UNIVERSITY OF CALIFORNIA,
IRVINE

# Using Synthetic Sphingolipids to Combat Obesity

DISSERTATION

submitted in partial satisfaction of the requirements
for the degree of

DOCTOR OF PHILOSOPHY

in Biological Sciences

by

Elizabeth Marie Selwan-Lewis

Dissertation Committee:
Professor Aimee Lara Edinger, Chair
Professor Marian Waterman
Associate Professor Michelle Digman
Assistant Professor Devon Lawson
Assistant Professor Wenqi Wang

2020

# DEDICATION

This dissertation is dedicated to

My Mom, my rock and

My Dad, my dragon slayer

Thank you for your unconditional love and support.

# TABLE OF CONTENTS

# LIST OF FIGURES

# ACKNOWLEDGMENTS

I would like to express my sincerest gratitude to my friends, family, mentors, and peers who have supported me along this long (very long) journey.

First and foremost, thank you to my outstanding mentor Dr. Aimee Edinger. Aimee is a true leader by example, who always strives to do the right thing and stays true to her values. Aimee has pushed me to always think critically and never take things at face value. Through all the challenges I faced in graduate school, Aimee was nothing but supportive, teaching me how to turn unanticipated roadblocks into opportunities for new directions. I truly would not have made it this far without her guidance, and I will forever mix, label and trust no one.

I would also like to thank my committee members Dr. Marian Waterman, Dr. Michelle Digman, Dr. Devon Lawson, and Dr. Wenqi Wang. I am grateful to these astounding scientists for their technical expertise and their commitment to my growth as a scientist.

Thank you to all that have supported my research: Dr. Michelle Digman and the LFD for technical assistance with FLIM, Dr. Adeela Syed at the Optical Biology Core for imaging, and Dr. Felix Grun at the Mass Spectrometery Core. Financial support was provided under the GAANN Fellowship, and National Cancer Institute of the National Institutes of Health under award number T32CA009054.

I am very thankful to all the past and current members of the Edinger Lab. The camaraderie and positivity made the late nights and long hours all the more bearable. A special thank you to Dr. Vaishali Jayashankar for her immense effort to elevate this project. I am grateful for the support for my personal as well as academic growth from Dr. Phong Luong and Andrea Ontiveros, as well as all of my graduate student lifting buddies who have come and gone.

Finally, I want to thank my friends and family for their patience and love throughout this process. Carla and Chuck, I apologize for all of the missed outings from experiments gone awry, but I promise no more canceling our adventures! To my Mom and Dad, look I did it – and here's proof that your daughter still exists. And finally, thank you to my husband Kevin for still bringing me doughnuts even though I left a mess in the kitchen from last night's bread baking.

# VITA

## Elizabeth Marie Selwan-Lewis

## EDUCATION

Ph.D., Biological Sciences, Department of Developmental and Cell Biology, University of California, Irvine — 2013 – 2020
Irvine, CA

B.S. Biochemistry, College of Sciences and Mathematics — 2009 – 2013
California Polytechnic State University, San Luis Obispo
San Luis Obispo, CA

## RESEARCH EXPERIENCE

University of California, Irvine — 2014 – 2020
Department of Developmental and Cell Biology
Advisor: Dr. Aimee Edinger

Dissertation research: Studies of the whole-body metabolic effects of SH-BC-893, a synthetic mimic of endogenous sphingolipids that block nutrient uptake. Investigating this pharmaceutical strategy in mouse models of diet-induced and congenital obesity. We are currently probing the mechanism by which SH-BC-893 ameliorates obesity and associated sequelae.

- Pioneered new area of research directions in the lab.
- Devised experiments and generated preliminary data for pilot studies resulting in award of a seed grant.
- Developed sample preparation and UPLC-MS/MS methodology to probe metabolism, enable pharmacokinetic analysis and guide in vivo dosing strategies of compounds. Optimized assay contributed to 2 publications.

Contributing project: Target deconvolution of tumor-suppressive natural and synthetic sphingolipids. Examined the cellular and molecular basis for differential sensitivity to lead compounds. Validated previously unrecognized protein targets suggesting feasibility of a unique polypharmacology approach for cancer, as well as illuminating novel mechanisms for growth control orchestrated by related endogenous sphingolipids.

- Implemented and performed functional biological assays to validate hits from datasets generated by collaborators.
- Utilized 2D and 3D cancer cell culture models in vitro as well as xenograft models in vivo.

Contributing project: Structure activity relationships of constrained FTY720 analogs as potential anti-cancer agents. *In collaboration with Dr. Stephen Hanessian, University of Montreal.*

- Performed bioassays for structure activity relationship studies.
- Supervised and managed execution of assays across lab personnel.
- Compiled data and communicated findings with synthetic chemist partners.
- Contributions to characterization of two series resulted in two publications.

California Polytechnic State University, San Luis Obispo 2010 - 2011
Department of Chemistry and Biochemistry
Advisor: Dr. Corinne Lehr
Undergraduate research: Investigation of microbes which oxidize arsenic/antimony

- Screened mutants for ability to oxidize arsenic and antimony using atomic absorption spectroscopy.
- Presented findings at ACS poster session.
- Helped validate a novel quantitative assay implemented as undergraduate chemistry laboratory module.

## PUBLICATIONS

- **Selwan, E.M,** Jayashankar, V., Hancock, S., Verlande, A., Chen, B., Hanessian, S., Masri, S., Turner, N., Edinger, A.L. Synthetic sphingolipid SH-BC-893 corrects high fat diet-induced mitochondrial fragmentation, obesity, and metabolic dysfunction. *In preparation.*

- Finicle, B.T., Ramirez, M.U., Liu, G., **Selwan, E.M.**, McCracken, A.N., Yu, J., Joo, Y., Nguyen, J., Ou, K., Roy, S.G., Mendoza, V.D., Corrales, D.V., Edinger, A.L. Sphingolipids inhibit endosomal recycling of nutrient transporters by inactivating ARF6. J Cell Sci (2018). 131(12): jcs213314.

- **Selwan, E.M.** and Edinger, A.L. Branched chain amino acid metabolism and cancer: the importance of keeping things in context. Transl Cancer Res (2017); 6(Suppl 3):S578-S584. doi: 10.21037/tcr.2017.05.05

- McCracken, A.N., McMonigle, R.J., Tessier, J., Fransson, R., Perryman, M.S., Chen, B., Keebaugh, A., **Selwan, E.M.**, Barr, S.A., Kim, S.M., Roy, S.G., Liu, G., Fallegger, D., Sernissi, L., Brandt, C., Moitessier, N., Snider, A.J., Clare, S., Müschen, M., Huwiler, A., Kleinman, M.T., Hanessian, S., Edinger, A.L. Phosphorylation of a constrained azacyclic FTY720 analog enhances anti-leukemic activity without inducing S1P receptor activation. Leukemia (2017). 31(3):669-677.

- Kim, S.M., Roy, S.G., Chen, B., Nguyen, T.M., McMonigle, R.J., McCracken, A.N., Zhang, Y., Kofuji S., Hou, J., **Selwan, E.M.**, Finicle, B.T., Nguyen, T.T., Ravi, A., Ramirez, M.U., Wiher, T., Guenther, G.G., Kono, M., Sasaki, A.T., Weisman, L.S., Potma, E.O., Tromberg, B.J., Edwards, R.A., Hanessian, S., Edinger, A.L. Targeting cancer metabolism by simultaneously disrupting parallel nutrient access pathways. J Clin Invest. (2016). 126(11):4088-4102.
- **Selwan, E.M.**, Finicle, B.T., Kim, S.M., Edinger AL. Attacking the supply wagons to starve cancer cells to death. FEBS Lett. (2016). 590(7):885-907.
- Chen, B., Roy, S.G., McMonigle, R.J., Keebaugh, A., McCracken, A.N., **Selwan, E.M.**, Fransson, R., Fallegger, D., Huwiler, A., Kleinman, M.T., Edinger, A.L., Hanessian S. Azacyclic FTY720 Analogues That Limit Nutrient Transporter Expression but Lack S1P Receptor Activity and Negative Chronotropic Effects Offer a Novel and Effective Strategy to Kill Cancer Cells in Vivo. ACS Chem Biol. (2016). 11(2):409-14.
- Hovereter, N., Zeller, M.D., McQuade, M.M., Girabaldi, A., Busch, A., **Selwan, E.M.**, Hertel, K.J., Baldi, P., Waterman, M.L. The TCF C-clamp DNA binding domain expands the Wnt transcriptome via alternative target recognition. Nucl. Acids Res. (2014). 42(22): 13615-13632.
- Lehr, C.R., Goscinski, N., Lewis, K,. Cross, N., Fylstra, N., **Selwan, E.M**. Kinetic Analysis of Sb(III): An Experiment for the Quantitative Analysis Laboratory. J. Chem. Edu. DOI: 10.1021/ed400021q

## PRESENTATIONS

**Poster Presentation**, “Starving triple negative breast cancers to death with sphingolipids that inactivate Arf6,” Keystone Symposia on Tumor Metabolism: Mechanisms and Targets. Whistler, BC, 2017.

**Poster Presentation**, “Characterization of the genes involved in antimony oxidation by Agrobacterium tumefaciens,” ACS National Research Conference. Denver, CO, 2011.

## HONORS AND AWARDS

GAANN (Graduate Assistant in Areas of National Need) fellowship 2018

NCI T32 Training Grant in Cancer Biology and Therapeutics 2015 – 2017

## TEACHING AND MENTORSHIP

University of California, Irvine
Teaching assistant – Bio93 (from DNA to Organisms) Fall 2016, 2017, 2019

- Created course content to supplement main lecture material in an active learning setting
- Led weekly discussion sections of 20-30 students

Bio199 undergraduate student Supervisor 2016 – 2019

- Mentored and supervised 4 undergraduate researchers.
- Trained to plan and execute experiments, analyze data, and critically evaluate scientific literature.

## PROFESSIONAL AFFILIATIONS

Association for Women in Science 2019 – present

Alpha Chi Sigma 2013 – present
*Professional member*

# ABSTRACT OF THE DISSERTATION

Using Synthetic Sphingolipids to Combat Obesity

By

Elizabeth Marie Selwan-Lewis

Doctor of Philosophy in Biological Sciences

University of California, Irvine, 2020

Professor Aimee Edinger, Chair

Obesity has reached epidemic status, threatening millions of lives and straining national economies and health-care systems. Obesity is a chronic disease with diverse etiologies, arising from complex interactions between genetic, physiologic, psychologic and environmental factors that can undermine one's ability to maintain a healthy weight. The current standard of care, behavioral and lifestyle interventions, has proven to be inadequate for a majority of obese patients thus use of pharmacotherapies has been proposed as an adjunct to lifestyle changes to overcome barriers to weight loss. However limited efficacy and poor safety prevent the widespread use of current pharmacotherapies, prompting the demand for new drug targets and novel therapeutics.

893 was previously characterized as a synthetic sphingolipid analog that simultaneously blocks multiple pathways of cellular nutrient uptake. Because chronic nutrient overload underlies much of obesity pathologies, we hypothesized that such a molecule would be an effective anti-obesity agent by putting cells on a diet, rather than a whole patient. To test this, we used 893 in an established mouse model of diet-induced obesity (DIO) that recapitulates the gradual weight gain and metabolic decline

that occurs in humans from passive overconsumption of energy dense foods. 893 safely restored normal body weight, reversed hepatic steatosis, and improved glucose homeostasis in obese mice maintained on a high-fat diet (HFD). 893 suppressed food intake and promoted whole body lipid metabolism *in vivo*. Prolonged HFD feeding induces ceramide-dependent mitochondrial fission that was directly blocked by 893 both *in vitro* and *in vivo*. This work demonstrates that 893 and related molecules represent a potential new strategy to tackle the growing obesity epidemic and highlights mitochondrial fission as a potential therapeutic target.

# CHAPTER 1

# Introduction

## 1.1 Obesity: A modern epidemic of supersized proportions

Since the World Health Organization (WHO) began to track obesity, rates have skyrocketed worldwide. A broad definition of obesity is having excessive fat mass at levels that pose various risks to health. Obesity is diagnosed by a body mass index (BMI weight in kg divided by height in $m^2$) of ≥ 30, although using BMI as a surrogate for obesity has its limitations (González-Muniesa et al., 2017). For example, Arnold Schwarzenegger, one of the greatest bodybuilders of his time, had a BMI of 30.6 when he was the epitome of leanness and won his first international title. Nevertheless, other measurements are not trivial and also come with caveats, and in most cases, BMI accurately portrays adiposity. Based on BMI, current estimates are that 13% of the world's population is obese (World Health Organization, 2018), and if just examining the US, 40% of adults are now obese (Hales, Carroll, Fryar, & Ogden, 2017). Even more alarming is the rise of obesity in children which has ballooned from 1% to 7% of children worldwide over the past 3 decades (World Health Organization, 2018). Unfortunately, most obese children today will likely become the obese adults of tomorrow. Obesity is a risk factor for many non-communicable diseases (NCDs) such as diabetes, heart disease, neurodegenerative disease, and many cancers (Guh et al., 2009). As NCD's are responsible for the majority of deaths worldwide, obesity imposes both a heavy personal and financial burden. In the US in 2014, obesity-related health care costs were estimated to be approximately $150 billion dollars, representing upwards of 5% of total

US health care spending (D. D. Kim & Basu, 2016). This large monetary impact together with the social, economic, and personal burden of obesity and its sequelae illustrates the critical unmet need for effective prevention and management strategies.

The WHO has set a seemingly modest goal of a zero-prevalence increase in obesity worldwide, however to this date no country has successfully met these criteria (Roberto et al., 2015). Achieving this will require a thorough understanding of the underlying causes of this unprecedented weight gain. At the most basic level, obesity results from a chronic state of positive energy balance; that is, energy intake in excess of what is expended. This definition is frequently linked to the first law of thermodynamics: energy in a closed system cannot be created or destroyed. In layman's terms, this is often reduced to calories in minus calories out determines your body weight. The high attrition rate for calorie restricted diets and frequent weight re-gain in obese individuals that do manage to lose weight indicates that this simple statement obscures the complexities of body weight control (Ochner, Barrios, Lee, & Pi-Sunyer, 2013). Indeed, because the etiology of obesity is so complex, some propose that obesity shouldn't be categorized as one entity rather it should be referred to as "obesities," akin to how we now view cancer (Karasu, 2016). Collectively, environmental and genetic factors contribute to the imbalance between food intake and energy expenditure and experimental design and interpretation should consider that the drivers of obesity and the effectiveness of interventions are likely to be highly context dependent.

### 1.2 Diet is a driver of the obesity epidemic

The exploding rates of obesity began in high-income countries such as the US, correlating to the central industrialization of food supplies (Cutler, Glaeser, & Shapiro, 2003). This allowed a plethora of foods to become widely available through new manufacturing techniques to enhance freshness and safety, while remaining cost effective and extremely tasty due to the addition of fat, sugar, artificial flavors and preservatives (Hall, 2018). As a result, industrialized foods became processed in such a way that make them irresistible especially when they were inexpensive and easily accessible (Cutler et al., 2003). Pervasive marketing from the food industry has exacerbated this issue by conditioning and misleading consumers to make unhealthy dietary choices. Children and adolescents are a particularly vulnerable population that are heavily targeted by the food industry and with the ubiquitous exposure to marketing through television and social media, are pre-disposed to continuously make poor dietary choices (Lobstein et al., 2015). Take for example, the chocolate hazelnut spread Nutella produced by the Ferrero company. In 2011 a California parent sued the company for marketing campaigns that portrayed the fat and sugar laden spread as a healthy and family friendly choice. Looking at the label, a brief glance at the top ingredients, sugar and palm oil, definitely state otherwise. A single serving covers 18% or 42% of the recommended daily fat or sugar intake, respectively. Besides, most people can't resist the chocolatey and nutty goodness and may easily exceed the measly 2 tbsp serving size. A common strategy for food companies is to obfuscate junk food characteristics by highlighting the positives, such labeling foods as "healthy" or designing marketing campaigns to create positive associations with branding (Hawkes

et al., 2015). Thus, the modern food system has created a dietary "recipe for disaster" collectively known as diet-induced obesity (DIO).

Understanding why dietary changes have led to such exaggerated weight gain is a critical question to address if we are to reverse the prevalence of obesity. The quest for the "holy grail" diet that can optimize human health and performance has brought forth a variety of dietary paradigms each claiming superiority for weight-loss properties. Upon further examination, meta-analysis of multiple dietary intervention studies reveals that there is no optimal diet; food composition does not affect long term weight loss as long as a sustainable calorie deficit is maintained (Gardner et al., 2018; Sacks et al., 2009). In contrast, the biochemical properties of obesogenic diets distinctly favor overconsumption and weight gain. Highly processed diets are less satiating in proportion to their caloric content than fresh foods triggering overeating (Poti, Braga, & Qin, 2017). A recent controlled trial illustrates this point nicely; when given unlimited access to a buffet composed of either exclusively unprocessed foods or calorie and macronutrient-matched ultra-processed offerings, individuals unknowingly consumed approximately 500 kcal extra, mostly from carbohydrates and fat, when they ate their fill of the processed foods (Hall et al., 2019). Beyond just satisfying energy requirements, the consumption of palatable food stimulates hedonic circuitries in the brain. Eating tasty high fat and high sugar food evokes a neurological response similar to that of addictive substances, which in turn can override homeostatic control of appetite (Leigh & Morris, 2018). Most often healthier diets are less palatable and do not have the same hedonic value, likely reinforcing preferences to unhealthy food choices (Kenny, 2011). Recent studies have suggested that high fat diets are associated with maladaptive

changes in the gut microbiome that may contribute to the development of obesity, possibly by increasing the metabolizable energy content or perturbing communication between the gut and brain (Martin, Osadchiy, Kalani, & Mayer, 2018). In summary, the quality and composition of one's diet influences energy balance in complex ways that are not completely understood.

The sheer caloric density of fat makes it easier to eat high-fat foods into a caloric surplus, but dietary fat in isolation is not sufficient to explain the magnitude of this ubiquitous issue. For example, ketogenic diets, loosely defined as very high fat, moderate protein, with minimal (<10% of kcal) carbohydrate have gained immense popularity for their promise to force individuals to preferentially burn fat stores. The key distinction between a typical "western" high fat diet and ketogenic diet is the relative macronutrient composition which creates a unique metabolic state from prolonged carbohydrate depletion (Kennedy et al., 2007). Once glucose stores are exhausted, fatty acids are released from adipocytes and converted into ketone bodies in the liver, where they can then be taken up by peripheral tissues and used to generate ATP (Newman & Verdin, 2014). There is no denying that weight loss can occur on a ketogenic diet, which is contentiously attributed to a metabolic advantage from relying on ketones as the primary source of fuel, as well as its appetite suppressive and thermogenic properties (Paoli, Rubini, Volek, & Grimaldi, 2013). While these diets may lead to weight loss in the short term, this may represent a tradeoff by eschewing fruits, whole grains, and legumes that provide key micronutrients (Joshi, Ostfeld, & McMacken, 2019). In contrast to ketogenic diets, obesogenic high fat diets that contain processed and refined carbohydrates interfere with homeostatic control of energy

balance, likely owing to their reward properties and differences in satiety (DiFeliceantonio et al., 2018; Hall et al., 2019).

What you eat matters, but so does when you eat it. Mammals have a central circadian clock located in the suprachiasmatic nucleus (SCN) of the hypothalamus that are set to so called zeitgebers, or time givers, such as light, to synchronize biological processes with shifts in the environment (Roenneberg & Merrow, 2016). This central clock in the SCN can entrain peripheral clocks in other tissues, however these can be regulated by their own zeitgebers. Food intake is a potent cue for peripheral clocks in metabolic tissues such as the liver, and consistent with this abundance of metabolites and the expression of many metabolic enzymes are under circadian control (Eckel-Mahan et al., 2012; Reinke & Asher, 2016). For example, enzymes that are involved with sugar uptake and metabolism peak early in the rodent active period, when most of their daily intake occurs (Reinke & Asher, 2016). The modern environment has forced many to desynchronize from normal sleep-wake times, for example shift-workers and so called 'social jet lag' arising from erratic meal times and sleep patterns over the week (Dibner & Schibler, 2015). Consistent with a disconnect between food intake and circadian oscillations in metabolism, shift workers are more prone to develop obesity than day workers (Q. Liu et al., 2018). In rodents, high-fat diets disrupt diurnal patterns in feeding behavior. When mice are only allowed to consume a high fat diet during their active period, they gain significantly less bodyweight than control mice allowed ad libitum access to the high-fat chow even though caloric intake remains equal (Hatori et al., 2012). Thus, meal timing can exacerbate the effects of an unhealthy diet. Considering that modern lifestyles are hallmarked by erratic work schedules, being

surrounded 24/7 by stimulating artificial lights, and seemingly endless access to food, the times at which we eat likely make a significant contribution to the epidemic of weight gain in humans.

The dramatic shift in the food environment has occurred rapidly yet the gene pool has remained relatively stable. The observation that we have not all equivocally become obese suggests that gene-environment interactions play a key role in determining individual adiposity (van der Klaauw & Farooqi, 2015). It has been hypothesized that from an evolutionary perspective, periods of starvation were more readily encountered and posed a larger threat to survival than nutrient excess (Sellayah, Cagampang, & Cox, 2014). Genetic selection would thus favor metabolic adaptations that promote efficient use and storage of fuel in times of feast to sustain viability in the inevitable famine to follow. In the current environment where overconsumption is unopposed by any risk of extended starvation, these protective responses have become maladaptive. Individuals who would have been well adapted to intermittent famine are now prone to obesity in the modern environment where food is rich and aplenty. Clearly there is a genetic component; family and twin studies correlating BMI have demonstrated that body weight is highly heritable, however the precise mechanisms remain poorly understood (Elks et al., 2012). In an attempt to develop a more nuanced understanding of contributing genetic factors, genome-wide association studies (GWAS) have been performed in diverse populations and have identified a number of gene loci associated with body weight variation. Gene and pathway analyses suggest that many identified genetic factors may either make individuals more prone to overeating, such as by modulating appetite, or change how individuals respond to the food they eat by

shifting nutrient use and/or partitioning (Locke et al., 2015; Shungin et al., 2015). While these associations are intriguing, it remains a challenge to establish causal relationships and mechanistic implications from these studies. In summary, it is important to consider that multiple genetic variants contribute to DIO susceptibility.

### 1.3 Molecular control of energy balance: The role of Leptin and Insulin

The discovery of leptin was the first direct evidence of a hormonal feedback system controlling food intake and energy expenditure. This began approximately 7 decades ago, when a genetic mutant obese mouse was discovered at the Jackson Laboratory with the putative gene aptly being named *Obese* (Ingalls, Dickie, & Snell, 1950). The *ob/ob* mouse strain displayed early onset obesity secondary to hyperphagia. Several years later another obese strain with a distinct mutation was discovered that almost completely phenocopied the *ob/ob* mouse, although in addition it developed severe diabetes and thus was dubbed the *Diabetes* gene, or the *db/db* mouse (Hummel, Coleman, & Lane, 1972). This led Dr. Douglas Coleman, the investigator responsible for the characterization of these mutants, to hypothesize that either of these mouse strains produced some unknown factor that was sufficient to cause obesity (Douglas L Coleman, 2010). He performed parabiosis experiments in which he surgically joined the circulatory systems of two mice to identify a putative feedback system that controlled adiposity. These led to striking results: when *db/db mice* were paired to a WT mouse, the WT mouse would become hypophagic and starve to death while the *db/db* symbiont continued to overeat and gain weight (D L Coleman & Hummel, 1969). Subsequently, pairing a *db/db* mouse with an *ob/ob* mouse also did not slow hyperphagia in the *db/db* mouse while the *ob/ob* mouse died of starvation.

Together, Dr. Coleman concluded that the *db/db* mouse was producing a satiety factor normally and the *db* gene was a defective receptor, while the *ob* mouse was lacking that satiety factor but had the functional receptor (D L Coleman, 1973). Additional observations suggested that the *db* protein was located centrally in the hypothalamus and the *ob* protein was in adipose tissue, but it wasn't until 1994 and 1995 when the *ob* and *db* gene products were cloned that these observations were validated. Injecting *ob/ob* mice with recombinant *ob* protein reduced body weight and increased energy expenditure, while having no effect on *db/db* mice (Halaas et al., 1995; Y. Zhang et al., 1994). Thus, the *ob* protein was named leptin derived from the Greek word leptos, meaning thin and its cognate receptor *db* was called the leptin receptor (Tartaglia et al., 1995). Together, these pivotal studies established the framework of a homeostatic system that functioned to regulate bodyweight.

Because leptin plays a key role in energy homeostasis, there have been many studies dissecting the molecular mechanisms underlying leptin's control of food intake. Leptin is synthesized and secreted by adipocytes and circulate in proportion to adiposity (Pan & Myers, 2018). Leptin levels rise after eating a meal, and basal levels rise as adipose tissue expands. Conversely, between meals and under conditions of fasting circulating levels of leptin drop. Although leptin was named for its proposed ability to prevent obesity, evidence favors the hypothesis that the leptin signaling axis communicates nutritional state as a mechanism to defend against starvation. In fact, the phenotype of *ob/ob* mice resembles that of starvation including infertility, reduction of thermogenesis, and an increase in stress hormone output (Ahima et al., 1996). Thus, the actions of leptin are not limited to the control of feeding behavior rather it signals an

integrated response to promote survival in the face of nutritional depletion. While the leptin receptor is expressed on many tissues, many of its effects are mediated through its signaling in the brain (Flak & Myers, 2016). Consistent with a dominant central mechanism of action, intracerebroventricular injections (ICV) of leptin are sufficient to cause weight loss at minute doses that do not reach peripheral circulation (Halaas et al., 1997). Thus, leptin provides a feedback loop from adipocyte to brain to communicate total energy stores and adjust behaviors to maintain metabolic homeostasis.

Within the brain the hypothalamus serves as a metabolic hub, integrating a variety of hormonal, neuronal and nutritional metabolic signals. Whole body energy status is sensed through afferent signals received by diverse hypothalamic nuclei, which in turn orchestrate physiological and behavioral responses to promote overall homeostasis. The arcuate nucleus (ARC) is a key locale within involved in regulation of energy balance that is a primary target of leptin. Within the ARC two populations of neurons function antagonistically to control food intake and energy expenditure, the anorexigenic (appetite suppressing) proopiomelanocortin (POMC) and the orexigenic (hunger enhancing) agouti-related peptide (AgRP) neurons (Flak & Myers, 2016). Both POMC and AgRP neurons express the leptin receptor but it is notably widely expressed in various regions of the brain (Flak & Myers, 2016). Upon reaching the ARC, leptin stimulates POMC neurons to produce and release anorexigenic peptides that reduce feeding and increase energy expenditure while concomitantly suppressing the activity of AgRP neurons (Pan & Myers, 2018). When leptin levels fall as under periods of energy depletion, inhibition of AgRP neurons is released which can both stimulate appetite and energy expenditure directly, while inhibiting the appetite suppressive POMC neurons

(Pan & Myers, 2018). Selective ablation of the leptin receptor in POMC or AgRP neurons is sufficient to cause a mild obese phenotype suggesting that this POMC/AgRP neuronal circuit is important for leptin-mediated control of food intake but is not solely responsible (Varela & Horvath, 2012). In summary, the direct effects of leptin on food intake are mediated primarily via leptin receptors expressed in neurons in the arcuate nucleus of the hypothalamus, although other regions of the brain may be involved.

It is important to recognize that mice lacking leptin signaling do not accurately model human obesity. Injecting recombinant leptin into *ob/ob* mice and humans with congenital leptin deficiencies, but not the majority of obese patients, triggers weight loss (Myers, Leibel, Seeley, & Schwartz, 2010). In most cases of human obesity leptin is not limiting. In fact, most obese patients are hyperleptinemic and are unresponsive to the effects of exogenous leptin, a state referred to as leptin resistance (Myers et al., 2010). Similar to humans, rodents fed a high fat diet develop peripheral and central leptin resistance as obesity progresses (Lin, Thomas, Storlien, & Huang, 2000). Sustained hyperleptinemia and leptin signaling is both necessary and sufficient to cause leptin resistance and weight gain, which remains unaffected by additional leptin administration (Enriori et al., 2007; Zhao et al., 2019). Modern obesogenic diets disrupt leptin signaling and leptin resistance is a key component underlying DIO however it can be reversed (Enriori et al., 2007). In fact, lowering leptin levels in obese mice can cause weight loss by reducing negative feedback and restoring hypothalamic leptin receptor signaling (Zhao et al., 2019). Because leptin-mediated signaling is such a powerful regulator of energy homeostasis effort has been directed towards identifying ways to re-sensitize obese patients to endogenous leptin (Andreoli, Donato, Cakir, & Perello, 2019). In

summary, while administering recombinant leptin is not a silver bullet to cure human obesity, restoring leptin signaling in obese patients is likely to be a successful therapeutic strategy.

So far, small molecules that have been found to sensitize to leptin work by reducing endoplasmic reticulum (ER) stress (Lee et al., 2016; J. Liu, Lee, Salazar Hernandez, Mazitschek, & Ozcan, 2015; L. Ozcan et al., 2009). DIO is known to induce chronic ER stress, a phenomenon by which cellular stressors trigger disruption in ER homeostasis leading to a set of adaptive responses to mitigate stress (U. Ozcan et al., 2004). While this acute response is beneficial in the short term, if unresolved it can create a pathological state. Consistent with this, genetic and pharmacological induction of ER stress causes hypothalamic leptin resistance (L. Ozcan et al., 2009; Won et al., 2009) and conversely, relieving ER stress can re-sensitize neurons to leptin and protect from DIO (L. Ozcan et al., 2009; X. Zhang et al., 2008). The ER forms extensive contact sites with mitochondria called mitochondria-associated membranes (MAMs) and maintaining these contacts is critical for proper ER function. MAMs also control mitochondrial dynamics. Mitochondria play a critical role in the cellular adaptations to nutritional status by undergoing distinct changes in morphology through cycles of fusion and fission through the recruitment of specific membrane-remodeling and adaptor proteins, and these changes are intricately tied to their function (Liesa & Shirihai, 2013). Under conditions of nutrient stress mitochondria will form highly tubular branched networks leading to an increase in oxidative metabolism to restore ATP levels (Liesa & Shirihai, 2013). When faced with nutrient overload these networks become highly fragmented, associated with an increase in reactive oxygen species and impaired

oxidative phosphorylation (Liesa & Shirihai, 2013). The saturated fatty acid palmitate is the most abundant fatty acid species in the blood, which is highly elevated in mice on a high-fat diet (Chaurasia & Summers, 2015). ICV administration of palmitate induces leptin resistance (Kleinridders et al., 2009), and the lipotoxic metabolite ceramide is derived from palmitate (Chaurasia & Summers, 2015). Interestingly, palmitate was recently shown to cause mitochondrial fragmentation in the liver through its conversion to ceramide (Hammerschmidt et al., 2019). Moreover, accumulation of hypothalamic ceramides induces ER stress (Contreras et al., 2014), and disrupting ER-mitochondria contacts in POMC neurons causes leptin resistance (Schneeberger et al., 2013). Therefore, the increased circulating levels of saturated fats like palmitate and lipotoxic species may contribute to leptin resistance in DIO by disrupting ER and mitochondrial function. The links between ER stress and mitochondrial morphology are clear, but mechanistic details remain to be defined. For example, while some studies conclude that increased mitochondrial-ER contacts are associated with metabolic dysfunction (Arruda et al., 2014), other studies draw the opposite conclusion (Schneeberger et al., 2013; Tubbs et al., 2014). Collectively, this suggests the roles of MAMs are likely to be context dependent. Dissecting the role of the ER and mitochondria in DIO will be important to understand the etiology of this disease and thus to develop effective therapies.

There is significant crosstalk between insulin and leptin signaling, and it is clear that insulin resistance also contributes to DIO and its sequelae (Könner & Brüning, 2012). As is the case for leptin, ER stress and mitochondrial fragmentation are associated with insulin resistance both in central and peripheral tissues. Under normal

conditions, insulin is secreted by pancreatic β-cells mainly in response to glucose and promotes blood glucose clearance by increasing its uptake into insulin-responsive tissues, while suppressing hepatic gluconeogenesis (Petersen & Shulman, 2018). Moreover, insulin acts as an anabolic hormone that increases lipogenesis, protein synthesis, and glycogenesis. In humans and mouse models of DIO insulin resistance is readily apparent often manifesting as reduced cellular glucose uptake from and failure for insulin to suppress hepatic glucose output, leading to hyperglycemia (Samuel & Shulman, 2012). Paradoxically, while many tissues are insulin-resistant, hyperinsulinemia still promotes hepatic lipogenesis, a state termed as selective insulin resistance (Könner & Brüning, 2012). In the liver, saturated fatty acids induce ER stress and mitochondrial fragmentation downstream of ceramide generation (Hammerschmidt et al., 2019). In hepatocytes, disrupting MAMs and triggering ER stress is sufficient to impair insulin signaling (U. Ozcan et al., 2004), while preventing mitochondrial fission or relieving ER stress can ameliorate HFD-induced insulin resistance (Jheng et al., 2012; L. Wang et al., 2015). Central administration of insulin under certain contexts suppresses food intake (Brown, Clegg, Benoit, & Woods, 2006), and can directly affect POMC and AgRP neuronal activity (Brüning et al., 2000; Dodd et al., 2018). Blunting hypothalamic insulin signaling leads to hyperphagia and obesity (Benoit et al., 2009; Obici, Feng, Karkanias, Baskin, & Rossetti, 2002). Together, this suggests that ER stress and mitochondrial disfunction promotes resistance to insulin in addition to leptin, both of which play major roles in the pathology of obesity.

### 1.4 Mouse models of obesity: pass the cheese, please

To crack the obesity epidemic, mouse models that accurately mimic the biology underlying human DIO will be essential. There are a number of animal models of obesity, each with their own utility. Characterization of traditional monogenic mouse models with obese phenotypes has paved the way for an era of discovery increasing our understanding of the pathways by which energy homeostasis is controlled, as was the case described for the *ob/ob* mice and leptin. However, the relevance of these models to the garden variety of obesity responsible for the widespread epidemic is questionable. The *ob/ob* and *db/db* mice represent a congenital absence of leptin, and this complete leptin deficiency is not the same as the manifestation of leptin resistance (Zhao et al., 2019). The absence of leptin in the perinatal period interferes with proper neuroendocrine development and can disrupt the circuits that control food intake and energy balance (Bouret & Simerly, 2004). This caveat is shared by conditional knockouts generated by cre-lox-mediated deletion in specific tissues during development. For example, studies examining POMC specific knockouts of mitochondrial fusion and fission factors lead to distinct phenotypes when Cre expression is induced in adulthood by administration of tamoxifen or doxycycline (Santoro et al., 2017; Schneeberger et al., 2013). Collectively, while these monogenic mouse models can be useful to elucidate mechanisms to understand obesity, these models may have limited predictive value for whether obesity interventions can be successfully translated to the majority of obese humans.

Individual adiposity clearly has a genetic component, however for most cases this arises from a complex interaction from many individual genes that occurs gradually

and subtly overtime (Barrett, Mercer, & Morgan, 2016). As argued above, the ubiquity of high fat and energy dense diets in modern society is a driving force for the burgeoning epidemic we face today. The polygenic nature of body weight in the majority of humans make it impossible to create a perfect genetically engineered animal model of obesity. Nonetheless, similar to what is seen in humans, mouse strains with different genetic backgrounds exhibit variable sensitivity to DIO, each developing different degrees of weight gain, region-specific adiposity, and hormonal resistance (Montgomery et al., 2013). The highly inbred C57BL6/J mice are relatively sensitive to high fat diet-induced obesity and while the sensitizing genetic factors are not fully characterized, male C57BL6 mice have become the standard model for DIO (C.-Y. Wang & Liao, 2012). When fed palatable diets that are high in fat, recapitulating the dietary environment thought to drive the increase in human adiposity, many laboratory rodents will gradually become obese and leptin resistant (Lin et al., 2000). Normal mouse chow contains 10% kcal from fat and commonly used DIO formulations contain either 45% or 60% kcal from fat. Many investigators use a 60% HFD for convenience and cost because it is more energy dense and mice become obese more quickly when compared to the 45% kcal from fat diet, but this may not be as physiologically relevant. The current recommended dietary fat content in the US as a % of kcal is suggested to be 20-35% (Rahavi, Altman, & Stoody, 2019), and a distortion equivalent from a mouse going from 10% to 60% is much less likely to be encountered as a human high fat diet. Taken together, the etiology of C57BL6/J male mice on a moderate 45% high fat diet are a good choice of model for the polygenic nature of human DIO.

## 1.5 Therapeutics for obesity

Because obesity is caused by persistent energy imbalance, any treatment for obesity must ultimately either increase energy expenditure or decrease food intake. Historically, obesity has been highly stigmatized from the medical community and misguidance from popular media, surmising that obesity was simply a result of poor behavioral choices and lack of willpower (Friedman, 2004). The conventional treatment for obesity has been a low-calorie diet with exercise and although there is a high value in good nutrition and physical activity for general health span, our growing body of knowledge about physiological mechanisms that regulate energy balance has challenged this oversimplified treatment paradigm (Ochner, Tsai, Kushner, & Wadden, 2015). For many obese patients, achieving and maintaining weight loss is an uphill battle against their biology as the neuroendocrine response to a calorie restricted diet is one that favors weight regain (Maclean, Bergouignan, Cornier, & Jackman, 2011; Ochner et al., 2013). Bariatric surgery is the most effective treatment by far but is high risk and invasive (Bray, Frühbeck, Ryan, & Wilding, 2016). Interestingly, weight rebound is much less common in patients that undergo surgery suggesting that the physiological adaptations underlying weight regain are blunted. As many individuals fail to lose and maintain a healthy weight with lifestyle interventions alone, pharmacotherapies have been suggested as an adjunct to help overcome these barriers to weight loss (Bessesen & Van Gaal, 2018).

For an anti-obesity drug to be approved, it must produce a weight loss of at least 5% greater in combination with behavioral intervention, than just intervention alone at one year (Bessesen & Van Gaal, 2018). It has been suggested that a 5% weight

reduction can produce clinically significant improvement in metabolic health and this is a seemingly low bar, yet many drugs have failed to meet these criteria (Bessesen & Van Gaal, 2018). As a weight loss drug needs to be taken chronically for it to work it must also meet stringent safety requirements. Past and current pharmacotherapies for weight management have performed poorly in practice because they were not efficacious, or they were deemed too toxic for long term use (Rodgers, Tschöp, & Wilding, 2012). In the 1930's the chemical dinitrophenol (DNP), a mitochondrial uncoupler, was prescribed as a miracle pill for its remarkable ability to cause weight loss without any conscious restriction of caloric intake (Colman, 2007). By dissipating the mitochondrial proton gradient, DNP diverts stored energy destined to become ATP into heat, causing a dramatic increase in metabolic rate and fat metabolism (Grundlingh, Dargan, El-Zanfaly, & Wood, 2011). Unfortunately, there really was no such thing as free lunch for users of DNP, and it was quickly banned by the FDA because of its severe side effects, namely fatal hyperthermia, and narrow therapeutic window (Grundlingh et al., 2011). Amphetamines and its derivatives have been used because of their thermogenic and anorectic properties, often in combination with other agents to reduce the potential of addiction and enhance efficacy. The combination of fenfluramine (a serotonergic) and phentermine (sympathomimetic) known as Fen/Phen, gained popularity after a clinical trial showed a mean weight loss of 15.9% in 34 weeks versus 4.9% in placebo (Weintraub et al., 1992). At the time it had a seemingly favorable safety profile but was later withdrawn due to the heightened risk of valvular heart disease from fenfluramine use, although phentermine is still in use today as described below (Srivastava & Apovian, 2018). Sibutramine was used to promote satiety but was also withdrawn post-

marketing due to cardiovascular side effects, a clear contraindication for a population already at enhanced risk for heart disease. As an alternative to sympathomimetics, a cannabinoid 1 (CB1) receptor antagonist Rimonabant was developed under the observation that CB1 receptor ligands like those in cannabis stimulate appetite (Di Marzo & Matias, 2005). Although Rimonabant was briefly approved in Europe, it was quickly withdrawn due to association with psychiatric adverse events such as anxiety, depression, and suicidal ideations (Rodgers et al., 2012; Sam, Salem, & Ghatei, 2011). As the history of anti-obesity pharmacotherapy has been plagued with failures not feasible for long term use, there is critical need for new targets and paradigms for drug discovery.

Most currently approved agents treat obesity by reducing food intake by targeting hypothalamic circuits that control appetite. The aforementioned sympathomimetic phentermine is the oldest approved therapy in the US and also the least expensive but is only prescribed for short-term use (up to three months) due to safety concerns. Low dose phentermine in combination with topiramate marketed as Qsymia, was more recently approved by the FDA having superior efficacy and safety versus phentermine alone (Srivastava & Apovian, 2018). The mechanism of appetite suppression by topiramate is not clear, but none the less this combination is contraindicated with cardiovascular disease. Lorcaserin was developed as a more selective serotonin receptor agonist drug with respect to fenfluramine, and acts on POMC neurons to reduce food intake (Heisler et al., 2002). It should not be taken with other serotonergic drugs due to risk of serotonin syndrome and considering antidepressant use has recently skyrocketed in the US population, lorcaserin may not be suitable for many. On

the other hand bupropion, a common antidepressant, in combination with naltrexone is approved for obesity under the trade name Contrave. Bupropion stimulates POMC neurons while naltrexone relieves negative feedback of POMC neurons, potentiating firing rate (Apovian, 2016). The GLP-1 agonist liraglutide was previously approved for the treatment of type 2 diabetes and the consistent observation that it caused weight loss led it to be tested and approved at a higher dose to enhance weight loss for patients with obesity. GLP-1 is an incretin hormone that acts both peripherally to stimulate insulin secretion and centrally to reduce appetite. Liraglutide also shows moderate efficacy and risk, but it has to be administered daily by subcutaneous injection and is also the costliest approved weight-loss drug (Srivastava & Apovian, 2018). Comparatively, meta-analysis of 5 currently US FDA approved drugs suggested that treatments that were most likely to be effective were also the ones with the highest chance of discontinuation due to adverse events (Khera et al., 2016). In summary, current approved drugs target hormonal circuits that regulate satiety and food intake, although the efficacy relative to risk leaves room for much improvement.

With no clear “home-run” pharmaceutical approved for treating obesity, a new distinct approach needs to be taken. Rather than limiting organismal food intake, it might be possible to reduce adiposity by limiting nutrient uptake at the cellular level. This was the premise of orlistat, a pancreatic and gastric lipase inhibitor that decreases fat absorption by the gut (Srivastava & Apovian, 2018). This peripheral mechanism doesn’t carry the cardiovascular and psychiatric liabilities as the above-mentioned drugs, but it comes with highly undesirable side effects such as oily stools and fecal urgency. It is also the least efficacious approved drug (Bessesen & Van Gaal, 2018).

This would limit nutrient uptake in principle but perhaps blocking uptake of only one macromolecule and being restricted to the gut may explain its poor efficacy. Interestingly, SGLT2 inhibitors, which prevent kidney reuptake of glucose, have also been reported to produce weight loss in non-diabetic obese patients (Bessesen & Van Gaal, 2018). While a considerable amount of glucose is lost in the urine, the caloric deficit is offset by compensatory increases in appetite from the reduction of glycemia (Pereira & Eriksson, 2019). By blocking the uptake of multiple nutrients and in different tissues a greater caloric deficit may be achieved. Sphingolipids are endogenous regulators of nutrient access that are conserved from yeast to man (Chung, Jenkins, Hannun, Heitman, & Obeid, 2000; Chung, Mao, Heitman, Hannun, & Obeid, 2001). In yeast, phytosphingosine is produced in response to heat stress causing the down-regulation of multiple amino acid permeases, creating a response similar to that of nutrient limitation that triggers adaptive growth arrest (Chung et al., 2001; Welsch, Roth, Goetschy, & Movva, 2004). Inspired by this, synthetic sphingolipid 893 was created to engage this pathway and prevent nutrient uptake by constitutively anabolic tumor cells (Chen et al., 2016; Romero Rosales et al., 2011). Both the endogenous mammalian sphingolipid ceramide and 893 cause downregulation of amino acid and glucose transporters, and 893 additionally reduces surface LDLr expression and LDL uptake (Chen et al., 2016; Guenther et al., 2008; S. M. Kim et al., 2016). Thus, 893 induces a coordinate downregulation in multiple nutrient uptake pathways, leading to profound nutrient stress. In various tumor models, 893 is very effective at killing cancer cells but non-toxic to normal cells, likely because the levels oscillate in the blood (Chen et al., 2016; S. M. Kim et al., 2016). This would create only periodic intervals of nutrient

limitation that spares normal tissue but is detrimental to tumors. We noticed that after treatment with 893 for 11 weeks in a genetically engineered mouse model of prostate cancer, the treated mice had greatly diminished inguinal fat pads relative to the vehicle mice, with no overt abnormalities in blood chemistry or damage to rapidly proliferating intestinal crypt cells (S. M. Kim et al., 2016). Together, this suggests that sphingolipids that mimic the effects of yeast phytosphingosine might restore energy balance by limiting cellular uptake and storage of nutrients.

The idea of using sphingolipids to treat obesity is innovative but not necessarily intuitive, as sphingolipids are generally considered to contribute to type II diabetes in obese patients (Chaurasia & Summers, 2015; Chavez & Summers, 2012). Ceramide in particular, which accumulates in tissues under lipid oversupply, has been vilified for its destructive roles in metabolic tissues. Mechanistically, ceramide dephosphorylates and inactivates AKT by either a PP2A or PKCζ dependent mechanism to antagonize insulin signaling. This in turn blocks insulin stimulated surface translocation of GLUT4 preventing glucose uptake, which when chronic can lead to hyperglycemia and insulin resistance. In rodent models of obesity blocking ceramide synthesis both genetically and pharmacologically can mitigate the development of insulin resistance (Chaurasia et al., 2019; Holland et al., 2007; Turpin et al., 2014; Turpin-Nolan et al., 2019). Notably, while ceramide and 893 both activate PP2A and downregulates nutrient transporters (Finicle et al., 2018), phosphoproteomic analysis comparing the effects of 893 and ceramide suggested that the changes in protein phosphorylation between 893 and ceramide only partially overlap (Kubiniok et al., 2019). Importantly, unlike ceramide, 893 did not inactivate AKT *in vitro* (Kubiniok et al., 2019). Mice treated chronically with 893

do not exhibit glucosuria suggesting 893 does not induce hyperglycemia. Encouraged by the apparent lack of systemic glucose intolerance and the dramatic fat loss observed in 893-treated tumor bearing mice, we reasoned that synthetic sphingolipids like 893 may have utility in diet-induced obesity.

### 1.6 Conclusions

In summary, the rapid expansion of obesity poses one of the greatest threats to the wellbeing of modern society. The constant availability of high-fat and energy dense foods has leveraged behavioral, physiological, and genetic vulnerabilities to create an environment conducive to promote overeating. Our understanding about the physiology of the obese state has expanded significantly, yet traditional treatment paradigms have failed to acknowledge the robust biological mechanisms that serve to resist weight loss. In the central chapter of this dissertation, we employ a mouse model of diet-induced obesity to explore the utility of apical inhibitors of nutrient access. In so doing, we unveil a novel mechanism by which synthetic sphingolipids can protect from overnutrition through effects on central and peripheral control of food intake and metabolism. These findings have profound implications on how we can target mitochondrial dynamics that underlie the pathogenesis of obesity.

## 1.7 References


Ahima, R. S., Prabakaran, D., Mantzoros, C., Qu, D., Lowell, B., Maratos-Flier, E., & Flier, J. S. (1996). Role of leptin in the neuroendocrine response to fasting. *Nature*, *382*(6588), 250–252. doi:10.1038/382250a0

Andreoli, M. F., Donato, J., Cakir, I., & Perello, M. (2019). Leptin resensitisation: a reversion of leptin-resistant states. *The Journal of Endocrinology*, *241*(3), R81–R96. doi:10.1530/JOE-18-0606

Apovian, C. M. (2016). Naltrexone/bupropion for the treatment of obesity and obesity with Type 2 diabetes. *Future cardiology*, *12*(2), 129–138. doi:10.2217/fca.15.79

Arruda, A. P., Pers, B. M., Parlakgül, G., Güney, E., Inouye, K., & Hotamisligil, G. S. (2014). Chronic enrichment of hepatic endoplasmic reticulum-mitochondria contact leads to mitochondrial dysfunction in obesity. *Nature Medicine*, *20*(12), 1427–1435. doi:10.1038/nm.3735

Barrett, P., Mercer, J. G., & Morgan, P. J. (2016). Preclinical models for obesity research. *Disease Models & Mechanisms*, *9*(11), 1245–1255. doi:10.1242/dmm.026443

Benoit, S. C., Kemp, C. J., Elias, C. F., Abplanalp, W., Herman, J. P., Migrenne, S., … Clegg, D. J. (2009). Palmitic acid mediates hypothalamic insulin resistance by altering PKC-theta subcellular localization in rodents. *The Journal of Clinical Investigation*, *119*(9), 2577–2589. doi:10.1172/JCI36714

Bessesen, D. H., & Van Gaal, L. F. (2018). Progress and challenges in anti-obesity pharmacotherapy. *The lancet. Diabetes & endocrinology*, *6*(3), 237–248. doi:10.1016/S2213-8587(17)30236-X

Bouret, S. G., & Simerly, R. B. (2004). Minireview: Leptin and development of hypothalamic feeding circuits. *Endocrinology*, *145*(6), 2621–2626. doi:10.1210/en.2004-0231

Bray, G. A., Frühbeck, G., Ryan, D. H., & Wilding, J. P. H. (2016). Management of obesity. *The Lancet*, *387*(10031), 1947–1956. doi:10.1016/S0140-6736(16)00271-3

Brown, L. M., Clegg, D. J., Benoit, S. C., & Woods, S. C. (2006). Intraventricular insulin and leptin reduce food intake and body weight in C57BL/6J mice. *Physiology & Behavior*, *89*(5), 687–691. doi:10.1016/j.physbeh.2006.08.008

Brüning, J. C., Gautam, D., Burks, D. J., Gillette, J., Schubert, M., Orban, P. C., … Kahn, C. R. (2000). Role of brain insulin receptor in control of body weight and reproduction. *Science*, *289*(5487), 2122–2125. doi:10.1126/science.289.5487.2122

Chaurasia, B., & Summers, S. A. (2015). Ceramides - Lipotoxic Inducers of Metabolic Disorders. *Trends in Endocrinology and Metabolism*, *26*(10), 538–550. doi:10.1016/j.tem.2015.07.006

Chaurasia, B., Tippetts, T. S., Mayoral Monibas, R., Liu, J., Li, Y., Wang, L., … Summers, S. A. (2019). Targeting a ceramide double bond improves insulin resistance and hepatic steatosis. *Science*, *365*(6451), 386–392. doi:10.1126/science.aav3722

Chavez, J. A., & Summers, S. A. (2012). A ceramide-centric view of insulin resistance. *Cell Metabolism*, *15*(5), 585–594. doi:10.1016/j.cmet.2012.04.002

Chen, B., Roy, S. G., McMonigle, R. J., Keebaugh, A., McCracken, A. N., Selwan, E., … Hanessian, S. (2016). Azacyclic FTY720 analogues that limit nutrient transporter expression but lack S1P receptor activity and negative chronotropic effects offer a novel and effective strategy to kill cancer cells in vivo. *ACS Chemical Biology*, *11*(2), 409–414. doi:10.1021/acschembio.5b00761

Chung, N., Jenkins, G., Hannun, Y. A., Heitman, J., & Obeid, L. M. (2000). Sphingolipids signal heat stress-induced ubiquitin-dependent proteolysis. *The Journal of Biological Chemistry*, *275*(23), 17229–17232. doi:10.1074/jbc.C000229200

Chung, N., Mao, C., Heitman, J., Hannun, Y. A., & Obeid, L. M. (2001). Phytosphingosine as a specific inhibitor of growth and nutrient import in Saccharomyces cerevisiae. *The Journal of Biological Chemistry*, *276*(38), 35614–35621. doi:10.1074/jbc.M105653200

Coleman, D L. (1973). Effects of parabiosis of obese with diabetes and normal mice. *Diabetologia*, *9*(4), 294–298. doi:10.1007/bf01221857

Coleman, D L, & Hummel, K. P. (1969). Effects of parabiosis of normal with genetically diabetic mice. *The American Journal of Physiology*, *217*(5), 1298–1304. doi:10.1152/ajplegacy.1969.217.5.1298

Coleman, Douglas L. (2010). A historical perspective on leptin. *Nature Medicine*, *16*(10), 1097–1099. doi:10.1038/nm1010-1097

Colman, E. (2007). Dinitrophenol and obesity: an early twentieth-century regulatory dilemma. *Regulatory Toxicology and Pharmacology*, *48*(2), 115–117. doi:10.1016/j.yrtph.2007.03.006

Contreras, C., González-García, I., Martínez-Sánchez, N., Seoane-Collazo, P., Jacas, J., Morgan, D. A., … López, M. (2014). Central ceramide-induced hypothalamic lipotoxicity and ER stress regulate energy balance. *Cell reports*, *9*(1), 366–377. doi:10.1016/j.celrep.2014.08.057

Cutler, D. M., Glaeser, E. L., & Shapiro, J. M. (2003). Why have americans become more obese? *Journal of Economic Perspectives*, *17*(3), 93–118. doi:10.1257/089533003769204371

Di Marzo, V., & Matias, I. (2005). Endocannabinoid control of food intake and energy balance. *Nature Neuroscience*, *8*(5), 585–589. doi:10.1038/nn1457

Dibner, C., & Schibler, U. (2015). Circadian timing of metabolism in animal models and humans. *Journal of Internal Medicine*, *277*(5), 513–527. doi:10.1111/joim.12347

DiFeliceantonio, A. G., Coppin, G., Rigoux, L., Edwin Thanarajah, S., Dagher, A., Tittgemeyer, M., & Small, D. M. (2018). Supra-Additive Effects of Combining Fat and Carbohydrate on Food Reward. *Cell Metabolism*, *28*(1), 33–44.e3. doi:10.1016/j.cmet.2018.05.018

Dodd, G. T., Michael, N. J., Lee-Young, R. S., Mangiafico, S. P., Pryor, J. T., Munder, A. C., … Tiganis, T. (2018). Insulin regulates POMC neuronal plasticity to control glucose metabolism. *eLife*, *7*. doi:10.7554/eLife.38704

Eckel-Mahan, K. L., Patel, V. R., Mohney, R. P., Vignola, K. S., Baldi, P., & Sassone-Corsi, P. (2012). Coordination of the transcriptome and metabolome by the circadian clock. *Proceedings of the National Academy of Sciences of the United States of America*, *109*(14), 5541–5546. doi:10.1073/pnas.1118726109

Elks, C. E., den Hoed, M., Zhao, J. H., Sharp, S. J., Wareham, N. J., Loos, R. J. F., & Ong, K. K. (2012). Variability in the heritability of body mass index: a systematic review and meta-regression. *Frontiers in endocrinology*, *3*, 29. doi:10.3389/fendo.2012.00029

Enriori, P. J., Evans, A. E., Sinnayah, P., Jobst, E. E., Tonelli-Lemos, L., Billes, S. K., … Cowley, M. A. (2007). Diet-induced obesity causes severe but reversible leptin resistance in arcuate melanocortin neurons. *Cell Metabolism*, *5*(3), 181–194. doi:10.1016/j.cmet.2007.02.004

Finicle, B. T., Ramirez, M. U., Liu, G., Selwan, E. M., McCracken, A. N., Yu, J., … Edinger, A. L. (2018). Sphingolipids inhibit endosomal recycling of nutrient transporters by inactivating ARF6. *Journal of Cell Science*, *131*(12). doi:10.1242/jcs.213314

Flak, J. N., & Myers, M. G. (2016). Minireview: CNS mechanisms of leptin action. *Molecular Endocrinology*, *30*(1), 3–12. doi:10.1210/me.2015-1232

Friedman, J. M. (2004). Modern science versus the stigma of obesity. *Nature Medicine*, *10*(6), 563–569. doi:10.1038/nm0604-563

Gardner, C. D., Trepanowski, J. F., Del Gobbo, L. C., Hauser, M. E., Rigdon, J., Ioannidis, J. P. A., … King, A. C. (2018). Effect of Low-Fat vs Low-Carbohydrate Diet on 12-Month Weight Loss in Overweight Adults and the Association With Genotype Pattern or Insulin Secretion: The DIETFITS Randomized Clinical Trial. *The Journal of the American Medical Association*, *319*(7), 667–679. doi:10.1001/jama.2018.0245

González-Muniesa, P., Mártinez-González, M.-A., Hu, F. B., Després, J.-P., Matsuzawa, Y., Loos, R. J. F., … Martinez, J. A. (2017). Obesity. *Nature reviews. Disease primers*, *3*, 17034. doi:10.1038/nrdp.2017.34

Grundlingh, J., Dargan, P. I., El-Zanfaly, M., & Wood, D. M. (2011). 2,4-dinitrophenol (DNP): a weight loss agent with significant acute toxicity and risk of death. *Journal of Medical Toxicology*, *7*(3), 205–212. doi:10.1007/s13181-011-0162-6

Guenther, G. G., Peralta, E. R., Rosales, K. R., Wong, S. Y., Siskind, L. J., & Edinger, A. L. (2008). Ceramide starves cells to death by downregulating nutrient transporter proteins. *Proceedings of the National Academy of Sciences of the United States of America*, *105*(45), 17402–17407. doi:10.1073/pnas.0802781105

Guh, D. P., Zhang, W., Bansback, N., Amarsi, Z., Birmingham, C. L., & Anis, A. H. (2009). The incidence of co-morbidities related to obesity and overweight: a systematic review and meta-analysis. *BMC Public Health*, *9*, 88. doi:10.1186/1471-2458-9-88

Halaas, J. L., Boozer, C., Blair-West, J., Fidahusein, N., Denton, D. A., & Friedman, J. M. (1997). Physiological response to long-term peripheral and central leptin infusion in lean and obese mice. *Proceedings of the National Academy of Sciences of the United States of America*, *94*(16), 8878–8883. doi:10.1073/pnas.94.16.8878

Halaas, J. L., Gajiwala, K. S., Maffei, M., Cohen, S. L., Chait, B. T., Rabinowitz, D., … Friedman, J. M. (1995). Weight-reducing effects of the plasma protein encoded by the obese gene. *Science*, *269*(5223), 543–546. doi:10.1126/science.7624777

Hales, C. M., Carroll, M. D., Fryar, C. D., & Ogden, C. L. (2017). Prevalence of obesity among adults and youth: United States, 2015–2016. *NCHS data brief, no 288. Hyattsville, MD: National Center for Health Statistics. 2017.*

Hall, K. D. (2018). Did the food environment cause the obesity epidemic? *Obesity*, *26*(1), 11–13. doi:10.1002/oby.22073

Hall, K. D., Ayuketah, A., Brychta, R., Cai, H., Cassimatis, T., Chen, K. Y., … Zhou, M. (2019). Ultra-Processed Diets Cause Excess Calorie Intake and Weight Gain: An Inpatient Randomized Controlled Trial of Ad Libitum Food Intake. *Cell Metabolism*, *30*(1), 67–77.e3. doi:10.1016/j.cmet.2019.05.008

Hammerschmidt, P., Ostkotte, D., Nolte, H., Gerl, M. J., Jais, A., Brunner, H. L., … Brüning, J. C. (2019). CerS6-Derived Sphingolipids Interact with Mff and Promote Mitochondrial Fragmentation in Obesity. *Cell*, *177*(6), 1536–1552.e23. doi:10.1016/j.cell.2019.05.008

Hatori, M., Vollmers, C., Zarrinpar, A., DiTacchio, L., Bushong, E. A., Gill, S., … Panda, S. (2012). Time-restricted feeding without reducing caloric intake prevents metabolic diseases in mice fed a high-fat diet. *Cell Metabolism*, *15*(6), 848–860. doi:10.1016/j.cmet.2012.04.019

Hawkes, C., Smith, T. G., Jewell, J., Wardle, J., Hammond, R. A., Friel, S., … Kain, J. (2015). Smart food policies for obesity prevention. *The Lancet*, *385*(9985), 2410–2421. doi:10.1016/S0140-6736(14)61745-1

Heisler, L. K., Cowley, M. A., Tecott, L. H., Fan, W., Low, M. J., Smart, J. L., … Elmquist, J. K. (2002). Activation of central melanocortin pathways by fenfluramine. *Science*, *297*(5581), 609–611. doi:10.1126/science.1072327

Holland, W. L., Brozinick, J. T., Wang, L.-P., Hawkins, E. D., Sargent, K. M., Liu, Y., … Summers, S. A. (2007). Inhibition of ceramide synthesis ameliorates glucocorticoid-, saturated-fat-, and obesity-induced insulin resistance. *Cell Metabolism*, *5*(3), 167–179. doi:10.1016/j.cmet.2007.01.002

Hummel, K. P., Coleman, D. L., & Lane, P. W. (1972). The influence of genetic background on expression of mutations at the diabetes locus in the mouse. I. C57BL-KsJ and C57BL-6J strains. *Biochemical Genetics*, *7*(1), 1–13. doi:10.1007/BF00487005

Ingalls, A. M., Dickie, M. M., & Snell, G. D. (1950). Obese, a new mutation in the house mouse. *The Journal of Heredity*, *41*(12), 317–318. doi:10.1093/oxfordjournals.jhered.a106073

Jheng, H.-F., Tsai, P.-J., Guo, S.-M., Kuo, L.-H., Chang, C.-S., Su, I.-J., … Tsai, Y.-S. (2012). Mitochondrial fission contributes to mitochondrial dysfunction and insulin resistance in skeletal muscle. *Molecular and Cellular Biology*, *32*(2), 309–319. doi:10.1128/MCB.05603-11

Joshi, S., Ostfeld, R. J., & McMacken, M. (2019). The Ketogenic Diet for Obesity and Diabetes-Enthusiasm Outpaces Evidence. *JAMA internal medicine*. doi:10.1001/jamainternmed.2019.2633

Karasu, S. R. (2016). The obesities: an overview of convergent and divergent paradigms. *American journal of lifestyle medicine*, *10*(2), 84–96. doi:10.1177/1559827614537773

Kennedy, A. R., Pissios, P., Otu, H., Roberson, R., Xue, B., Asakura, K., … Maratos-Flier, E. (2007). A high-fat, ketogenic diet induces a unique metabolic state in mice. *American Journal of Physiology. Endocrinology and Metabolism*, *292*(6), E1724–39. doi:10.1152/ajpendo.00717.2006

Kenny, P. J. (2011). Reward mechanisms in obesity: new insights and future directions. *Neuron*, *69*(4), 664–679. doi:10.1016/j.neuron.2011.02.016

Khera, R., Murad, M. H., Chandar, A. K., Dulai, P. S., Wang, Z., Prokop, L. J., … Singh, S. (2016). Association of Pharmacological Treatments for Obesity With Weight Loss and Adverse Events: A Systematic Review and Meta-analysis. *The Journal of the American Medical Association*, *315*(22), 2424–2434. doi:10.1001/jama.2016.7602

Kim, D. D., & Basu, A. (2016). Estimating the Medical Care Costs of Obesity in the United States: Systematic Review, Meta-Analysis, and Empirical Analysis. *Value in Health*, *19*(5), 602–613. doi:10.1016/j.jval.2016.02.008

Kim, S. M., Roy, S. G., Chen, B., Nguyen, T. M., McMonigle, R. J., McCracken, A. N., … Edinger, A. L. (2016). Targeting cancer metabolism by simultaneously disrupting parallel nutrient access pathways. *The Journal of Clinical Investigation*, *126*(11), 4088–4102. doi:10.1172/JCI87148

Kleinridders, A., Schenten, D., Könner, A. C., Belgardt, B. F., Mauer, J., Okamura, T., … Brüning, J. C. (2009). MyD88 signaling in the CNS is required for development of fatty acid-induced leptin resistance and diet-induced obesity. *Cell Metabolism*, *10*(4), 249–259. doi:10.1016/j.cmet.2009.08.013

Könner, A. C., & Brüning, J. C. (2012). Selective insulin and leptin resistance in metabolic disorders. *Cell Metabolism*, *16*(2), 144–152. doi:10.1016/j.cmet.2012.07.004

Kubiniok, P., Finicle, B. T., Piffaretti, F., McCracken, A. N., Perryman, M., Hanessian, S., … Thibault, P. (2019). Dynamic Phosphoproteomics Uncovers Signaling Pathways Modulated by Anti-oncogenic Sphingolipid Analogs. *Molecular & Cellular Proteomics*, *18*(3), 408–422. doi:10.1074/mcp.RA118.001053

Lee, J., Liu, J., Feng, X., Salazar Hernández, M. A., Mucka, P., Ibi, D., … Ozcan, U. (2016). Withaferin A is a leptin sensitizer with strong antidiabetic properties in mice. *Nature Medicine*, *22*(9), 1023–1032. doi:10.1038/nm.4145

Leigh, S.-J., & Morris, M. J. (2018). The role of reward circuitry and food addiction in the obesity epidemic: An update. *Biological Psychology*, *131*, 31–42. doi:10.1016/j.biopsycho.2016.12.013

Liesa, M., & Shirihai, O. S. (2013). Mitochondrial dynamics in the regulation of nutrient utilization and energy expenditure. *Cell Metabolism*, *17*(4), 491–506. doi:10.1016/j.cmet.2013.03.002

Lin, S., Thomas, T. C., Storlien, L. H., & Huang, X. F. (2000). Development of high fat diet-induced obesity and leptin resistance in C57Bl/6J mice. *International Journal of Obesity and Related Metabolic Disorders*, *24*(5), 639–646. doi:10.1038/sj.ijo.0801209

Liu, J., Lee, J., Salazar Hernandez, M. A., Mazitschek, R., & Ozcan, U. (2015). Treatment of obesity with celastrol. *Cell*, *161*(5), 999–1011. doi:10.1016/j.cell.2015.05.011

Liu, Q., Shi, J., Duan, P., Liu, B., Li, T., Wang, C., … Lu, Z. (2018). Is shift work associated with a higher risk of overweight or obesity? A systematic review of observational studies with meta-analysis. *International Journal of Epidemiology*, *47*(6), 1956–1971. doi:10.1093/ije/dyy079

Lobstein, T., Jackson-Leach, R., Moodie, M. L., Hall, K. D., Gortmaker, S. L., Swinburn, B. A., … McPherson, K. (2015). Child and adolescent obesity: part of a bigger picture. *The Lancet*, *385*(9986), 2510–2520. doi:10.1016/S0140-6736(14)61746-3

Locke, A. E., Kahali, B., Berndt, S. I., Justice, A. E., Pers, T. H., Day, F. R., … Yang, J. (2015). Genetic studies of body mass index yield new insights for obesity biology. *Nature*, *518*(7538), 197–206. doi:10.1038/nature14177

Maclean, P. S., Bergouignan, A., Cornier, M.-A., & Jackman, M. R. (2011). Biology's response to dieting: the impetus for weight regain. *American Journal of Physiology. Regulatory, Integrative and Comparative Physiology*, *301*(3), R581–600. doi:10.1152/ajpregu.00755.2010

Martin, C. R., Osadchiy, V., Kalani, A., & Mayer, E. A. (2018). The Brain-Gut-Microbiome Axis. *Cellular and molecular gastroenterology and hepatology*, *6*(2), 133–148. doi:10.1016/j.jcmgh.2018.04.003

Montgomery, M. K., Hallahan, N. L., Brown, S. H., Liu, M., Mitchell, T. W., Cooney, G. J., & Turner, N. (2013). Mouse strain-dependent variation in obesity and glucose homeostasis in response to high-fat feeding. *Diabetologia*, *56*(5), 1129–1139. doi:10.1007/s00125-013-2846-8

Myers, M. G., Leibel, R. L., Seeley, R. J., & Schwartz, M. W. (2010). Obesity and leptin resistance: distinguishing cause from effect. *Trends in Endocrinology and Metabolism*, *21*(11), 643–651. doi:10.1016/j.tem.2010.08.002

Newman, J. C., & Verdin, E. (2014). Ketone bodies as signaling metabolites. *Trends in Endocrinology and Metabolism*, *25*(1), 42–52. doi:10.1016/j.tem.2013.09.002

Obici, S., Feng, Z., Karkanias, G., Baskin, D. G., & Rossetti, L. (2002). Decreasing hypothalamic insulin receptors causes hyperphagia and insulin resistance in rats. *Nature Neuroscience*, *5*(6), 566–572. doi:10.1038/nn0602-861

Ochner, C. N., Barrios, D. M., Lee, C. D., & Pi-Sunyer, F. X. (2013). Biological mechanisms that promote weight regain following weight loss in obese humans. *Physiology & Behavior*, *120*, 106–113. doi:10.1016/j.physbeh.2013.07.009

Ochner, C. N., Tsai, A. G., Kushner, R. F., & Wadden, T. A. (2015). Treating obesity seriously: when recommendations for lifestyle change confront biological adaptations. *The lancet. Diabetes & endocrinology*, *3*(4), 232–234. doi:10.1016/S2213-8587(15)00009-1

Ozcan, L., Ergin, A. S., Lu, A., Chung, J., Sarkar, S., Nie, D., … Ozcan, U. (2009). Endoplasmic reticulum stress plays a central role in development of leptin resistance. *Cell Metabolism*, *9*(1), 35–51. doi:10.1016/j.cmet.2008.12.004

Ozcan, U., Cao, Q., Yilmaz, E., Lee, A.-H., Iwakoshi, N. N., Ozdelen, E., … Hotamisligil, G. S. (2004). Endoplasmic reticulum stress links obesity, insulin action, and type 2 diabetes. *Science*, *306*(5695), 457–461. doi:10.1126/science.1103160

Pan, W. W., & Myers, M. G. (2018). Leptin and the maintenance of elevated body weight. *Nature Reviews. Neuroscience*, *19*(2), 95–105. doi:10.1038/nrn.2017.168

Paoli, A., Rubini, A., Volek, J. S., & Grimaldi, K. A. (2013). Beyond weight loss: a review of the therapeutic uses of very-low-carbohydrate (ketogenic) diets. *European Journal of Clinical Nutrition*, *67*(8), 789–796. doi:10.1038/ejcn.2013.116

Pereira, M. J., & Eriksson, J. W. (2019). Emerging Role of SGLT-2 Inhibitors for the Treatment of Obesity. *Drugs*, *79*(3), 219–230. doi:10.1007/s40265-019-1057-0

Petersen, M. C., & Shulman, G. I. (2018). Mechanisms of insulin action and insulin resistance. *Physiological Reviews*, *98*(4), 2133–2223. doi:10.1152/physrev.00063.2017

Poti, J. M., Braga, B., & Qin, B. (2017). Ultra-processed Food Intake and Obesity: What Really Matters for Health-Processing or Nutrient Content? *Current obesity reports*, *6*(4), 420–431. doi:10.1007/s13679-017-0285-4

Rahavi, E. B., Altman, J. M., & Stoody, E. E. (2019). Dietary guidelines for americans, 2015–2020: national nutrition guidelines. In J. M. Rippe (ed.), *Lifestyle Medicine* (pp. 101–110). Third edition. | Boca Raton : Taylor & Francis, 2019.: CRC Press. doi:10.1201/9781315201108-7

Reinke, H., & Asher, G. (2016). Circadian clock control of liver metabolic functions. *Gastroenterology*, *150*(3), 574–580. doi:10.1053/j.gastro.2015.11.043

Roberto, C. A., Swinburn, B., Hawkes, C., Huang, T. T.-K., Costa, S. A., Ashe, M., … Brownell, K. D. (2015). Patchy progress on obesity prevention: emerging examples, entrenched barriers, and new thinking. *The Lancet*, *385*(9985), 2400–2409. doi:10.1016/S0140-6736(14)61744-X

Rodgers, R. J., Tschöp, M. H., & Wilding, J. P. H. (2012). Anti-obesity drugs: past, present and future. *Disease Models & Mechanisms*, *5*(5), 621–626. doi:10.1242/dmm.009621

Roenneberg, T., & Merrow, M. (2016). The circadian clock and human health. *Current Biology*, *26*(10), R432–43. doi:10.1016/j.cub.2016.04.011

Romero Rosales, K., Singh, G., Wu, K., Chen, J., Janes, M. R., Lilly, M. B., … Edinger, A. L. (2011). Sphingolipid-based drugs selectively kill cancer cells by down-regulating nutrient transporter proteins. *The Biochemical Journal*, *439*(2), 299–311. doi:10.1042/BJ20110853

Sacks, F. M., Bray, G. A., Carey, V. J., Smith, S. R., Ryan, D. H., Anton, S. D., … Williamson, D. A. (2009). Comparison of weight-loss diets with different compositions of fat, protein, and carbohydrates. *The New England Journal of Medicine*, *360*(9), 859–873. doi:10.1056/NEJMoa0804748

Sam, A. H., Salem, V., & Ghatei, M. A. (2011). Rimonabant: from RIO to ban. *Journal of obesity*, *2011*, 432607. doi:10.1155/2011/432607

Samuel, V. T., & Shulman, G. I. (2012). Mechanisms for insulin resistance: common threads and missing links. *Cell*, *148*(5), 852–871. doi:10.1016/j.cell.2012.02.017

Santoro, A., Campolo, M., Liu, C., Sesaki, H., Meli, R., Liu, Z.-W., … Diano, S. (2017). DRP1 suppresses leptin and glucose sensing of POMC neurons. *Cell Metabolism*, *25*(3), 647–660. doi:10.1016/j.cmet.2017.01.003

Schneeberger, M., Dietrich, M. O., Sebastián, D., Imbernón, M., Castaño, C., Garcia, A., … Claret, M. (2013). Mitofusin 2 in POMC neurons connects ER stress with leptin resistance and energy imbalance. *Cell*, *155*(1), 172–187. doi:10.1016/j.cell.2013.09.003

Sellayah, D., Cagampang, F. R., & Cox, R. D. (2014). On the evolutionary origins of obesity: a new hypothesis. *Endocrinology*, *155*(5), 1573–1588. doi:10.1210/en.2013-2103

Shungin, D., Winkler, T. W., Croteau-Chonka, D. C., Ferreira, T., Locke, A. E., Mägi, R., … Justice, A. E. (2015). New genetic loci link adipose and insulin biology to body fat distribution. *Nature*, *518*(7538), 187–196. doi:10.1038/nature14132

Srivastava, G., & Apovian, C. M. (2018). Current pharmacotherapy for obesity. *Nature Reviews. Endocrinology*, *14*(1), 12–24. doi:10.1038/nrendo.2017.122

Tartaglia, L. A., Dembski, M., Weng, X., Deng, N., Culpepper, J., Devos, R., … Tepper, R. I. (1995). Identification and expression cloning of a leptin receptor, OB-R. *Cell*, *83*(7), 1263–1271. doi:10.1016/0092-8674(95)90151-5

Tubbs, E., Theurey, P., Vial, G., Bendridi, N., Bravard, A., Chauvin, M.-A., … Rieusset, J. (2014). Mitochondria-associated endoplasmic reticulum membrane (MAM) integrity is required for insulin signaling and is implicated in hepatic insulin resistance. *Diabetes*, *63*(10), 3279–3294. doi:10.2337/db13-1751

Turpin, S. M., Nicholls, H. T., Willmes, D. M., Mourier, A., Brodesser, S., Wunderlich, C. M., … Brüning, J. C. (2014). Obesity-induced CerS6-dependent C16:0 ceramide production

promotes weight gain and glucose intolerance. *Cell Metabolism*, *20*(4), 678–686. doi:10.1016/j.cmet.2014.08.002

Turpin-Nolan, S. M., Hammerschmidt, P., Chen, W., Jais, A., Timper, K., Awazawa, M., … Brüning, J. C. (2019). CerS1-Derived C18:0 Ceramide in Skeletal Muscle Promotes Obesity-Induced Insulin Resistance. *Cell reports*, *26*(1), 1–10.e7. doi:10.1016/j.celrep.2018.12.031

van der Klaauw, A. A., & Farooqi, I. S. (2015). The hunger genes: pathways to obesity. *Cell*, *161*(1), 119–132. doi:10.1016/j.cell.2015.03.008

Varela, L., & Horvath, T. L. (2012). Leptin and insulin pathways in POMC and AgRP neurons that modulate energy balance and glucose homeostasis. *EMBO Reports*, *13*(12), 1079–1086. doi:10.1038/embor.2012.174

Wang, C.-Y., & Liao, J. K. (2012). A mouse model of diet-induced obesity and insulin resistance. *Methods in Molecular Biology*, *821*, 421–433. doi:10.1007/978-1-61779-430-8_27

Wang, L., Ishihara, T., Ibayashi, Y., Tatsushima, K., Setoyama, D., Hanada, Y., … Nomura, M. (2015). Disruption of mitochondrial fission in the liver protects mice from diet-induced obesity and metabolic deterioration. *Diabetologia*, *58*(10), 2371–2380. doi:10.1007/s00125-015-3704-7

Weintraub, M., Sundaresan, P. R., Madan, M., Schuster, B., Balder, A., Lasagna, L., & Cox, C. (1992). Long-term weight control study. I (weeks 0 to 34). The enhancement of behavior modification, caloric restriction, and exercise by fenfluramine plus phentermine versus placebo. *Clinical Pharmacology and Therapeutics*, *51*(5), 586–594. doi:10.1038/clpt.1992.69

Welsch, C. A., Roth, L. W. A., Goetschy, J. F., & Movva, N. R. (2004). Genetic, biochemical, and transcriptional responses of Saccharomyces cerevisiae to the novel immunomodulator FTY720 largely mimic those of the natural sphingolipid phytosphingosine. *The Journal of Biological Chemistry*, *279*(35), 36720–36731. doi:10.1074/jbc.M406179200

Won, J. C., Jang, P.-G., Namkoong, C., Koh, E. H., Kim, S. K., Park, J.-Y., … Kim, M.-S. (2009). Central administration of an endoplasmic reticulum stress inducer inhibits the anorexigenic effects of leptin and insulin. *Obesity*, *17*(10), 1861–1865. doi:10.1038/oby.2009.194

World Health Organization. (2018, February 16). Obesity and overweight. Retrieved February 15, 2020, from https://www.who.int/en/news-room/fact-sheets/detail/obesity-and-overweight

Zhang, X., Zhang, G., Zhang, H., Karin, M., Bai, H., & Cai, D. (2008). Hypothalamic IKKbeta/NF-kappaB and ER stress link overnutrition to energy imbalance and obesity. *Cell*, *135*(1), 61–73. doi:10.1016/j.cell.2008.07.043

Zhang, Y., Proenca, R., Maffei, M., Barone, M., Leopold, L., & Friedman, J. M. (1994). Positional cloning of the mouse obese gene and its human homologue. *Nature*, *372*(6505), 425–432. doi:10.1038/372425a0

Zhao, S., Zhu, Y., Schultz, R. D., Li, N., He, Z., Zhang, Z., … Scherer, P. E. (2019). Partial leptin reduction as an insulin sensitization and weight loss strategy. *Cell Metabolism*, *30*(4), 706–719.e6. doi:10.1016/j.cmet.2019.08.005

# CHAPTER 2

## Synthetic sphingolipid SH-BC-893 corrects high fat diet-induced mitochondrial fragmentation, obesity, and metabolic dysfunction

Elizabeth Selwan[1*], Vaishali Jayashankar[1*], Sarah E. Hancock[3], Amandine Verlande[2], Bin Chen[4], Stephen Hanessian[4], Selma Masri[2], Nigel Turner[3], and Aimee L. Edinger[1,*]

[1]Department of Developmental and Cell Biology, University of California Irvine, Irvine, CA 92697, USA
[2]Department of Biological Chemistry, University of California Irvine, Irvine, CA 92697, USA
[3]School of Medical Sciences, University of New South Wales, Sydney, NSW, 2052, Australia
[4]Department of Chemistry, Université de Montréal, Montréal, Québec H3C 3J7, Canada

* These authors contributed equally

### 2.1 Abstract

Lifestyle changes have proven insufficient to curb the obesity epidemic; therapeutics that can safely promote weight loss are needed. Here we show that a drug-like sphingolipid, SH-BC-893 (893), restores normal body weight, reverses hepatic steatosis, and improves systemic glucose tolerance in obese mice consuming a high fat diet (HFD). Ceramide generation in HFD-fed mice leads to increased mitochondrial fission which contributes to metabolic dysfunction by producing leptin and insulin resistance. *In vitro*, 893 prevents palmitate-induced mitochondrial fragmentation downstream of ceramide generation by blocking recruitment of the

fission factor DRP1. *In vivo*, acute administration of 893 reverses mitochondrial fragmentation in the livers of mice with HFD-induced obesity. Intriguingly, 893 fails to produce weight loss in obese, leptin-deficient *ob/ob* mice where mitochondrial morphology is not disrupted. Together, these results suggest that 893 or related molecules could be used to treat obesity and other diseases associated with unbalanced mitochondrial fission.

## 2.2 Introduction

Obesity has emerged as a serious epidemic. According to the World Health Organization, an estimated 13% of the world's adult population was obese in 2016, a number that has nearly tripled since 1975. Even more alarming is the accelerating prevalence of obesity in children. Worldwide, over 340 million children aged 5-19 were overweight or obese in 2016; most of these children will eventually become obese adults. Because obesity and related comorbidities are leading causes of preventable and pre-mature death(Abdelaal, le Roux, & Docherty, 2017), these statistics reflect a staggering social and economic burden. While the drivers of the growing obesity epidemic are multi-factorial, over-consumption of calorie dense, high-fat foods clearly contributes (Swinburn et al., 2011). These hypercaloric diets synergize with environmental and genetic factors to create a chronic positive energy balance that leads to excessive adiposity. While dietary modification and increasing exercise are an integral part of any interventional program, lifestyle changes have proven insufficient to resolve obesity in most patients. The "eat less" and "move more" approach ignores the complex physiologic, psychological, and genetic factors that prevent some patients from maintaining a negative energy balance (Roberto et al., 2015). There is thus a critical unmet need for medical therapies that can complement lifestyle interventions and help individuals overcome barriers to successful long-term weight loss. Bariatric surgery is highly effective in many patients, but is also invasive and can be accompanied by serious complications (Nguyen & Varela, 2017). Pharmacotherapies are potential adjunct, or even primary, treatments, with most affecting food intake (Srivastava & Apovian, 2018). Our growing understanding of the circuits that control energy intake and expenditure, especially the hormonal cross-talk between peripheral tissues and complex neural circuitry, has identified a number of targets amenable to pharmacological

intervention. The discovery of the hormone leptin and subsequent dissection of its multifaceted effects on satiety and energy expenditure offers hope that obesity could be treated by modulating leptin signaling (Andreoli, Donato, Cakir, & Perello, 2019). Although pharmacological administration of leptin has dramatic effects in the rare patients with obesity driven by leptin deficiency, leptin itself has limited therapeutic potential. The majority of obese individuals are leptin resistant, a phenotype that has been traced to disruptions in the balance of mitochondrial fission and fusion (Galloway & Yoon, 2013; Schrepfer & Scorrano, 2016; Wai & Langer, 2016). While leptin sensitizing agents have yet to reach patients, many other signaling pathways regulating appetite and satiety have been targeted (Timper & Brüning, 2017). Currently, all FDA-approved weight-loss agents affect these peripheral and central regulators of food intake, with the exception of Orlistat which reduces fat absorption from the gut (Srivastava & Apovian, 2018). Unfortunately, existing treatments for obesity are only marginally effective and plagued by toxicities and side effects (Bessesen & Van Gaal, 2018; Srivastava & Apovian, 2018). This poorly stocked armamentarium and the expanding scope of the obesity epidemic provides a strong impetus to develop and test innovative therapeutic approaches.

Nutrient delivery to tissues in excess of their demand initiates the metabolic dysfunction that leads to obesity and its lethal sequelae. Limiting cellular access to circulating nutrients might provide resistance to, or even reverse, the negative consequences of organismal hyper-nutrition and offer many of the benefits of dietary restriction while maintaining satiety. Natural sphingolipids restrict access to nutrients by engaging evolutionarily-conserved signaling pathways that trigger the down-regulation of cell surface nutrient transporter proteins (Chung,

Mao, Heitman, Hannun, & Obeid, 2001; Skrzypek, Nagiec, Lester, & Dickson, 1998). The orally bio-available and water-soluble sphingolipid analog, SH-BC-893 (893, Figure 2.1a), activates these same signaling nodes, reducing the uptake of glucose, amino acids, and low density lipoprotein particles while also limiting nutrient generation via lysosomal catabolism (Garret G Guenther et al., 2008; Kim et al., 2016; Romero Rosales et al., 2011). 893 starves nutrient-addicted, constitutively anabolic cancer cells to death. However, the intermittent nutrient stress it produces with daily administration is well-tolerated by non-transformed cells, even rapidly proliferating cells in the bone marrow and intestinal crypts (Kim et al., 2016). Intriguingly, in addition to restricting prostate tumor growth, 893 appeared to reduce inguinal fat mass without an obvious loss of lean mass and did not produce hyperglycemia in mice fed standard chow. These findings suggested that 893 might have favorable effects on whole-body energy homeostasis. Here we establish that 893 reverses established obesity, corrects metabolic dysfunction, and prevents fragmentation of the mitochondrial network in mice maintained on a HFD.

## 2.3 Results

**893 restores normal body weight and adiposity in mice maintained on a HFD.** To evaluate 893 (Figure 2.1a) as an intervention protecting from over-nutrition, a cohort of mice with increased adiposity was generated. Six-week old male, C57BL/6J mice were fed a 45% kcal from fat rodent diet (HFD) for 45 days. A 45% HFD was selected to mimic obesogenic diets in humans, taking into account the relatively low fat content of a standard rodent diet and numerous studies demonstrating that chronic feeding of this diet is sufficient to increase adiposity and produce metabolic defects in male C57BL/6J mice (Speakman, 2019; N Turner et al., 2013). An age-matched cohort of control mice were maintained on a standard chow diet (10% kcal from fat) throughout the study. After 45 days, the average body weight of HFD-fed mice was approximately 130% that of chow-fed mice (Figure 2.1b and Figure S2.1a,b). Using quantitative nuclear magnetic resonance imaging, fat mass represented 21% of the body weight of mice that had consumed the HFD for 45 days and 12% of body weight in controls fed the standard diet; changes in lean body mass were of lesser magnitude (Figure S2.1c-f). At this point, HFD-fed mice were randomly assigned to receive vehicle (water), 60 mg/kg, or 120 mg/kg 893 by oral gavage. These doses of 893 are sufficient to inhibit tumor growth and reduce amino acid-dependent mTORC1 signaling without toxicity as assessed by blood chemistry, complete blood count, and liver and small intestine histology (Kim et al., 2016). Based on the plasma pharmacokinetics of orally administered 893 ($t_{max}$ = 4 h, $t_{1/2}$ = 10.6 h, Figure S2.1g), mice were treated Mondays, Wednesdays, and Fridays at ZT8.5, 3.5 hours prior to the onset of the dark cycle when mice become active (ZT12). While the vehicle-treated group continued to gain weight as expected, mice treated with 60 mg/kg or 120 mg/kg 893 exhibited dose-dependent weight loss despite continued consumption of the HFD (Figure

2.1b,c and Figure S2.1a). In the group receiving 120 mg/kg 893, the rate of weight loss slowed after 10 days. After 2 weeks (6 doses of 893), the body weight of mice eating the HFD and treated with 120 mg/kg 893 was no longer statistically different from that of mice continuously fed a standard chow diet (Figure 2.1b and Figure S2.1a); the 60 mg/kg group no longer gained weight, but did not match chow-fed controls. Despite continued treatment with the high dose of 893, weight loss plateaued once body weight matched that of standard diet controls (Figure 2.1b,c). The majority of the dose-dependent weight loss in 893-treated mice was due to a decline in fat mass with little change in lean mass indicating that overall body composition was improved (Figure 2.1d-g and Figure S2.1a, h, and i). Mice treated with 60 mg/kg 893 gained fat mass at a similar rate to mice fed a standard diet (Figure 2.1d) indicating that this dose was sufficient to prevent adiposity resulting from HFD feeding. As in our prior study (Kim et al., 2016), these doses of 893 were well-tolerated; toxicity was not observed over the course of treatment, and the behavior of 893-treated mice was overtly normal throughout the study. These results indicate that 893 restores normal adiposity and body weight in previously obese mice despite continuous feeding of a HFD.

Exercise can mitigate the negative effects of hyper-nutrition. When provided with a running wheel, mice will voluntarily run 2-10 km per night, slowing the body weight and fat gain that normally accompany HFD feeding and improving metabolic status (Bell, Spencer, & Sherriff, 1995). To benchmark the effects of 893 against voluntary exercise and to determine whether the beneficial effects of these interventions are additive, 16 male, C57BL/6J mice that had been fed a HFD for 7 weeks were individually housed, provided with running wheels, and randomly assigned to receive vehicle or 120 mg/kg 893 on the Monday/Wednesday/Friday

schedule. Rodent running activity declines under stress (Garland et al., 2011), and monitoring the duration and distance of voluntary wheel running also provides a holistic measure of overall mouse health. HFD-fed mice receiving vehicle ran an average daily distance of 2.8 ± 0.7 km over the course of the experiment, a value that was not significantly different from the 893-treated group (2.8 ± 1.2 km, Figure 2.1h,i). The average time spent on running wheels each day was also equivalent in vehicle- and 893-treated groups (Figure S2.1j,k). Exercise activity was generally well-matched between the groups on a given day (Figure 2.1h and Figure S2.1j) suggesting that day to day differences in activity were likely related to uncontrolled variations in the environment. As expected, voluntary exercise led to weight loss in vehicle-treated mice maintained on a HFD that leveled off after the first week of intervention (Figure 2.1j,k and Figure S2.1a). HFD-fed mice receiving vehicle and housed with a running wheel exhibited a similar body weight loss to 893-treated mice maintained in normal caging. Mice both provided with a running wheel and treated with 893 exhibited even greater weight loss than observed with either treatment alone. In keeping with published studies (Bell et al., 1995), wheel running reduced fat mass while maintaining lean mass in all groups (Figure 2.1l-o and Figure S2.1a, l, and m). Together, these results demonstrate that 893 reduces adiposity and body weight to an equivalent extent and additively with voluntary exercise and confirm that the effects of 893 on body weight are unrelated to morbidity or malaise.

**893 corrects metabolic defects associated with HFD feeding.** Chronic over-nutrition leads to toxic lipid accumulation (lipotoxicity) in muscle and liver (Shulman, 2014). Excessive hepatic lipid accumulation can lead to liver fibrosis and inflammation (non-alcoholic steatohepatitis) and cancer (Haas, Francque, & Staels, 2016). As expected, the livers of vehicle-treated mice

maintained on the HFD accumulated excess lipids (Figure 2.2a) (N Turner et al., 2013). Strikingly, treatment with 120 mg/kg 893 eliminated hepatic steatosis in HFD-fed mice. Unbiased lipidomic analysis revealed that the majority of the lipids that accumulated in the liver on the HFD were triacylglycerols (Figure 2.2b). Ceramides, particularly C16:0 ceramide in the liver and C18:0 ceramide in muscle, also increase with HFD feeding and contribute to the insulin resistance that accompanies diet-induced obesity (Holland et al., 2007; Montgomery et al., 2016; N Turner et al., 2013; Nigel Turner et al., 2018; Turpin et al., 2014; Turpin-Nolan et al., 2019). Consistent with published studies, trends towards elevated hepatic C16:0 ceramide and muscle C18:0 ceramide levels were observed in HFD-fed mice (Figure 2.2b and Figure S2.2a,b). Treating HFD-fed mice with 893 restored liver C16:0 ceramide to the level seen in chow-fed controls; a downward trend in C18:0 ceramide was also observed in quadriceps muscle. Thus, 893 prevented the accumulation of toxic lipid species in HFD-fed mice.

Insulin resistance is a hallmark of the metabolic syndrome and develops rapidly in male C57BL/6 mice fed a 45% HFD (N Turner et al., 2013). Both genetic and pharmacologic experiments indicate that elevated ceramide levels play a central role in the development of insulin resistance in diet-induced obesity (Chaurasia et al., 2019; Holland et al., 2007; Montgomery et al., 2016; N Turner et al., 2013; Nigel Turner et al., 2018; Turpin et al., 2014; Turpin-Nolan et al., 2019). Ceramide disrupts insulin-dependent signaling in part by reducing AKT phosphorylation and thus GLUT4 translocation to the plasma membrane leading to sustained elevations in plasma glucose (Chavez & Summers, 2012; Summers, Garza, Zhou, & Birnbaum, 1998). Although 893 shares ceramide's ability to activate protein phosphatase 2A (PP2A), 893 does not reduce AKT activity (Kim et al., 2016; Kubiniok et al., 2019). Indeed,

ceramide, but not 893, interfered with insulin-stimulated AKT activation in 3T3-L1 adipocytes (Figure 2.2c,d). Consistent with this result, the AKT inhibitor MK-2206, but not 893, impeded insulin-stimulated glucose uptake in adipocytes (Figure 2.2e); constitutive glucose uptake in fibroblasts was reduced by 893 as expected (Figure S2.2c) (G G Guenther et al., 2014; Kim et al., 2016). Normalization of ceramide levels in liver and possibly skeletal muscle (Figure 2.2b and Figure S2.2a,b) without AKT inhibition (Figure 2.2c-e) suggested that treatment with 893 might restore insulin sensitivity in mice maintained on a HFD. Vehicle-treated mice fed the 45% fat diet for 12 weeks exhibited fasting hyperglycemia as expected (Figure 2.2f). However, 25 days of treatment with 120 mg/kg 893 three days a week normalized both fasting glucose and glucose disposal in HFD-fed mice as demonstrated by an oral glucose tolerance test (OGTT) (Figure 2.2f-h and Figure S2.2d); the 60 mg/kg dose produced an intermediate effect. Consistent with the lack of effect on insulin-stimulated glucose uptake in adipocytes *in vitro* (Figure 2.2e), normal clearance of glucose was observed even when plasma 893 concentrations were at their peak (Figure S2.2e,f). In sum, 12 doses of 120 mg/kg 893 over 4 weeks was sufficient to correct the hepatic lipid accumulation, fasting hyperglycemia, and insulin resistance associated with HFD feeding in male, C57BL/6J mice.

**893 reduces food intake in lean and HFD-fed mice.** To examine the acute effects of 893 on whole body metabolism, indirect calorimetry was performed on mice naïve to treatment. Male C57BL/6J mice were maintained on the SD or HFD for 10-12 weeks and then treated with vehicle or 120 mg/kg 893 by gavage at ZT8.5. The effect of 893 on the respiratory exchange ratio (RER) was determined using metabolic cages that mimic the home cage environment. RER, the ratio between the amount of $CO_2$ produced and the $O_2$ consumed, reflects relative

whole-body fuel substrate utilization, with a value close to 0.7 indicating that fat is primarily being utilized and a value of 1.0 indicating that carbohydrates are the main fuel source. As expected, vehicle-treated mice exhibited diurnal fluctuations in substrate utilization, as indicated by the RER values, that were blunted in HFD-fed mice (Figure 2.3a,b). HFD-fed mice exhibited lower RER values during both light and dark cycles. Treatment with 893 reduced the RER in mice fed either the SD or the HFD (Figure 2.3c-f). Consistent with the pharmacokinetic properties of 893 (Figure S2.1g), RER returned to control values 24 h after 893 treatment (Figure 2.3c-f). Animals were similarly responsive to a second treatment with 893 given 48 h after the first. In contrast with the clear reduction in RER, energy expenditure calculated using the Weir formula was not significantly affected by 893 (Figure S2.3a,b). A trend towards reduced activity as measured by XY beam breaks (Figure S2.3c,d) may relate to decreased food seeking behavior (see below) given the equivalent use of running wheels by vehicle- and 893-treated mice (Figure 2.1h,i and Figure S2.1j,k). In summary, indirect calorimetry revealed that 893 reduces the RER without affecting activity or energy expenditure.

If 893-treated animals are losing weight but not expending more energy, fewer calories must be available to metabolically-active tissues. Continuous monitoring in metabolic caging revealed that 893 reduced food intake (Figure 2.4a-d). This trend was apparent in both mice fed the SD and in mice maintained on the HFD for 10-12 weeks although the effect was more pronounced in the HFD group. When these studies were repeated in mice maintained on the HFD for 22 weeks, suppression of food intake and body weight loss may have been increased (Figure 2.4e,f and Figure S2.4a). To determine whether the reduction in food consumption was sufficient to account for the suppression of RER by 893 (Figure 2.3c-f), a paired feeding study

was performed. Providing untreated, HFD-fed mice with only the reduced amount of food eaten by 893-treated mice between ZT12 and ZT24 resulted in an equivalent reduction in RER (Figure 2.4g). Thus, the reduced RER in 893-treated mice (Figure 2.3c-f) likely stems from reduced carbohydrate availability and increased utilization of fat stores rather than from primary changes in how dietary components are metabolized. Consistent with this model, normalizing food intake by gavaging chow-fed mice at ZT12 with a liquid diet containing the number of calories consumed from ZT12-ZT15 by lean, vehicle control mice eliminated the effects of 893 on the RER (Figure 2.3c,d and Figure S2.4b,c). When access to solid food was restored at ZT17, a trend towards reduced RER was again observed. When administered in the morning at ZT2 rather than in the afternoon at ZT8.5, 893 still appeared to decrease both food intake and RER although statistical significance was not achieved during the light period, most likely because 893 levels peaked when mice were inactive and food intake was low (Figure S2.4d-h). Taken together, data collected in metabolic cages suggest that 893 produces weight loss by limiting calorie intake.

Because adipokines play a central role in controlling feeding behavior (Funcke & Scherer, 2019; Pan & Myers, 2018), the observation that 893's effects on food intake might be proportional to body weight was intriguing (Figure 2.4e,f). Leptin is secreted by adipocytes in proportion to their triglyceride content, conveying signals to the CNS about peripheral energy stores (Pan & Myers, 2018). In HFD-fed mice, chronic increases in adiposity lead to elevations in circulating leptin with no accompanying decrease in food intake, a state that has been termed leptin-resistant (El-Haschimi, Pierroz, Hileman, Bjørbaek, & Flier, 2000). Several compounds have been described that restore sensitivity to leptin and decrease food intake in

HFD-fed mice (Lee et al., 2016; J. Liu, Lee, Salazar Hernandez, Mazitschek, & Ozcan, 2015). To explore the possibility that 893 also functioned as a leptin-sensitizing agent, food intake and body weight were measured in 18 week old lean, male C57BL/6J mice treated with a suboptimal dose of leptin intraperitoneally at ZT8.5 (Breslow et al., 1999; Levin, Nelson, Gurney, Vandlen, & de Sauvage, 1996; Mistry, Swick, & Romsos, 1997). Peripheral administration of 2 mg/kg leptin was not sufficient to decrease food intake or body weight in these mice (Figure 2.5a-d). Similar to feeding studies conducted in metabolic cages (Figure 2.4a,b,e and f), 893-treatment produced a trend towards reduced food intake and body weight in chow-fed mice singly-housed in standard caging (Figure 2.5a-d). Administering 2 mg/kg leptin along with 893 appeared to further reduce food intake and body weight. These results suggest that 893 may sensitize mice to the anorexigenic effects of leptin.

To more rigorously assess whether leptin mediated the effects of 893 on food intake and body weight, *ob/ob* mice that completely lack leptin were treated with 893 at ZT8.5. Hyperphagic, leptin-deficient *ob/ob* mice became obese on the standard chow diet provided by University Lab Animal Resources (16% kcal from fat) as expected and were used in experiments once they attained an equivalent body weight to C57BL/6J mice fed the HFD for 24 weeks (Figure 2.5e). Intriguingly, 893 decreased food intake in 893-treated *ob/ob* mice (Figure 2.5f,g). However, as 893-treated *ob/ob* mice still ate more than 893-treated, wild type, HFD-fed controls of equivalent body weight (Figure 2.5e,f), leptin is likely required for the full suppression of food intake by 893. While a single dose of 893 produced significant weight loss over the next 24 h in HFD-fed mice, 893 only prevented weight gain in *ob/ob* mice (Figure 2.5h and Figure S2.4a). Interestingly, upon repeated dosing with 893, *ob/ob* mice continued to gain

weight. While six doses of 120 mg/kg 893 given 3 days a week for 2 weeks reduced the body weight of HFD-fed mice by 10% (Figure 2.1b,c), 893-treated *ob/ob* mice exhibited a 5% weight gain over this period (Figure 2.5i,j). Body weight gain in 893-treated *ob/ob* mice paralleled that observed in *ob/ob* mice receiving vehicle despite a modest, cumulative decrease in food intake (Figure 2.5i-k). The failure of 893-treated *ob/ob* mice to lose weight despite consuming fewer calories (Figure 2.5g-k) is consistent with paired feeding studies showing that decreased food intake is insufficient to produce the weight loss seen upon leptin administration in *ob/ob* mice (Breslow et al., 1999; Levin et al., 1996). While there was a slight trend towards improvement, 893 also failed to correct fasting hyperglycemia or restore glucose tolerance in *ob/ob* mice (Figure 2.5l and Figure S2.4i) as it did in HFD-fed mice (Figure 2.2f-h and Figure S2.2d). In summary, the failure of 893 to fully suppress food intake, reduce body weight, or normalize glucose handing in *ob/ob* mice indicates that endogenous leptin is necessary for the full metabolic effects of 893.

**893 protects from HFD-induced mitochondrial fragmentation.** Chronic consumption of a HFD diet leads to disruptions in mitochondrial dynamics that favor fission over fusion.(Cunarro, Casado, Lugilde, & Tovar, 2018; Galloway & Yoon, 2013; Schrepfer & Scorrano, 2016; Wai & Langer, 2016) Through mechanisms that are incompletely defined, this imbalance in mitochondrial dynamics leads to both leptin and insulin resistance in multiple tissues (Filippi et al., 2017; Hammerschmidt et al., 2019; Jheng et al., 2012; Schneeberger et al., 2013; Sebastián et al., 2012; Smith et al., 2013; Wang et al., 2015). Ceramide accumulation is causally linked to this mitochondrial fragmentation (Hammerschmidt et al., 2019). 893 reduced hepatic levels of C16:0 ceramide (Figure 2.2b and Figure S2.2a), and a compound structurally

similar to 893, FTY720, inhibits CerS6, the ceramide synthase that produces the C16:0 ceramide that triggers mitochondrial fission (Hammerschmidt et al., 2019; Nigel Turner et al., 2018). This finding raised the possibility that 893 protects HFD-fed mice from obesity by reducing ceramide production and preserving normal mitochondrial morphology. This model was initially explored in murine embryonic fibroblasts (MEFs), a cell type with a highly tubular mitochondrial network that simplifies detection of increased mitochondrial fission. Palmitate supplementation, which increases C16:0 ceramide levels, produced dramatic mitochondrial fragmentation in MEFs (Figure 2.6a-d and Figures 2.5 and 6) (Hammerschmidt et al., 2019). As expected, blocking ceramide production with either the serine palmitoyl transferase inhibitor myriocin or the ceramide synthase inhibitor Fumonisin B1 prevented palmitate-induced morphological changes, maintaining mitochondrial tubule length (aspect ratio and branch length) and preventing the increase in mitochondrial roundness (Figure S2.7a-d). Similar to these ceramide synthesis inhibitors, 893 preserved a tubular, branched mitochondrial network in palmitate-treated cells (Figure 2.6a-d and Figure S2.6). In addition, 893 blocked the palmitate-induced recruitment of the GTPase that mediates fission, DRP1, to mitochondrial membranes without affecting DRP1 protein expression levels (Figure 2.6e-h). However, 893 did not reduce palmitate-induced ceramide production under these conditions (Figure 2.6i). Indeed, the effects of 893 on mitochondrial dynamics lie downstream of ceramide generation as 893 also blocked mitochondrial fragmentation in response to exogenous short or long chain ceramides (Figure 2.6j-m and Figure S2.7e-h). The previously described leptin sensitizer, celastrol,(J. Liu et al., 2015) did not maintain normal mitochondrial morphology in palmitate-supplemented cells (Figure S2.7i-l). In fact, celastrol fragmented the mitochondrial network similar to palmitate, reducing mitochondrial aspect ratio and branching and increasing

roundness, suggesting that 893 and celastrol work through distinct mechanisms. Intriguingly, 893 also reversed mitochondrial fragmentation induced by an oncogenic form of KRAS suggesting that it blocks mitochondrial fission in response to additional stimuli (Figure 2.6n-q). Together, these findings raise the possibility that 893 protects mice from HFD-induced obesity by preventing the mitochondrial fragmentation that occurs downstream of increased ceramide accumulation.

To evaluate whether 893 also affects mitochondrial morphology in mice maintained on a HFD, mitochondria were visualized in intact, freshly-resected livers using NADH autofluorescence and confocal microscopy. When evaluating mitochondrial morphology, light microscopy has two, significant advantages over electron microscopy: 1) the 3D architecture of the mitochondrial network is readily apparent, and 2) quantitative measurements of mitochondrial shape can be made in a large number of cells in an unbiased manner using image analysis software (Figure S2.8). In addition, evaluating mitochondrial morphology in the intact, viable organ avoids artifacts introduced by tissue processing or lengthy cell isolation procedures. Because the morphology of hepatocyte mitochondria varies over the circadian cycle (Jacobi et al., 2015), vehicle- and 893-treated mice were sacrificed in pairs over a time period where 893 significantly reduced the RER and food intake in HFD-fed mice, between ZT12.5 and ZT17 (Figure 2.3e,f and Figure 2.4c,d). Consistent with published reports (Galloway, Lee, Brookes, & Yoon, 2014; Galloway et al., 2012; Hammerschmidt et al., 2019), mitochondria in the livers of mice chronically maintained on a HFD were larger and more spherical than those in the livers of mice fed standard chow (Figure 2.7a-c). Administration of 893 to naïve, HFD-fed mice at ZT8.5 caused a dramatic change in the morphology of hepatic mitochondria, increasing their

tubularity (increased aspect ratio) and reducing their roundness. 893 did not alter the morphology of hepatic mitochondria in mice consuming the matched standard chow. Thus, 893 reverses HFD-diet induced changes in mitochondrial morphology in the livers of male C57BL/6J mice offering a potential mechanism by which leptin and insulin sensitivity might be restored.

The failure of 893 to reduce body weight in leptin-deficient *ob/ob* mice (Figure 2.5h-j) offered an opportunity to test whether its anti-obesogenic effects are linked to mitochondrial dynamics. Mitochondrial morphology has not been extensively evaluated in *ob/ob* mice. A report that fission is increased in *ob/ob* livers was based on the finding that mitochondrial area was reduced in TEM sections (Theurey et al., 2016); however, area in electron micrographs does not provide a complete picture of 3D mitochondrial morphology. In fact, despite the expected presence of abundant lipid droplets, mitochondria in hepatocytes isolated from *ob/ob* mice are tubulated and grossly indistinguishable from wild type controls by light microscopy (Arruda et al., 2014). Consistent with this non-quantitative observation in cultured *ob/ob* hepatocytes and despite the fact that *ob/ob* mice were obese and exhibited grossly apparent hepatic steatosis, the mitochondria in freshly resected, viable livers collected from *ob/ob* mice between ZT12.5 and ZT17 were highly tubular (Figure 2.7b-d and Figure S2.9). In fact, hepatic mitochondria in *ob/ob* livers appeared more tubulated and less round than those present in the livers of wild type mice consuming standard rodent chow. These results reveal a previously unrecognized difference in mitochondrial morphology between obese *ob/ob* and wild type, HFD-fed mice that underscores the divergent pathophysiology of the metabolic disturbances in these models with leptin deficiency and leptin resistance, respectively. In summary, the failure of 893 to reduce

body weight in leptin-deficient *ob/ob* mice suggests that 893's metabolic effects stem from the reversal of unbalanced mitochondrial fission and are mediated in part by leptin.

## 2.4 Discussion

Here we show that an orally-bioavailable, synthetic sphingolipid, SH-BC-893, restores normal body weight, adiposity, and glucose tolerance and reverses hepatic steatosis in male, C57BL/6J mice maintained on a HFD (Figures 2.1-2.2). A significant reduction in food intake in 893-treated mice likely makes a major contribution to the restoration of energy homeostasis in treated animals (Figure 2.4). However, the observation that 893 reduces food intake in *ob/ob* mice without producing weight loss (Figure 2.5f-k) suggests that 893's anti-obesogenic effects extend beyond limiting calorie intake. The failure of 893 to fully normalize food intake, reduce body weight, or restore normal glucose handling in leptin-deficient *ob/ob* mice (Figure 2.5f-l) and a trend towards enhanced sensitivity to exogenous leptin (Figure 2.5a-d) suggest that a significant fraction of 893's anti-obesogenic effects are mediated by leptin. The ability of 893 to oppose mitochondrial fission (Figures 2.6 and 2.7) provides a potential mechanism for leptin sensitization (Figure 2.7e). Chronic consumption of a HFD enhances mitochondrial fission in the liver (Figure 2.7a-c), hypothalamic neurons, muscle, and white adipose tissue (Galloway et al., 2012; Hammerschmidt et al., 2019; Jheng et al., 2012; R. Liu et al., 2014; Schneeberger et al., 2013; Smith et al., 2013). Inhibiting mitochondrial fission by deleting DRP1 or over-expressing MFN2 in anorexigenic POMC neurons sensitizes to leptin (Santoro et al., 2017; Schneeberger et al., 2013). Conversely, promoting fission by knocking out the mitochondrial fusion protein MFN2 in POMC neurons produces leptin resistance (Schneeberger et al., 2013). Fragmentation of the mitochondrial network also contributes to insulin resistance. Limiting

mitochondrial fission via dominant-negative DRP1 expression, deletion of DRP1, or treatment with the small molecule DRP1 inhibitor Mdivi1 increases insulin sensitivity in liver and skeletal muscle and limits HFD-induced obesity and hepatic steatosis (Galloway et al., 2014; Jheng et al., 2012; Smith et al., 2013; Wang et al., 2015). On the other hand, promoting mitochondrial fission in liver or muscle by reducing expression of the fusion protein MFN2 produces insulin resistance (R. Liu et al., 2014; Sebastián et al., 2012). Importantly, increased mitochondrial fission is also associated with increased adiposity and metabolic dysfunction in humans. Patients homozygous for a missense mutation in *MFN2* have fragmented, spherical adipocyte mitochondria and a dramatic upper body adipose tissue over-growth syndrome (Rocha et al., 2017). Large, round mitochondria have also been observed in pancreatic β cells of patients with type 2 diabetes (Anello et al., 2005). In sum, a large body of evidence collected in both mouse models and in humans indicates that enhanced mitochondrial fission contributes to obesity and its metabolic sequelae, providing a likely mechanism for the anti-obesogenic actions of 893.

While initially surprising, the observation that 893 reduces food intake, but not body weight, in leptin-deficient *ob/ob* mice (Figure 2.5f-k) is consistent with published paired feeding studies (Breslow et al., 1999; Levin et al., 1996), and the proposal that 893's metabolic effects stem from the suppression of mitochondrial fission (Figure 2.7e). As discussed above, mitochondrial fission is enhanced in mice with HFD-induced obesity. However, hepatic mitochondria in obese *ob/ob* mice fed a standard chow diet are tubulated, not large and round as they are in HFD-fed mice (Figure 2.7a-d and Figure S2.9). These results in freshly resected livers are consistent with published images of isolated *ob/ob* hepatocytes which possess a normal mitochondrial

network (Arruda et al., 2014). The lack of leptin in *ob/ob* mice creates a starvation-like state;(Garthwaite, Martinson, Tseng, Hagen, & Menahan, 1980) starvation promotes mitochondrial fusion (Schrepfer & Scorrano, 2016; Wai & Langer, 2016). Regardless of the pathophysiology underlying this phenotypic difference, tubular mitochondrial morphology in *ob/ob* mice (Figure 2.7b-d and Figure S2.9) indicates that all forms of obesity are not rooted in altered mitochondrial dynamics and suggests that 893 will be most effective in those with this etiology. Importantly, even though mitochondria were not fragmented in the *ob/ob* model or in wild type mice eating a SD (Figure 2.7a-d and Figure S2.9), 893's ability to oppose mitochondrial fission could still explain the reduction in food intake in treated animals (Figures 2.4a,b and 5f,g, and k). Blocking mitochondrial fission in the POMC neurons of chow-fed mice reduces food intake even though mitochondrial dynamics and leptin signaling are not basally perturbed (Santoro et al., 2017). Inhibiting mitochondrial fission sensitizes anorexigenic POMC neurons to more than just leptin. Excitation by glucose is also increased, stimulating α-MSH secretion (Parton et al., 2007); α-MSH also mediates the anorexic effects of leptin. *Ob/ob* mice are robustly hyperglycemic (Figure 2.5l and Figure S2.4i) (Levin et al., 1996; Van den Bergh et al., 2008). Thus, 893 may trigger POMC neuron activation in these leptin-deficient mice by increasing glucose sensitivity. As consuming a HFD interferes with glucose-induced α-MSH release from POMC neurons (Parton et al., 2007), increased sensitivity to elevated circulating glucose levels (Figure 2.2f-h) may also contribute to the reduction in food intake in HFD-fed animals (Figure 2.4c-e). A non-mutually exclusive hypothesis is that 893 reduces food intake in *ob/ob* mice by increasing sensitivity to insulin. In wild type mice, intracerebroventricular insulin administration reduces food intake through an α-MSH-dependent pathway (Benoit et al., 2002; Varela & Horvath, 2012). *Ob/ob* mice are hyperinsulinemic (Garthwaite et al., 1980; Levin et

al., 1996; Van den Bergh et al., 2008), and blocking mitochondrial fission sensitizes to insulin (Jheng et al., 2012; Smith et al., 2013; Wang et al., 2015). In sum, 893 may reduce food intake by sensitizing hypothalamic neurons to leptin, glucose, and/or insulin secondary to a block in mitochondrial fission.

Although 893 prevented DRP1 recruitment to mitochondria downstream of ceramide production (Figure 2.6a-m), additional experiments will be required to fully elucidate the molecular mechanism underlying its suppression of mitochondrial fission. DRP1 is regulated by phosphorylation (Wai & Langer, 2016). As 893 activates protein phosphatase 2A (PP2A) (Kim et al., 2016), it could alter DRP1 phosphorylation directly or indirectly. One caveat of proposing a PP2A-dependent mechanism to explain the block in DRP1 recruitment in 893-treated cells is that ceramide also activates PP2A (Ruvolo, 2016), but increases DRP1 recruitment (Hammerschmidt et al., 2019). As 893 and ceramide differentially affect AKT phosphorylation (Figure 2.2c,d), they may also have differential effects on DRP1 phosphorylation. However, the absence of mitochondrial fission or fusion factors from published 893- or ceramide-regulated phosphoproteomes(Kubiniok et al., 2019) suggests alternate modes of regulation may be involved. 893 may instead interfere with ceramide binding to MFF, a protein that anchors DRP1 to the outer mitochondrial membrane (Hammerschmidt et al., 2019). Given that mitochondrial-ER contact sites (mitochondrial associated membranes, MAMs) control both mitochondrial fission and leptin and insulin sensitivity (Theurey & Rieusset, 2017), 893 may modulate the number or composition of mitochondrial-ER contact sites. Defining 893's mechanism of action could reveal previously unrecognized actions of natural sphingolipids. 893 is closely related to and produces similar

phenotypes as the fungal sphingolipid phytosphingosine (Perryman et al., 2016). Intriguingly, dietary supplementation with phytosphingosine improves glucose metabolism in HFD-fed mice (Murakami et al., 2013) and in humans (Snel et al., 2010). Clearly, further study of 893 and natural sphingolipids in the context of mitochondrial dynamics is warranted.

893 was initially developed and tested as an anti-cancer agent (Chen et al., 2016; Kim et al., 2016). The present results may provide mechanistic insight into its ability to suppress tumor growth and progression. Mitochondrial fission is enhanced in many cancer cells; a fragmented mitochondrial network is hypothesized to contribute to the anaerobic glycolysis that promotes tumor growth (Lima et al., 2018; Senft & Ronai, 2016). In fact, a bias towards mitochondrial fission is essential for RAS-mediated tumorigenesis (Nagdas et al., 2019; Serasinghe et al., 2015). 893 is active against a range of cancer cells, including many with activating mutations in RAS (Kim et al., 2016). As 893 also produced dramatic mitochondrial hypertubulation in KRAS G12D knock-in MEFs (Figure 2.6n-q), suppression of mitochondrial fission may contribute to 893's anti-neoplastic activity in KRAS-mutant colorectal cancer xenografts (Kim et al., 2016). Other reports suggest that mitochondrial fission is favored in tumors because it promotes stemness and maintains tumor initiating cells (Katajisto et al., 2015; Xie et al., 2015), Interestingly, 893 not only slowed autochthonous prostate tumor growth, it also maintained tumors in a more differentiated state (Kim et al., 2016). Given that the energy dependent process of migration requires trafficking of mitochondria to the leading edge and mitochondrial transport depends on fission (Senft & Ronai, 2016), the present work suggests that 893 might additionally subvert cancer metastasis by blocking mitochondrial fission. Finally, as obesity itself promotes cancer (Park, Morley, Kim, Clegg, & Scherer, 2014), 893's ability to reduce

caloric intake and adiposity may enhance its anti-neoplastic effects. In summary, the systemic metabolic effects of 893 uncovered in the present study complement the previously described cell autonomous anti-cancer effects of 893.

Given that dietary and behavioral interventions have failed to slow the expansion of the obesity epidemic, effective medical therapies for obesity are a critical unmet need (Srivastava & Apovian, 2018). Historically, obesity therapies have been severely limited by low and/or transient efficacy and unacceptable toxicities. At least in male, C57BL/6J mice with HFD-induced obesity, 893 is robustly efficacious, rapidly restoring body weight and metabolic parameters to levels seen in controls eating a standard diet (Figs. 1 and 2). Whether 893 is equally effective in other obesity models and in female mice merits further study. Importantly, 893 is also well tolerated (Figure 2.1h,i and Figure S2.1j,k), even upon chronic administration at the elevated, anti-cancer dose (Kim et al., 2016). Although 893's low toxicity may at first seem surprising, it is important to take into account that plasma levels of 893 will rise and fall with alternate day dosing (Figure S2.1g). While 893's low micromolar potency might be improved, its favorable pharmacological properties (84% oral bioavailability, 10.6 h half-life) and robust efficacy with relatively infrequent dosing (Figure 2.1b,c) make 893 itself worthy of further pre-clinical evaluation. Combinations with complementary interventions such as physical exercise (Figure 2.1h-o), which up-regulates the mitochondrial fusion proteins MFN1 and MFN2 (Cartoni et al., 2005), should also be explored. Given that unbalanced mitochondrial fission is linked to the lethal sequelae of obesity such as non-alcoholic steatohepatitis, kidney failure, cardiomyopathy, and blood vessel damage, a compound with 893's mechanism of action could have a major, positive impact on human health.(Galloway & Yoon, 2013;

Schrepfer & Scorrano, 2016; Wai & Langer, 2016) In conclusion, the finding that a synthetic sphingolipid corrects defects resulting from the accumulation of endogenous ceramide by opposing mitochondrial fission opens multiple avenues for future study.

## 2.5 Acknowledgements

The authors would like to thank the following UCI colleagues for generously sharing equipment, reagents, and/or providing technical advice: Raquel Chamorro and Bruce Blumberg (EchoMRI), Carl Cottman (running wheels), Felix Grun (LC-MS/MS), Mei Kong (3T3-L1 cells), Wenqi Wang (DS-Fi3 color camera), Adela Syeed and Michelle Digman (in vivo imaging), and Maggie Goodson (indirect calorimetry). We would also like to thank Matheus Viana and Susanne Rafelski (Allen Institute for Cell Science, Seattle WA) for providing advice regarding quantification of mitochondrial networks. This project was supported by: a Proof of Product grant from Beall Applied Innovation to ALE; the National Center for Research Resources and the National Center for Advancing Translational Sciences, National Institutes of Health, through Grant UL1 TR001414; a National Health and Medical Research Council of Australia project grant (1126135) to NT; and by grants from the National Institutes of Health, the Concern Foundation for Cancer Research, and the V Foundation for Cancer Research to SM. ES was supported by the National Cancer Institute of the National Institutes of Health under award number T32CA009054 and by Graduate Assistance in Areas of National Need (GAANN) grant P200A120207; AV was supported by a Hitachi-Nomura postdoctoral fellowship. The authors also wish to acknowledge the support of the Chao Family Comprehensive Cancer Center Optical Biology Center and Experimental Tissue Resource shared resources, supported by the National Cancer Institute of the National Institutes of Health under award number P30CA062203. Subsidized access to the UNSW Bioanalytical Mass Spectrometry Facility is also gratefully acknowledged. The content is solely the responsibility of the authors and does not necessarily represent the official views of the National Institutes of Health.

## 2.6 Author Contributions

All authors contributed to the conception or design of the work and analysis of data. ES, VJ, SEH, and AV acquired the data. BC synthesized SH-BC-893. SM, SH, NT, and ALE supervised the research. ES, VJ, and ALE drafted the manuscript and all authors revised and approved the final version.

## 2.7 Competing Interest Statement

SH and ALE are founders of Siege Pharmaceuticals which is developing SH-BC-893 for use in cancer and other diseases. Other authors declare no competing interests.

## 2.8 Materials and methods

*General animal procedures*

All animal experiments were performed in accordance with the Institutional Animal Care and Use Committee of University of California, Irvine. Male mice were used in all experiments. C57BL/6J mice (stock no 000664) and *ob/ob* mice (stock no 000632) were purchased from the Jackson Laboratory and were acclimated for at least 7 d prior to beginning experiments. Mice were housed under a 12:12 h light-dark cycle at 20-22°C in groups of 4-5. Cages contained 1/8" corncob bedding (7092A, Envigo, Huntingdon, UK) enriched with ~6 g of cotton fiber nestlets (Ancare Corp., Bellmore,NY). Access to food and water was ad libitum unless otherwise specified. For HFD studies, 8 week old C57BL/6J males were randomly assigned to either a 45% kcal from fat diet (HFD; D12451, Research Diets Inc., New Brunswick, NJ) or 10% kcal from fat diet designed to match D12451 for other components (SD; D12450B, Research Diets Inc). Mice were maintained on these diets for up to 22 weeks as indicated. *Ob/ob* mice were fed the vivarium stock diet which contained 16% kcal from fat (2020x, Envigo). On rare occasions (3 times out of >500 gavage doses), animals required euthanasia due to gavage errors. One *ob/ob* mouse died during Echo MRI for unknown reasons. Inadvertent pharyngeal administration of gavage solution during removal of the feeding tube occurred in 4 cases but did not require euthanasia. In these instances, bubbles emerged from the animals' noses and excessive nose rubbing was observed immediately after dosing. Data from these animals were censored from analysis as indicated below for specific procedures. Polypropylene feeding tubes (20 g x 38 mm; Instech Laboratories Inc., Plymouth, PA) were utilized for gavage and dipped into a 1 g/ml sucrose solution immediately prior to treatment to induce salivation.

*Weight loss intervention study*

HFD-fed mice were randomly assigned to experimental groups receiving either vehicle (water) or 893 at 60 mg/kg or 120 mg/kg by oral gavage on Mondays, Wednesdays, and Fridays. Mice were maintained on the HFD throughout the study. The SD group was treated with vehicle on the same schedule. Group size was initially n=10; one animal from the 60 mg/kg group that was euthanized due to gavage error was excluded from the analysis making this group n=9. All treatments and measurements were performed between ZT8 and ZT10 unless otherwise noted. Body weight and food consumption were monitored Monday-Friday. Body composition was determined weekly in live animals using an EchoMRI™ Body Composition Analyzer (EchoMRI™ Corp., Singapore). Mice were euthanized and tissues collected 4 h after treatment. Where indicated, mice were fasted for 6 h (Figures 2.2f-h and 5l).

*Voluntary cage running*

To monitor voluntary exercise, sixteen mice were singly housed in home cages equipped with running wheels; initially n=8. A magnet was affixed to each 240 mm wheel and a bicycle odometer (Sigma BC509, Sigma Sports, Chicago) used to count the number of wheel revolutions and time spent on running on the wheels. Distance run was calculated by the equation (*#revolutions x running wheel circumference = distance)*. The wheels were cleaned and randomly re-assigned weekly to each cage to control for differences in wheel performance. Two animals in the 893-treated group were euthanized due to gavage errors and were excluded from the analysis resulting in n=6.

*Blood glucose measurements and oral glucose tolerance tests (OGTT)*

Mice were fasted for 6 h prior to blood glucose testing at ZT10. When 893 treatment was combined with an OGTT, mice were treated at ZT4. Once baseline fasting blood glucose was determined using a handheld blood glucose meter (Prodigy Diabetes Care, Charlotte, NC) and a drop of blood collected from a tail vein nick, mice were gavaged with an oral glucose solution (20% w/v in water, 2 g/kg bodyweight) and blood glucose measured in a drop of tail vein blood at 0, 15, 30, 60 and 120 min. The area under the curve was determined using Graphpad Prism software.

*Indirect calorimetry*

Metabolic parameters were measured using the Phenomaster system (TSE Systems Inc., Chesterfield, MO). The climate chamber was set to 21°C and 50% humidity with a 12:12 h light-dark cycle. Mice were singly housed inside the chamber and acclimated for 48 h prior to data collection. $VO_2$, $VCO_2$, and food intake was measured every 27 min. Respiratory exchange ratio (RER) was calculated using the formula RER = $VCO_2/VO_2$. Energy expenditure was calculated using the equation EE = $1.44(3.941 \times VO_2 + 1.106 \times VCO_2)$. In the indirect calorimetry studies in Figure 2.3 and Figure S2.3, C57BL/6J mice were maintained on the HFD or SD for 10-12 weeks prior to evaluation and were naïve to therapy. Mice were serially evaluated in cohorts of 4 vehicle- and 4 893-treated mice using 8 metabolic cages. Treatment was by gavage at ZT8.5, 893 was administered at 120 mg/kg in water. To evaluate the effect of morning treatment (Figure S2.4d-h), vehicle or 120 mg/kg 893 was administered at ZT2 to 18 week old C57BL/6J males on a standard diet. Liquid diet experiments (Figure S2.4b,c) were

also performed on 18 week old C57BL/6J males; mice were treated with 893 at ZT8.5 and food access was restricted at ZT11. Liquid feed (AIN-76, BioServ, Flemington, NJ) was prepared at 1000 kcal/L in milli-Q water and at ZT12, mice were gavaged with 400 µL (0.4kcal) of diet, corresponding to approximately 3 h of ad libitum consumption of standard chow. For the pair feeding study (Figure 2.4g), RER was monitored over 12 h in mice maintained on the HFD for 22 weeks (31 weeks of age); pair-fed mice were used after a 48 h wash-out period and provided with the average amount of food they ate over 24 h after 893 treatment (92.5 mg or 0.4 kcal).

Data was excluded from these analyses as follows. During measurements of one SD cohort (4 vehicle- and 4 893-treated mice), a leak in the reference $CO_2$ system was detected; the $O_2$ and $CO_2$ data was censored until the leak was corrected (70-74 h). Feeding and activity measurements were not compromised and were still analyzed. Occasionally, uneaten food was found on the floor of the cage precluding use of the hopper sensor to accurately monitor food intake. In these instances, food intake data was censored for the prior 24 h period (days 2 and 3 for mouse 8 (SD + 893) and mouse 8 (SD + vehicle), and day 3 for mouse 8 (HFD + 893) and mouse 1 (HFD + vehicle) in Figure 2.4a-e). A sensor malfunction due to the mouse dislodging the hopper also resulted in the exclusion of food intake data (mouse 5 (SD + vehicle) days 2-4, Figure 2.4a,b, and e). In rare cases, inadvertent pharyngeal administration of gavage material occurred. These mice were not euthanized, but food intake, calorimetry, and activity data from these animals was excluded from the analysis for 1 week after this event (mouse 2 (HFD + 893) after the second treatment on day 3 and mouse 5 (HFD + 893) after the first dose on day 1, Figure 2.3e,f and 4c-f).

*Home-cage feeding studies*

Mice were singly housed and allowed to acclimate for 72 h before food intake was monitored. Food consumption was determined by monitoring the weight of food in the hopper. Initial food and body weight measurements were taken at ZT9 and final measurements were taken 16 h later to capture the active period where most consumption occurred. Home cage feeding studies were performed with C57BL/6J mice maintained on a HFD for 24 weeks (33 weeks of age), or *ob/ob* mice at 8 wk of age. Mice received vehicle or 120 mg/kg 893 by gavage at ZT8.5. For experiments involving leptin, 18 week old, SD fed (16% kcal from fat, 2020x, Envigo) C57BL/6J mice received vehicle or 120 mg/kg 893 by gavage at ZT8.5. At ZT11.5, vehicle (20 mM Tris-Cl, pH 8.0) or 2 mg/kg recombinant mouse leptin (498-OB, R&D Systems, Minneapolis, MN) was delivered by intraperitoneal injection. The same 8 mice were used for all treatments following a 48 h washout period, and treatments were administered in the following order: vehicle, 893, leptin, and leptin + 893. All data collected from one mouse was excluded due to inadvertent pharyngeal administration during gavage reducing the n from 8 to 7 (Figure 2.5a-d). One *ob/ob* mouse that failed to gain weight on the chow diet (bodyweight >20% less than littermates) was excluded from all analyses. One *ob/ob* mouse died during Echo MRI for unknown reasons after 6 d of treatment with 893; data from this mouse was analyzed prior to death.

*Lipidomic profiling*

Lipids were extracted from liver and quadriceps tissue using a modified MTBE method (Abbott et al., 2013; Matyash, Liebisch, Kurzchalia, Shevchenko, & Schwudke, 2008). Briefly, 10 mg/ml of tissue was homogenized in ice-cold 150 mM ammonium acetate using a bead

homogenizer (1.4 mm ceramic) kept below 4°C using liquid nitrogen vapor (Precellys 24 homogenizer with Cryolys cooling unit, Bertin Technologies, Montigny-le-Bretonneux, France). From this, 20 µl of homogenized tissues were added to glass vials containing MTBE and methanol (3:1 v/v, with 0.01% BHT), alongside 10 µl of an internal standard solution containing 10 µM each: phosphatidylcholine (PC) 17:0/17:0, phosphatidylethanolamine (PE) 17:0/17:0, phosphatidylserine (PS) 17:0/17:0, phosphatidylglycerol (PG) 17:0/17:0, lysophosphatidylcholine (LPC) 17:0, lysophosphatidylethanolamine (LPE) 14:0, ceramide (Cer) d18:1/17:0, dihydrosphingomyelin d18:0/12:0, diacylglycerol (DAG) 17:0/17:0, D5-triacylglycerol (TAG) 48:0, and cholesteryl ester (CE) 22:1. Samples were allowed to rotate at 4°C overnight prior to the addition of 1 volume of ice-cold 150 mM ammonium acetate. Samples were vortexed thoroughly prior to centrifugation (2000 *x* g, 5 min) to enable phase separation. The upper organic phase was removed to a new vial and dried under a stream of nitrogen with gentle heating (37°C). The dried lipids were reconstituted in chloroform:methanol:water (60:30:4.5 v/v/v) and kept at -20°C until analysis.

Extracted lipids were analyzed by liquid chromatography-mass spectrometry (LC-MS) using a Dionex Ultimate 3000 LC pump and Q Exactive Plus mass spectrometer equipped with a heated electrospray ionization (HESI) source (Thermo Fisher Scientific) (Bird, Marur, Sniatynski, Greenberg, & Kristal, 2011; Hu et al., 2008; Nigel Turner et al., 2018). Lipids were separated on a Water ACQUITY C18 reverse phase column (2.1 x 100 mm, 1.7 µm pore size, Waters Corp., Milford, MA) using a binary gradient, where mobile phase A consisted of acetonitrile:water (6:4 v/v) and B of isopropanol: acetonitrile (9:1 v/v). Both mobile phases A and B contained 10 mM ammonium formate and 0.1% formic acid, the flow rate was 0.26 ml/min, and the column oven was heated to 60°C. Source conditions were as follows: a spray

voltage of 4.0 and 3.5 kV in positive and negative ion modes respectively, capillary temperature of 290°C, S lens RF of 50, and auxiliary gas heater temperature of 250°C. Nitrogen was used as both source and collision gas, with sheath and auxillary gas flow rate set at 20 and 5 (arbitrary units) respectively. Data were acquired in full scan/data-dependent MS2 mode (full scan resolution 70,000 FWHM, max ion injection time 50 ms, scan range *m/z* 200-1500), with the 10 most abundant ions being subjected to collision-induced dissociation using an isolation window of 1.5 Da and a normalized stepped collision energy of 15/27 eV, with product ions detected at a resolution of 17,500. An exclusion list for background ions was developed using extraction blanks, and mass calibration was performed in both positive and negative ionization modes prior to analysis to ensure mass accuracy of 5 ppm in full scan mode.

Lipids were analyzed using MS-DIAL (Tsugawa et al., 2015). Lipids were detected in both positive and negative ionization modes using a minimum peak height of $1x10^4$ cps, a MS1 tolerance of 5 ppm and MS2 tolerance of 10 ppm, and a minimum identification score of 50%. Identified peaks were aligned with a retention time tolerance of 0.5 min. Exported aligned data were background subtracted and quantified from internal standards using the statistical package R. One-way ANOVA with Tukey *post-hoc* analysis was used to identify differences between groups with statistical significance set at an adjusted $P < 0.05$.

*Targeted metabolite quantification*

Plasma pharmacokinetic analysis of 893 was performed by Pharmaron Corporation (Beijing, China).

C16:0 ceramide levels were quantified in cells using the method described in (Kasumov et al., 2010) with minor modifications. Cultured cells were washed twice in PBS and scraped into 250 µL of HPLC grade water and flash frozen until time of analysis. On the day of analysis, samples were thawed, and an aliquot used for protein quantification. Fifty ng of C17:0 ceramide prepared in ethanol (#22532, Cayman Chemical, Ann Arbor, MI) was added into 200 µL of the thawed cell suspension as an internal standard to control for varying extraction efficiency; 750 µL of an ice-cold 1:2 choroform/methanol mixture was then added. Samples were sonicated for 30 min and phase separation induced by the addition of 250 µL each of chloroform and HPLC-grade water. Samples were centrifuged at 4°C for 10 min and the lower lipid phase transferred to a clean tube. The remaining protein and aqueous layers were re-extracted with an additional 500 µL of chloroform. Lipid phases were combined and then dried under vacuum. Dried extract was re-constituted in 100% acetonitrile immediately before analysis. Samples were analyzed by ultra-performance liquid chromatography tandem mass spectrometry (UPLC-MS/MS) using a Waters Micromass Quattro Premier XE equipped with a Waters ACQUITY BEH C4 column (Waters Corp.). Samples were resolved starting at 60% mobile phase A (10 mM ammonium acetate and 0.05% formic acid in water) to 98% mobile phase B (60:40 acetonitrile:isopropanol) over 3 min with a linear gradient, held at 98% B for 1 min, then the column was equilibrated with 60% A for 1 min. The mass spectrometer was operated in positive ion mode with the following parameters: cone voltage 20 V, source temperature 125°C, desolvation temperature 400°C. Ion transition channels for MS/MS were 538 → 264 for C16:0 ceramide and 552 → 264 for C17:0 ceramide, both with a dwell time of 285 ms. Standard curves prepared from C16:0 ceramide (#860516, Avanti Polar Lipids,

Alabaster, AL) dissolved in ethanol were used for quantitation and were linear from 4.1 nM – 1,000 nM, with an $R^2$ of 0.98 or greater.

*Cell culture*

3T3-L1 cells (a kind gift from Dr. Mei Kong (UC Irvine)) were maintained in DMEM with 10% FBS and 1% penicillin-streptomycin until induced to differentiate. 3T3-L1 pre-adipocytes were differentiated as described in (Valley et al., 2016) with slight modifications. Briefly, pre-adipocytes were grown to confluence. After 2 d, cells were induced with maintenance media containing 500 µM IBMX (I5879, Sigma-Aldrich, St. Louis, MO), 1 µM dexamethasone (D4902, Sigma-Aldrich), 5 µg/mL bovine insulin (I0516, Sigma-Aldrich), and 5 µM troglitazone (50-115-0786, ApexBio). Media was changed every 2-3 d for 7 d. On day 7 post-induction, media was changed to maintenance media + 5 µg/mL bovine insulin. On day 9 post-induction, media was changed to maintenance media. Mature adipocytes were used 12-14 d post-induction for all experiments. LSL-KrasG12D mouse embryonic fibroblasts (MEFs) with and without Cre-mediated deletion of the STOP cassette were obtained from David Tuveson (Cold Spring Harbor Laboratory, Cold Spring Harbor New York, USA) in 2000. *p53*$^{flox/flox}$ MEFs were derived in house (2015) from C57BL/6 mice using standard techniques and immortalized by transient expression of Cre recombinase and deletion of *p53*. MEFs were cultured and maintained in DMEM with 10% FBS and 1% penicillin-streptomycin. Stock solution of palmitic acid (ACROS Organics, cat# AC129702500) was prepared at 100 mM in ethanol. Palmitate (250 µM) was conjugated to 1% (w/v) fatty-acid free bovine serum albumin (Sigma, A8806) in DMEM at 37°C for 20 min. For all immunofluorescence assays, 8,000 MEFs were seeded into 8-chamber

slides (Cellvis, cat# C8-1.5H-N) 12-16 h before treatment. Cells were pre-treated with 893 (5 μM in water), myriocin (10 μM in methanol), Fumonisin-B1 (30 μM in DMSO), or celastrol (500 nM in DMSO) for 3 h followed by a 3 h treatment with BSA-conjugated palmitate mixture or BSA alone. Where cells were treated with C2-ceramide (50 μM in DMSO) or C16-ceramide (100 μM in ethanol) for 3 h, cells were pre-treated with 893 for 3 h. LSL or $KRAS^{G12D}$ MEFs were treated with 893 (5 μM) for 6 h prior to fixation.

*Western blot analysis*

Mature adipocytes were serum starved for 16 h then treated with vehicle, ceramide, or 893 in serum-free media supplemented with 0.2% fatty-acid free BSA for 3 h after which 100 nM insulin was added for 15 min. To determine total DRP1 protein levels, 100,000 MEFs were seeded into a 6-well plate for 16 h, pre-treated for 3 h with vehicle or 893 (5 μM) followed by a 3 h incubation in BSA or BSA-palmitate (250 μM). Cells were washed once with cold PBS, then lysed in cold RIPA buffer (140 mM NaCl, 10 mM Tris pH 8.0, 1% Triton X-100, 0.1% SDS, 1% sodium deoxycholate) with cOmplete™ protease inhibitor (Cat no. 11697498001, Millipore Sigma, St. Louis, MO) and phosSTOP™ phosphatase inhibitor (Cat no. 4906837001, Millipore Sigma). Samples were incubated on ice for 10 min and insoluble material removed by centrifugation (9000 x g for 10 min at 4°C). Protein content was quantified in the supernatant using the Pierce™ BCA Protein Assay Kit (Thermo-Fisher Scientific, Waltham, MA). Equal amounts of protein were prepared in NuPAGE® LDS Sample Buffer (NP0007, Invitrogen) containing 50 mM DTT, and heated at 70°C for 10 min. Proteins were resolved on a NuPAGE® 4-12% Bis-Tris protein gel (NP0336, Invitrogen, Carlsbad, CA) and subsequently

transferred to a nitrocellulose membrane. Membranes were blocked in 5% BSA in TBST for 1 h, then probed with primary antibodies overnight at 4°C. Antibodies used were rabbit-anti-AKT pS473 at 1:1,000 (#4058, Cell Signaling Technology, Danvers, MA), rabbit-anti-AKT at 1:1,000 (#4685, Cell Signaling Technology), rabbit-anti-DRP1 at 1:1,000 (#8570, Cell Signaling Technology), and mouse anti-tubulin at 1:10,000 (T8328, Millipore Sigma, St. Louis, MO). Blots were then washed 3X in TBST and incubated in 800CW-conjugated goat anti-rabbit (#926-32211, Li-COR, Lincoln, NB) and 680LT-conjugated goat anti-mouse (#925-68020, Li-COR) secondary antibodies at 1:10,000 in 5% BSA in TBST for 1 h. Blots were washed then imaged using a Li-COR Odyssey CLx instrument. Band intensity was quantified using Image Studio Lite V5.2 software (Li-COR).

*Glucose uptake assays*

Glucose uptake assays were performed using the Glucose-Glo™ uptake Kit according to manufacturer's instructions (cat# J1342, Promega, Madison, WI). For basal glucose uptake in MEFs, cells were plated the night before in 96-well black, clear-bottom plates. Cells were treated for 3 h, washed once in PBS, then pulsed with 1 mM 2-DG in glucose-free media containing their respective drug treatments. After 10 min, the reaction was quenched and developed according to manufacturer's protocol. To assay insulin-stimulated glucose uptake, mature adipocytes in 96-well black clear-bottom plates were serum starved for 16 h. Cells were treated in serum-free media supplemented with 0.2% fatty-acid free BSA for 3 h. Cells were washed once in PBS and incubated in glucose-free media with their respective drug treatments, with or without 100 nM bovine insulin, for 15 min. A concentrated 2-DG stock was

added directly to wells for 10 min (1 mM final concentration), then the reaction stopped and developed according to manufacturer's protocol.

*Microscopy*

MEFs were washed twice with PBS and fixed with 4% paraformaldehyde for 10 min at RT. Cells were permeabilized with 0.3% Triton X-100 in blocking buffer containing 10% fetal bovine serum for 20 min at 37°C followed by overnight incubation with mouse anti-citrate synthase (sc-390693, Santa Cruz Biotechnology; dilution, 1:200) or rabbit-anti-DRP1 at 1:1000 (#8570, Cell Signaling Technology) at 4°C. Cells were then washed twice with PBS and incubated with AlexaFluor 488 goat anti-mouse (A28175, Invitrogen) or AlexaFluor 594 donkey anti-rabbit (A32754, Invitrogen) secondary antibodies at RT followed by 5 min incubation with 1 µg/ml DAPI and 2 washes in PBS. For NADH autofluorescence studies, mice were gavaged with vehicle or 120 mg/kg 893 at ZT8.5 (4-10.5 h before sacrifice between ZT12.5 and ZT18). Post sacrifice, livers were excised, washed 3X with PBS, placed in DMEM supplemented with 10% FBS and 1% penicillin-streptomycin, and immediately imaged. NADH/NADPH autofluorescence was detected with 740 nm excitation and 450 ± 50 nm detectors using a Mai Tai two-photon laser. Fluorescence microscopy was performed on a Zeiss LSM 780 confocal using a 63X oil objective with a 1.7 numerical aperture (NA). All images presented are 16-bit images from 8-15 Z-stacks with 0.5 micron steps. At least 8-12 non-overlapping fields of view were obtained. Images were obtained using Zeiss Zen 2.3 image acquisition software. To analyze the co-localization between DRP1/citrate synthase signals, Mander's overlap coefficient (MOC) was calculated using the JACOP co-localization plug-in of ImageJ v.1.52e (NIH) post background subtraction per field basis; 40 cells were analyzed from 2 biological replicates. For H&E staining, livers were fixed in formalin, dehydrated in ethanol, and

processed by the Experimental Tissue Research pathology core facility at UCI and evaluated on a Nikon Ti2-F inverted epifluorescence microscope equipped with a DS-Fi3 color camera. Five non-overlapping fields were acquired from 3 different liver sections obtained from 3 mice per group (SD, HFD or HFD + 120 mg/kg 893) and representative images shown.

*Morphometric quantification of mitochondrial networks*

Schematics describing the quantitative analysis of mitochondrial networks are provided as Figures 2.5 (*in vitro*) and 8 (*in vivo*). Analysis was performed using ImageJ software as described in (Chaudhry, Shi, & Luciani, 2019). Briefly, maximum projections from Z-stacks were pre-processed to remove background, manually thresholded as necessary to accurately capture mitochondria, and binarized images evaluated using the analyze particles tool (roundness = 4 × area/π × width and aspect ratio = width/height) or skeletonized and analyzed using the analyze skeleton 2D/3D function (branch length). Cell boundaries were manually delimited using the brightfield channel. For in vivo samples, noise was reduced with the despeckle function; branch length was not calculated for in vivo samples as hepatic mitochondria are minimally branched. In vitro analysis was performed on 40 cells (20 cells from each of the 2 biological replicates) from 6-10 non-overlapping fields of view. In each cell, 100-500 objects were evaluated and averaged; average values from 40 individual cells were used to generate averages for each condition. To demonstrate the spread of the data for individual objects, Figure S2.6 depicts the values for 3,000 – 8,000 objects from 20 cells. In vivo analysis was performed on a per field basis using 8-12 non-overlapping fields collected for each animal.

*Statistical analysis*

Mean ± SEM is presented except where otherwise indicated in the legends. All experimental data is from ≥3 independent biological replicates except where otherwise indicated in the legends. Statistical analysis was performed using Graphpad Prism software except for lipid profiling when the statistical package R was used. Corrections for multiple comparisons were made as indicated in the legends and adjusted *P*-values reported: ns, not significant, $P \geq 0.05$; *, $P < 0.05$; **, $P < 0.01$; ***, $P < 0.001$.

## 2.9 References


Abbott, S. K., Jenner, A. M., Mitchell, T. W., Brown, S. H. J., Halliday, G. M., & Garner, B. (2013). An improved high-throughput lipid extraction method for the analysis of human brain lipids. *Lipids*, *48*(3), 307–318. https://doi.org/10.1007/s11745-013-3760-z

Abdelaal, M., le Roux, C. W., & Docherty, N. G. (2017). Morbidity and mortality associated with obesity. *Annals of Translational Medicine*, *5*(7), 161. https://doi.org/10.21037/atm.2017.03.107

Andreoli, M. F., Donato, J., Cakir, I., & Perello, M. (2019). Leptin resensitisation: a reversion of leptin-resistant states. *The Journal of Endocrinology*, *241*(3), R81–R96. https://doi.org/10.1530/JOE-18-0606

Anello, M., Lupi, R., Spampinato, D., Piro, S., Masini, M., Boggi, U., … Marchetti, P. (2005). Functional and morphological alterations of mitochondria in pancreatic beta cells from type 2 diabetic patients. *Diabetologia*, *48*(2), 282–289. https://doi.org/10.1007/s00125-004-1627-9

Arruda, A. P., Pers, B. M., Parlakgül, G., Güney, E., Inouye, K., & Hotamisligil, G. S. (2014). Chronic enrichment of hepatic endoplasmic reticulum-mitochondria contact leads to mitochondrial dysfunction in obesity. *Nature Medicine*, *20*(12), 1427–1435. https://doi.org/10.1038/nm.3735

Bell, R. R., Spencer, M. J., & Sherriff, J. L. (1995). Diet-induced obesity in mice can be treated without energy restriction using exercise and/or a low fat diet. *The Journal of Nutrition*, *125*(9), 2356–2363. https://doi.org/10.1093/jn/125.9.2356

Benoit, S. C., Air, E. L., Coolen, L. M., Strauss, R., Jackman, A., Clegg, D. J., … Woods, S. C. (2002). The catabolic action of insulin in the brain is mediated by melanocortins. *The Journal of Neuroscience*, *22*(20), 9048–9052.

Bessesen, D. H., & Van Gaal, L. F. (2018). Progress and challenges in anti-obesity pharmacotherapy. *The Lancet. Diabetes & Endocrinology*, *6*(3), 237–248. https://doi.org/10.1016/S2213-8587(17)30236-X

Bird, S. S., Marur, V. R., Sniatynski, M. J., Greenberg, H. K., & Kristal, B. S. (2011). Serum lipidomics profiling using LC-MS and high-energy collisional dissociation fragmentation: focus on triglyceride detection and characterization. *Analytical Chemistry*, *83*(17), 6648–6657. https://doi.org/10.1021/ac201195d

Breslow, M. J., Min-Lee, K., Brown, D. R., Chacko, V. P., Palmer, D., & Berkowitz, D. E. (1999). Effect of leptin deficiency on metabolic rate in ob/ob mice. *The American Journal of Physiology*, *276*(3), E443–9. https://doi.org/10.1152/ajpendo.1999.276.3.E443

Cartoni, R., Léger, B., Hock, M. B., Praz, M., Crettenand, A., Pich, S., … Russell, A. P. (2005). Mitofusins 1/2 and ERRalpha expression are increased in human skeletal muscle after physical exercise. *The Journal of Physiology*, *567*(Pt 1), 349–358. https://doi.org/10.1113/jphysiol.2005.092031

Chaudhry, A., Shi, R., & Luciani, D. S. (2019). A pipeline for multidimensional confocal analysis of mitochondrial morphology, function and dynamics in pancreatic β-cells. *American Journal of Physiology. Endocrinology and Metabolism*. https://doi.org/10.1152/ajpendo.00457.2019

Chaurasia, B., Tippetts, T. S., Mayoral Monibas, R., Liu, J., Li, Y., Wang, L., … Summers, S. A. (2019). Targeting a ceramide double bond improves insulin resistance and hepatic steatosis. *Science*, *365*(6451), 386–392. https://doi.org/10.1126/science.aav3722

Chavez, J. A., & Summers, S. A. (2012). A ceramide-centric view of insulin resistance. *Cell Metabolism*, *15*(5), 585–594. https://doi.org/10.1016/j.cmet.2012.04.002

Chen, B., Roy, S. G., McMonigle, R. J., Keebaugh, A., McCracken, A. N., Selwan, E., … Hanessian, S. (2016). Azacyclic FTY720 analogues that limit nutrient transporter expression but lack S1P receptor activity and negative chronotropic effects offer a novel and effective strategy to kill cancer cells in vivo. *ACS Chemical Biology*, *11*(2), 409–414. https://doi.org/10.1021/acschembio.5b00761

Chung, N., Mao, C., Heitman, J., Hannun, Y. A., & Obeid, L. M. (2001). Phytosphingosine as a specific inhibitor of growth and nutrient import in Saccharomyces cerevisiae. *The Journal of Biological Chemistry*, *276*(38), 35614–35621. https://doi.org/10.1074/jbc.M105653200

Cunarro, J., Casado, S., Lugilde, J., & Tovar, S. (2018). Hypothalamic mitochondrial dysfunction as a target in obesity and metabolic disease. *Frontiers in Endocrinology*, *9*, 283. https://doi.org/10.3389/fendo.2018.00283

El-Haschimi, K., Pierroz, D. D., Hileman, S. M., Bjørbaek, C., & Flier, J. S. (2000). Two defects contribute to hypothalamic leptin resistance in mice with diet-induced obesity. *The Journal of Clinical Investigation*, *105*(12), 1827–1832. https://doi.org/10.1172/JCI9842

Filippi, B. M., Abraham, M. A., Silva, P. N., Rasti, M., LaPierre, M. P., Bauer, P. V., … Lam, T. K. T. (2017). Dynamin-Related Protein 1-Dependent Mitochondrial Fission Changes in the Dorsal Vagal Complex Regulate Insulin Action. *Cell Reports*, *18*(10), 2301–2309. https://doi.org/10.1016/j.celrep.2017.02.035

Funcke, J.-B., & Scherer, P. E. (2019). Beyond adiponectin and leptin: adipose tissue-derived mediators of inter-organ communication. *Journal of Lipid Research*, *60*(10), 1648–1684. https://doi.org/10.1194/jlr.R094060

Galloway, C. A., Lee, H., Brookes, P. S., & Yoon, Y. (2014). Decreasing mitochondrial fission alleviates hepatic steatosis in a murine model of nonalcoholic fatty liver disease. *American Journal of Physiology. Gastrointestinal and Liver Physiology*, *307*(6), G632–41. https://doi.org/10.1152/ajpgi.00182.2014

Galloway, C. A., Lee, H., Nejjar, S., Jhun, B. S., Yu, T., Hsu, W., & Yoon, Y. (2012). Transgenic control of mitochondrial fission induces mitochondrial uncoupling and relieves diabetic oxidative stress. *Diabetes*, *61*(8), 2093–2104. https://doi.org/10.2337/db11-1640

Galloway, C. A., & Yoon, Y. (2013). Mitochondrial morphology in metabolic diseases. *Antioxidants & Redox Signaling*, *19*(4), 415–430. https://doi.org/10.1089/ars.2012.4779

Garland, T., Schutz, H., Chappell, M. A., Keeney, B. K., Meek, T. H., Copes, L. E., … Eisenmann, J. C. (2011). The biological control of voluntary exercise, spontaneous physical activity and daily energy expenditure in relation to obesity: human and rodent perspectives. *The Journal of Experimental Biology*, *214*(Pt 2), 206–229. https://doi.org/10.1242/jeb.048397

Garthwaite, T. L., Martinson, D. R., Tseng, L. F., Hagen, T. C., & Menahan, L. A. (1980). A longitudinal hormonal profile of the genetically obese mouse. *Endocrinology*, *107*(3), 671–676. https://doi.org/10.1210/endo-107-3-671

Guenther, G G, Liu, G., Ramirez, M. U., McMonigle, R. J., Kim, S. M., McCracken, A. N., … Edinger, A. L. (2014). Loss of TSC2 confers resistance to ceramide and nutrient deprivation. *Oncogene*, *33*(14), 1776–1787. https://doi.org/10.1038/onc.2013.139

Guenther, Garret G, Peralta, E. R., Rosales, K. R., Wong, S. Y., Siskind, L. J., & Edinger, A. L. (2008). Ceramide starves cells to death by downregulating nutrient transporter proteins. *Proceedings of the National Academy of Sciences of the United States of America*, *105*(45), 17402–17407. https://doi.org/10.1073/pnas.0802781105

Haas, J. T., Francque, S., & Staels, B. (2016). Pathophysiology and mechanisms of nonalcoholic fatty liver disease. *Annual Review of Physiology*, *78*, 181–205. https://doi.org/10.1146/annurev-physiol-021115-105331

Hammerschmidt, P., Ostkotte, D., Nolte, H., Gerl, M. J., Jais, A., Brunner, H. L., … Brüning, J. C. (2019). CerS6-Derived Sphingolipids Interact with Mff and Promote Mitochondrial Fragmentation in Obesity. *Cell*, *177*(6), 1536–1552.e23. https://doi.org/10.1016/j.cell.2019.05.008

Holland, W. L., Brozinick, J. T., Wang, L.-P., Hawkins, E. D., Sargent, K. M., Liu, Y., … Summers, S. A. (2007). Inhibition of ceramide synthesis ameliorates glucocorticoid-, saturated-fat-, and obesity-induced insulin resistance. *Cell Metabolism*, *5*(3), 167–179. https://doi.org/10.1016/j.cmet.2007.01.002

Hu, C., van Dommelen, J., van der Heijden, R., Spijksma, G., Reijmers, T. H., Wang, M., … Hankemeier, T. (2008). RPLC-ion-trap-FTMS method for lipid profiling of plasma: method validation and application to p53 mutant mouse model. *Journal of Proteome Research*, *7*(11), 4982–4991. https://doi.org/10.1021/pr800373m

Jacobi, D., Liu, S., Burkewitz, K., Kory, N., Knudsen, N. H., Alexander, R. K., … Lee, C.-H. (2015). Hepatic bmal1 regulates rhythmic mitochondrial dynamics and promotes metabolic fitness. *Cell Metabolism*, *22*(4), 709–720. https://doi.org/10.1016/j.cmet.2015.08.006

Jheng, H.-F., Tsai, P.-J., Guo, S.-M., Kuo, L.-H., Chang, C.-S., Su, I.-J., … Tsai, Y.-S. (2012). Mitochondrial fission contributes to mitochondrial dysfunction and insulin resistance in skeletal muscle. *Molecular and Cellular Biology*, *32*(2), 309–319. https://doi.org/10.1128/MCB.05603-11

Kasumov, T., Huang, H., Chung, Y.-M., Zhang, R., McCullough, A. J., & Kirwan, J. P. (2010). Quantification of ceramide species in biological samples by liquid chromatography electrospray ionization tandem mass spectrometry. *Analytical Biochemistry*, *401*(1), 154–161. https://doi.org/10.1016/j.ab.2010.02.023

Katajisto, P., Döhla, J., Chaffer, C. L., Pentinmikko, N., Marjanovic, N., Iqbal, S., … Sabatini, D. M. (2015). Stem cells. Asymmetric apportioning of aged mitochondria between daughter cells is required for stemness. *Science*, *348*(6232), 340–343. https://doi.org/10.1126/science.1260384

Kim, S. M., Roy, S. G., Chen, B., Nguyen, T. M., McMonigle, R. J., McCracken, A. N., … Edinger, A. L. (2016). Targeting cancer metabolism by simultaneously disrupting parallel nutrient access

pathways. *The Journal of Clinical Investigation*, *126*(11), 4088–4102. https://doi.org/10.1172/JCI87148

Kubiniok, P., Finicle, B. T., Piffaretti, F., McCracken, A. N., Perryman, M., Hanessian, S., … Thibault, P. (2019). Dynamic Phosphoproteomics Uncovers Signaling Pathways Modulated by Anti-oncogenic Sphingolipid Analogs. *Molecular & Cellular Proteomics*, *18*(3), 408–422. https://doi.org/10.1074/mcp.RA118.001053

Lee, J., Liu, J., Feng, X., Salazar Hernández, M. A., Mucka, P., Ibi, D., … Ozcan, U. (2016). Withaferin A is a leptin sensitizer with strong antidiabetic properties in mice. *Nature Medicine*, *22*(9), 1023–1032. https://doi.org/10.1038/nm.4145

Levin, N., Nelson, C., Gurney, A., Vandlen, R., & de Sauvage, F. (1996). Decreased food intake does not completely account for adiposity reduction after ob protein infusion. *Proceedings of the National Academy of Sciences of the United States of America*, *93*(4), 1726–1730. https://doi.org/10.1073/pnas.93.4.1726

Lima, A. R., Santos, L., Correia, M., Soares, P., Sobrinho-Simões, M., Melo, M., & Máximo, V. (2018). Dynamin-Related Protein 1 at the Crossroads of Cancer. *Genes*, *9*(2). https://doi.org/10.3390/genes9020115

Liu, J., Lee, J., Salazar Hernandez, M. A., Mazitschek, R., & Ozcan, U. (2015). Treatment of obesity with celastrol. *Cell*, *161*(5), 999–1011. https://doi.org/10.1016/j.cell.2015.05.011

Liu, R., Jin, P., Yu, L., Wang, Y., Han, L., Shi, T., & Li, X. (2014). Impaired mitochondrial dynamics and bioenergetics in diabetic skeletal muscle. *Plos One*, *9*(3), e92810. https://doi.org/10.1371/journal.pone.0092810

Matyash, V., Liebisch, G., Kurzchalia, T. V., Shevchenko, A., & Schwudke, D. (2008). Lipid extraction by methyl-tert-butyl ether for high-throughput lipidomics. *Journal of Lipid Research*, *49*(5), 1137–1146. https://doi.org/10.1194/jlr.D700041-JLR200

Mistry, A. M., Swick, A. G., & Romsos, D. R. (1997). Leptin rapidly lowers food intake and elevates metabolic rates in lean and ob/ob mice. *The Journal of Nutrition*, *127*(10), 2065–2072. https://doi.org/10.1093/jn/127.10.2065

Montgomery, M. K., Brown, S. H. J., Lim, X. Y., Fiveash, C. E., Osborne, B., Bentley, N. L., … Turner, N. (2016). Regulation of glucose homeostasis and insulin action by ceramide acyl-chain length: A beneficial role for very long-chain sphingolipid species. *Biochimica et Biophysica Acta*, *1861*(11), 1828–1839. https://doi.org/10.1016/j.bbalip.2016.08.016

Murakami, I., Mitsutake, S., Kobayashi, N., Matsuda, J., Suzuki, A., Shigyo, T., & Igarashi, Y. (2013). Improved high-fat diet-induced glucose intolerance by an oral administration of phytosphingosine. *Bioscience, Biotechnology, and Biochemistry*, *77*(1), 194–197. https://doi.org/10.1271/bbb.120644

Nagdas, S., Kashatus, J. A., Nascimento, A., Hussain, S. S., Trainor, R. E., Pollock, S. R., … Kashatus, D. F. (2019). Drp1 Promotes KRas-Driven Metabolic Changes to Drive Pancreatic Tumor Growth. *Cell Reports*, *28*(7), 1845–1859.e5. https://doi.org/10.1016/j.celrep.2019.07.031

Nguyen, N. T., & Varela, J. E. (2017). Bariatric surgery for obesity and metabolic disorders: state of the art. *Nature Reviews. Gastroenterology & Hepatology*, *14*(3), 160–169. https://doi.org/10.1038/nrgastro.2016.170

Pan, W. W., & Myers, M. G. (2018). Leptin and the maintenance of elevated body weight. *Nature Reviews. Neuroscience*, *19*(2), 95–105. https://doi.org/10.1038/nrn.2017.168

Park, J., Morley, T. S., Kim, M., Clegg, D. J., & Scherer, P. E. (2014). Obesity and cancer--mechanisms underlying tumour progression and recurrence. *Nature Reviews. Endocrinology*, *10*(8), 455–465. https://doi.org/10.1038/nrendo.2014.94

Parton, L. E., Ye, C. P., Coppari, R., Enriori, P. J., Choi, B., Zhang, C.-Y., … Lowell, B. B. (2007). Glucose sensing by POMC neurons regulates glucose homeostasis and is impaired in obesity. *Nature*, *449*(7159), 228–232. https://doi.org/10.1038/nature06098

Perryman, M. S., Tessier, J., Wiher, T., O'Donoghue, H., McCracken, A. N., Kim, S. M., … Hanessian, S. (2016). Effects of stereochemistry, saturation, and hydrocarbon chain length on the ability of synthetic constrained azacyclic sphingolipids to trigger nutrient transporter down-regulation, vacuolation, and cell death. *Bioorganic & Medicinal Chemistry*, *24*(18), 4390–4397. https://doi.org/10.1016/j.bmc.2016.07.038

Roberto, C. A., Swinburn, B., Hawkes, C., Huang, T. T.-K., Costa, S. A., Ashe, M., … Brownell, K. D. (2015). Patchy progress on obesity prevention: emerging examples, entrenched barriers, and new thinking. *The Lancet*, *385*(9985), 2400–2409. https://doi.org/10.1016/S0140-6736(14)61744-X

Rocha, N., Bulger, D. A., Frontini, A., Titheradge, H., Gribsholt, S. B., Knox, R., … Semple, R. K. (2017). Human biallelic MFN2 mutations induce mitochondrial dysfunction, upper body adipose hyperplasia, and suppression of leptin expression. *eLife*, *6*. https://doi.org/10.7554/eLife.23813

Romero Rosales, K., Singh, G., Wu, K., Chen, J., Janes, M. R., Lilly, M. B., … Edinger, A. L. (2011). Sphingolipid-based drugs selectively kill cancer cells by down-regulating nutrient transporter proteins. *The Biochemical Journal*, *439*(2), 299–311. https://doi.org/10.1042/BJ20110853

Ruvolo, P. P. (2016). The broken "Off" switch in cancer signaling: PP2A as a regulator of tumorigenesis, drug resistance, and immune surveillance. *BBA Clinical*, *6*, 87–99. https://doi.org/10.1016/j.bbacli.2016.08.002

Santoro, A., Campolo, M., Liu, C., Sesaki, H., Meli, R., Liu, Z.-W., … Diano, S. (2017). DRP1 suppresses leptin and glucose sensing of POMC neurons. *Cell Metabolism*, *25*(3), 647–660. https://doi.org/10.1016/j.cmet.2017.01.003

Schneeberger, M., Dietrich, M. O., Sebastián, D., Imbernón, M., Castaño, C., Garcia, A., … Claret, M. (2013). Mitofusin 2 in POMC neurons connects ER stress with leptin resistance and energy imbalance. *Cell*, *155*(1), 172–187. https://doi.org/10.1016/j.cell.2013.09.003

Schrepfer, E., & Scorrano, L. (2016). Mitofusins, from Mitochondria to Metabolism. *Molecular Cell*, *61*(5), 683–694. https://doi.org/10.1016/j.molcel.2016.02.022

Sebastián, D., Hernández-Alvarez, M. I., Segalés, J., Sorianello, E., Muñoz, J. P., Sala, D., … Zorzano, A. (2012). Mitofusin 2 (Mfn2) links mitochondrial and endoplasmic reticulum function with insulin signaling and is essential for normal glucose homeostasis. *Proceedings of the National*

*Academy of Sciences of the United States of America*, *109*(14), 5523–5528. https://doi.org/10.1073/pnas.1108220109

Senft, D., & Ronai, Z. A. (2016). Regulators of mitochondrial dynamics in cancer. *Current Opinion in Cell Biology*, *39*, 43–52. https://doi.org/10.1016/j.ceb.2016.02.001

Serasinghe, M. N., Wieder, S. Y., Renault, T. T., Elkholi, R., Asciolla, J. J., Yao, J. L., … Chipuk, J. E. (2015). Mitochondrial division is requisite to RAS-induced transformation and targeted by oncogenic MAPK pathway inhibitors. *Molecular Cell*, *57*(3), 521–536. https://doi.org/10.1016/j.molcel.2015.01.003

Shulman, G. I. (2014). Ectopic fat in insulin resistance, dyslipidemia, and cardiometabolic disease. *The New England Journal of Medicine*, *371*(12), 1131–1141. https://doi.org/10.1056/NEJMra1011035

Skrzypek, M. S., Nagiec, M. M., Lester, R. L., & Dickson, R. C. (1998). Inhibition of amino acid transport by sphingoid long chain bases in Saccharomyces cerevisiae. *The Journal of Biological Chemistry*, *273*(5), 2829–2834. https://doi.org/10.1074/jbc.273.5.2829

Smith, M. E., Tippetts, T. S., Brassfield, E. S., Tucker, B. J., Ockey, A., Swensen, A. C., … Bikman, B. T. (2013). Mitochondrial fission mediates ceramide-induced metabolic disruption in skeletal muscle. *The Biochemical Journal*, *456*(3), 427–439. https://doi.org/10.1042/BJ20130807

Snel, M., Sleddering, M. A., Pijl, H., Nieuwenhuizen, W. F., Frölich, M., Havekes, L. M., … Jazet, I. M. (2010). The effect of dietary phytosphingosine on cholesterol levels and insulin sensitivity in subjects with the metabolic syndrome. *European Journal of Clinical Nutrition*, *64*(4), 419–423. https://doi.org/10.1038/ejcn.2009.154

Speakman, J. R. (2019). Use of high-fat diets to study rodent obesity as a model of human obesity. *International Journal of Obesity*, *43*(8), 1491–1492. https://doi.org/10.1038/s41366-019-0363-7

Srivastava, G., & Apovian, C. M. (2018). Current pharmacotherapy for obesity. *Nature Reviews. Endocrinology*, *14*(1), 12–24. https://doi.org/10.1038/nrendo.2017.122

Summers, S. A., Garza, L. A., Zhou, H., & Birnbaum, M. J. (1998). Regulation of insulin-stimulated glucose transporter GLUT4 translocation and Akt kinase activity by ceramide. *Molecular and Cellular Biology*, *18*(9), 5457–5464. https://doi.org/10.1128/mcb.18.9.5457

Swinburn, B. A., Sacks, G., Hall, K. D., McPherson, K., Finegood, D. T., Moodie, M. L., & Gortmaker, S. L. (2011). The global obesity pandemic: shaped by global drivers and local environments. *The Lancet*, *378*(9793), 804–814. https://doi.org/10.1016/S0140-6736(11)60813-1

Team, R. C. (n.d.). *R: A language and environment for statistical computing.* R Foundation for Statistical Computing.

Theurey, P., & Rieusset, J. (2017). Mitochondria-Associated Membranes Response to Nutrient Availability and Role in Metabolic Diseases. *Trends in Endocrinology and Metabolism*, *28*(1), 32–45. https://doi.org/10.1016/j.tem.2016.09.002

Theurey, P., Tubbs, E., Vial, G., Jacquemetton, J., Bendridi, N., Chauvin, M.-A., … Rieusset, J. (2016). Mitochondria-associated endoplasmic reticulum membranes allow adaptation of mitochondrial

metabolism to glucose availability in the liver. *Journal of Molecular Cell Biology*, *8*(2), 129–143. https://doi.org/10.1093/jmcb/mjw004

Timper, K., & Brüning, J. C. (2017). Hypothalamic circuits regulating appetite and energy homeostasis: pathways to obesity. *Disease Models & Mechanisms*, *10*(6), 679–689. https://doi.org/10.1242/dmm.026609

Tsugawa, H., Cajka, T., Kind, T., Ma, Y., Higgins, B., Ikeda, K., … Arita, M. (2015). MS-DIAL: data-independent MS/MS deconvolution for comprehensive metabolome analysis. *Nature Methods*, *12*(6), 523–526. https://doi.org/10.1038/nmeth.3393

Turner, N, Kowalski, G. M., Leslie, S. J., Risis, S., Yang, C., Lee-Young, R. S., … Bruce, C. R. (2013). Distinct patterns of tissue-specific lipid accumulation during the induction of insulin resistance in mice by high-fat feeding. *Diabetologia*, *56*(7), 1638–1648. https://doi.org/10.1007/s00125-013-2913-1

Turner, Nigel, Lim, X. Y., Toop, H. D., Osborne, B., Brandon, A. E., Taylor, E. N., … Don, A. S. (2018). A selective inhibitor of ceramide synthase 1 reveals a novel role in fat metabolism. *Nature Communications*, *9*(1), 3165. https://doi.org/10.1038/s41467-018-05613-7

Turpin, S. M., Nicholls, H. T., Willmes, D. M., Mourier, A., Brodesser, S., Wunderlich, C. M., … Brüning, J. C. (2014). Obesity-induced CerS6-dependent C16:0 ceramide production promotes weight gain and glucose intolerance. *Cell Metabolism*, *20*(4), 678–686. https://doi.org/10.1016/j.cmet.2014.08.002

Turpin-Nolan, S. M., Hammerschmidt, P., Chen, W., Jais, A., Timper, K., Awazawa, M., … Brüning, J. C. (2019). CerS1-Derived C18:0 Ceramide in Skeletal Muscle Promotes Obesity-Induced Insulin Resistance. *Cell Reports*, *26*(1), 1–10.e7. https://doi.org/10.1016/j.celrep.2018.12.031

Valley, M. P., Karassina, N., Aoyama, N., Carlson, C., Cali, J. J., & Vidugiriene, J. (2016). A bioluminescent assay for measuring glucose uptake. *Analytical Biochemistry*, *505*, 43–50. https://doi.org/10.1016/j.ab.2016.04.010

Van den Bergh, A., Vanderper, A., Vangheluwe, P., Desjardins, F., Nevelsteen, I., Verreth, W., … Herijgers, P. (2008). Dyslipidaemia in type II diabetic mice does not aggravate contractile impairment but increases ventricular stiffness. *Cardiovascular Research*, *77*(2), 371–379. https://doi.org/10.1093/cvr/cvm001

Varela, L., & Horvath, T. L. (2012). Leptin and insulin pathways in POMC and AgRP neurons that modulate energy balance and glucose homeostasis. *EMBO Reports*, 13(12), 1079–1086. https://doi.org/10.1038/embor.2012.174

## 2.10 Figures

### Figure 2.1

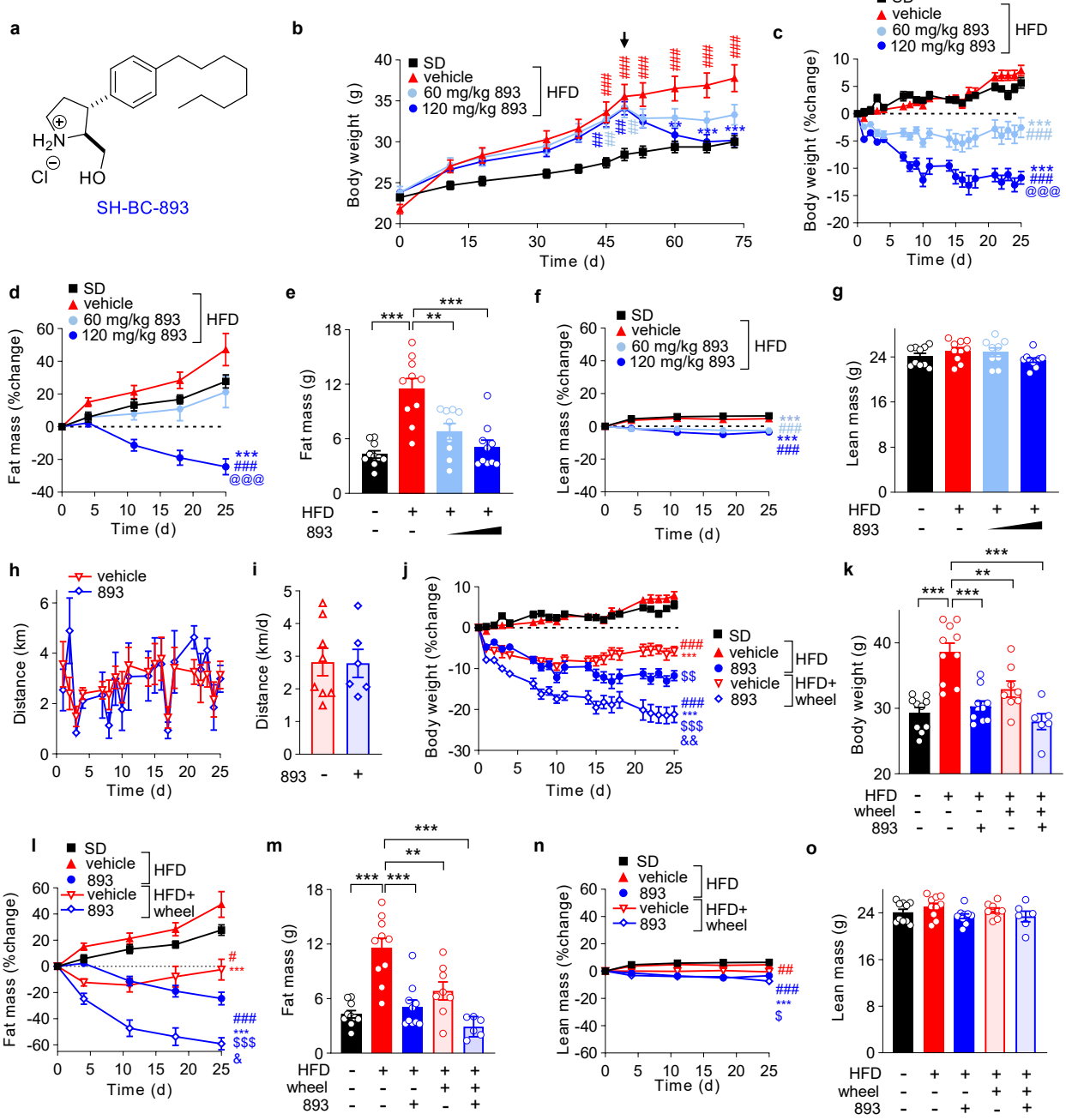

**Figure 2.1: 893 restores normal weight in mice maintained on a high fat diet**

**a,** Structure of 893. **b,** Body weight of mice fed a standard diet and gavaged with vehicle (SD, n=10) or fed a high fat diet (HFD) and gavaged with vehicle (n=10), 60 mg/kg (n=9), or 120 mg/kg (n=10) 893 on Mondays, Wednesdays, and Fridays beginning on day 49. **c,d,** Percent change in body weight (**c**) or fat mass (**d**) during treatment (days 49-73) for mice in (**b**). **e,** As in (**d**) but at the end of treatment (day 73). **f,g,** As in (**d**,**e**) but lean mass was measured. **h,i,** Distance run over 24 h by day (**h**) or averaged over the treatment period (**i**) for HFD-fed mice treated with vehicle (n=8) or 893 (120 mg/kg, n=6) and housed with a running wheel. **j,** As in (**c**), but including the mice provided with running wheels shown in (**h,i**). **k,** Body weight at the end of treatment (day 73) for the mice in (**j**). **l,m,** Percent (**l**) or absolute (**m**) fat mass measured weekly (**l**) or at the end of the study (**m**) in the mice in (**j**). **n,o,** As in (**l,m**) but for lean mass. In (**b-o**), mean ± SEM is shown. Using a one-way ANOVA with Tukey's correction (**b-g** and **j-o**) or an unpaired, two-tailed t test (**h,i**): one symbol, $P < 0.05$; two symbols, $P < 0.01$; or three symbols, $P < 0.001$. Statistics compare indicated group to SD (#), HFD + vehicle (*), 60 mg/kg 893 (@), HFD + vehicle + wheel ($), or HFD +120 mg/kg 893 (&). For clarity, all *P*-values for (**b-d, f, j, l, n**) are presented in Extended Data Fig. 1a.

## Figure 2.2

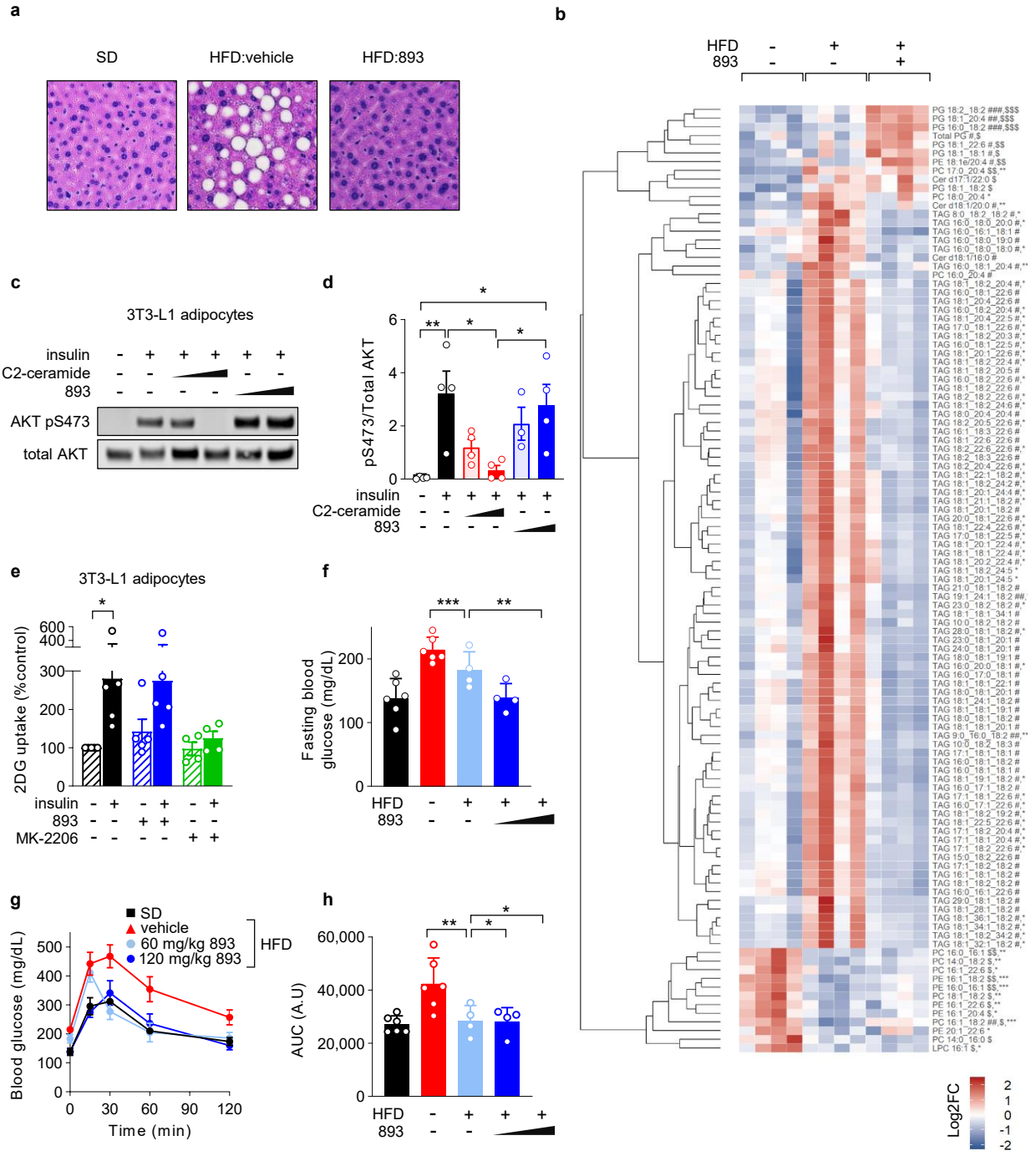
a
SD
HFD:vehicle
HFD:893
b
HFD
893
c
3T3-L1 adipocytes
insulin
C2-ceramide
893
AKT pS473
total AKT
d
pS473/Total AKT
e
3T3-L1 adipocytes
2DG uptake (%control)
MK-2206
f
Fasting blood glucose (mg/dL)
g
SD
vehicle
60 mg/kg 893
120 mg/kg 893
HFD
Blood glucose (mg/dL)
Time (min)
h
AUC (A.U)
Log2FC

**Figure 2.2: 893 corrects metabolic defects in mice fed a high fat diet**

**a**, Representative images of H&E stained livers from SD, HFD + vehicle, or HFD + 120 mg/kg 893 mice shown in **Figure 2.1** at the end of treatment. **b,** Heat map depicting hepatic lipids that were significantly different in SD, HFD + vehicle, or HFD + 120 mg/kg 893 at the end of treatment (day 73). PG, phosphatidylglycerol; PE, phosphatidylethanolamine; PC, phosphatidylcholine; Cer, ceramide; TAG, triacylglycerol; and LPC, lysophosphatidylcholine. **c,d** Insulin-stimulated (100 nm for 15 min) AKT activation in 3T3-L1 adipocytes pre-treated with C2-ceramide (50 or 100 μM) or 893 (5 or 10 μM) for 3 h. Representative western blot (**c**) or quantification (**d**) of 4 biological replicates except for 5 μM 893 where n=3. **e,** Insulin-stimulated glucose uptake in 3T3-L1 adipocytes after 3 h of treatment with vehicle (n=5), 893 (10 μM, n=5) or MK-2206 (2 μM, n=3). **f,** Fasting blood glucose from mice in **Fig. 1** after 25 d of treatment. SD + vehicle and HFD + vehicle (n=6), HFD + 60 or 120 mg/kg 893 (n=4). **g,h** Blood glucose levels (**g**) or area under the curve AUC (**h**) during an oral glucose tolerance test performed in the mice in (**f**). Blood glucose values for each mouse shown in Extended Data Fig. 2d. For **d-h**, mean ± SEM shown. In (**d, f,** and **h**) using a one-way ANOVA with Tukey's correction or an unpaired, two-tailed t test (**e**), *, $P < 0.05$; **, $P < 0.01$; ***, $P < 0.001$; unmarked, not significant, $P > 0.05$. In (**b**), comparisons are made between SD and HFD (*), HFD + vehicle and HFD + 120 mg/kg 893 (#), or SD and HFD + 120 mg/kg 893 ($) using a one-way ANOVA with Tukey's correction for multiple comparisons.

## Figure 2.3

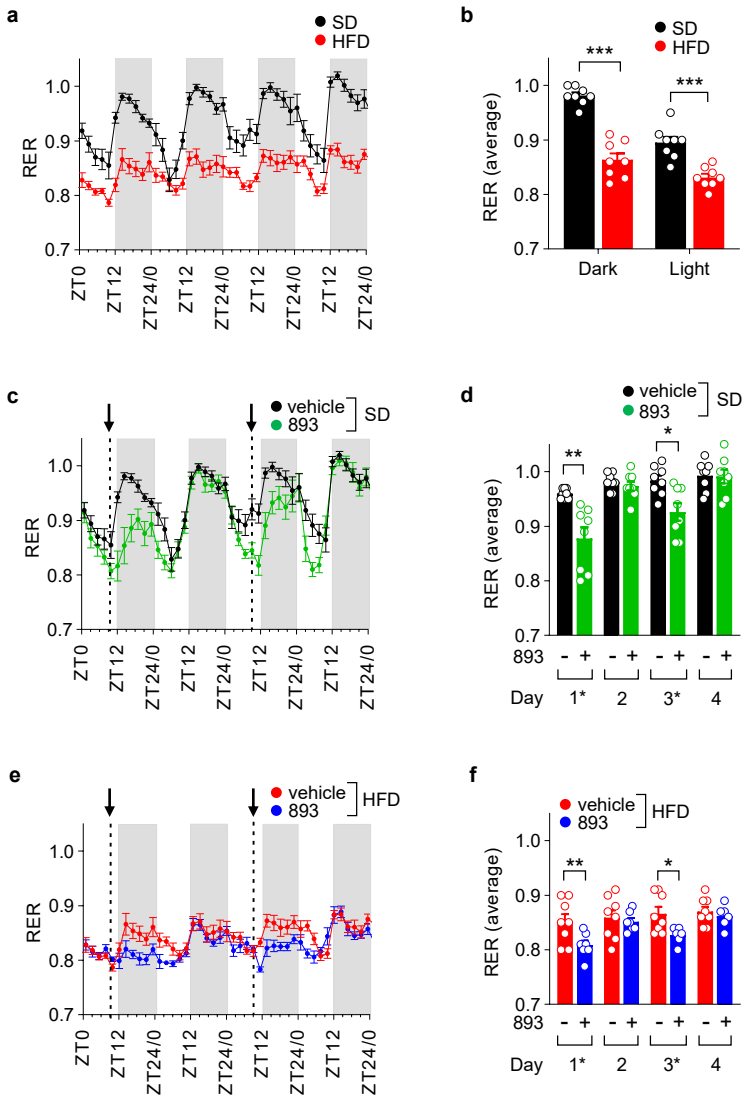


**Figure 2.3: 893 reduces the respiratory exchange ratio**
**a,b,** Respiratory exchange ratio (RER) of mice fed either a SD (n=8) or HFD (n=8) for 10-12 weeks. The means of 4 measurements over 108 minutes (**a**) or average value over all of the dark (ZT12-ZT24) or light (ZT0-ZT12) cycles (**b**) shown. **c,d,** As in (**a,b**), but in mice maintained on a SD treated with vehicle (n=8) or 120 mg/kg 893 (n=8) p.o. at ZT8.5 on days 1 (first exposure) and 3. The means of 4 measurements over 108 minutes (**c**) or daily averages (**d**) are presented, treatment indicated with arrows (**c**) or * (**d**). **e,f,** As in (**c,d**) but in mice maintained on a HFD treated with vehicle (n=8) or 120 mg/kg 893 (n=6-7). In **b**, **d**, and **f**, means ± SEM shown; using unpaired, two-tailed t tests to compare conditions, *, $P < 0.05$; **, $P < 0.01$; ***, $P < 0.001$; unmarked, not significant, $P > 0.05$.

## Figure 2.4

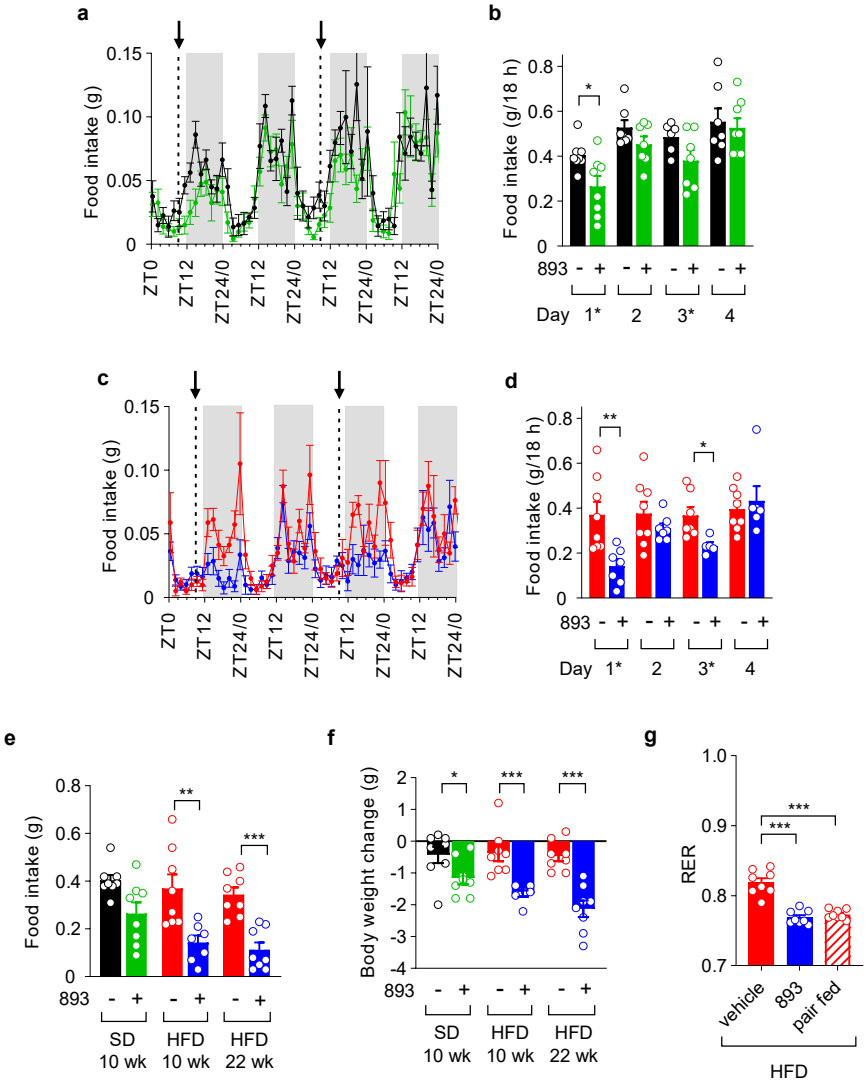


**Figure 2.4: 893 reduces food intake**

**a,b,** Food intake during the indirect calorimetry studies in **Figure 2.3** shown as the mean of 4 measurements taken over 108 min (**a**) or averaged from ZT12-ZT24 (**b**). Mice were fed a SD and treated with vehicle (n=6-8) or 120 mg/kg 893 (n=7-8) by gavage (arrows (**a**) or * (**b**)) on days 1 (first exposure) and 3 at ZT8.5. **c**,**d**, As in (**a**,**b**), but in mice maintained on a HFD treated with vehicle (n=7-8) or 893 (n=5-7). **e,** Food intake between ZT12 and ZT24 in mice fed a SD for 10 weeks (n=8), a HFD for 10 weeks (n=7), or a HFD for 22 weeks (n=8) were treated once at ZT8.5 with vehicle or 120 mg/kg 893 by gavage. **f**, Body weight change in mice in (**e**). **g,** Average RER between ZT12-ZT24 in mice fed a HFD for 22 weeks and then treated with vehicle (n=8), 120 mg/kg 893 (n=8), or pair fed the average amount of food eaten during this period by 893-treated mice (n=8). Using unpaired, two-tailed t tests to compare vehicle- and 893-treated mice (**b**, **d**, **e**, and **f**) or a one-way ANOVA with Tukey's correction (**g**), *, $P < 0.05$; **, $P < 0.01$; ***, $P < 0.001$; unmarked, not significant, $P > 0.05$.

## Figure 2.5

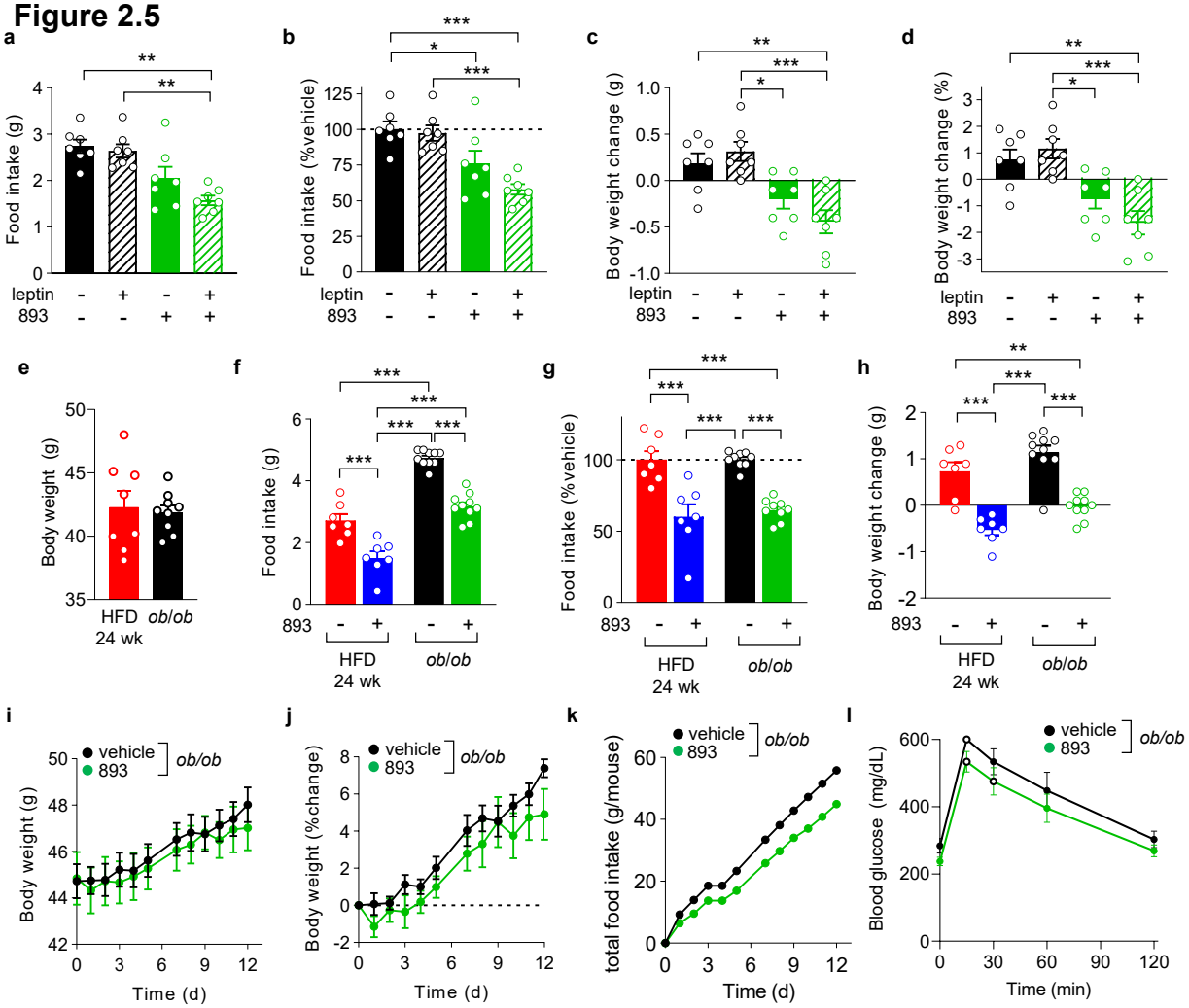


**Figure 2.5: Leptin contributes to the metabolic effects of 893.**
**a,b,** Food intake (**a**) or percent intake relative to vehicle-treated mice (**b**) between ZT8.5 and ZT2.5 (18 h) in 18 week-old mice fed a 16% kcal from fat chow diet and treated with vehicle (saline) or 2 mg/kg leptin i.p. at ZT11.5 and with vehicle (water) or 120 mg/kg 893 by gavage at ZT8.5; all groups, n=7. **c,d,** Body weight (**c**) or body weight change (**d**) in mice in (**a,b**). **e,** Body weight of wild type C57BL/6J mice fed a HFD for 24 weeks (n=8) or 10 week old *ob/ob* mice (n=9) fed a 16% kcal from fat chow diet prior to treatment with 893. **f,g,** Food intake (**f**) or percent food intake relative to vehicle (**g**) between ZT8.5 and ZT2.5 (18 h) in the mice in (**e**) after a single oral dose of vehicle or 120 mg/kg 893. For both treatments, wild type, n=7 and *ob/ob*, n=9. **h,** Body weight change in mice shown in (**f,g**). **i,j,** Body weight (**i**) or percent change in body weight (**j**) in *ob/ob* mice treated Monday, Wednesday, and Friday with vehicle (n=4) or 120 mg/kg 893 (n=4) by gavage for 2 weeks. **k**, Cumulative food intake in the mice in (**i,j**); all 4 mice receiving each treatment were maintained in one cage and thus n=1. **l**, Oral glucose tolerance test performed in the mice in (**i,j**) 14 d after the initiation of treatment; n=4. Open circles indicate where some blood glucose values exceeded the limit of detection (>600 mg/dL) and were assigned a value of 600 mg/dL; all data points are reported in Figure S2.4i. Means ± SEM shown except (**k**) where the value for each cage is shown. Using a one-way ANOVA (**a-d** and **f-h**) or unpaired, two-tailed t tests (**e, i, j,** and **l**),* $P < 0.05$; **, $P < 0.01$; ***, $P < 0.001$; unmarked, not significant, $P > 0.05$.

# Figure 2.6

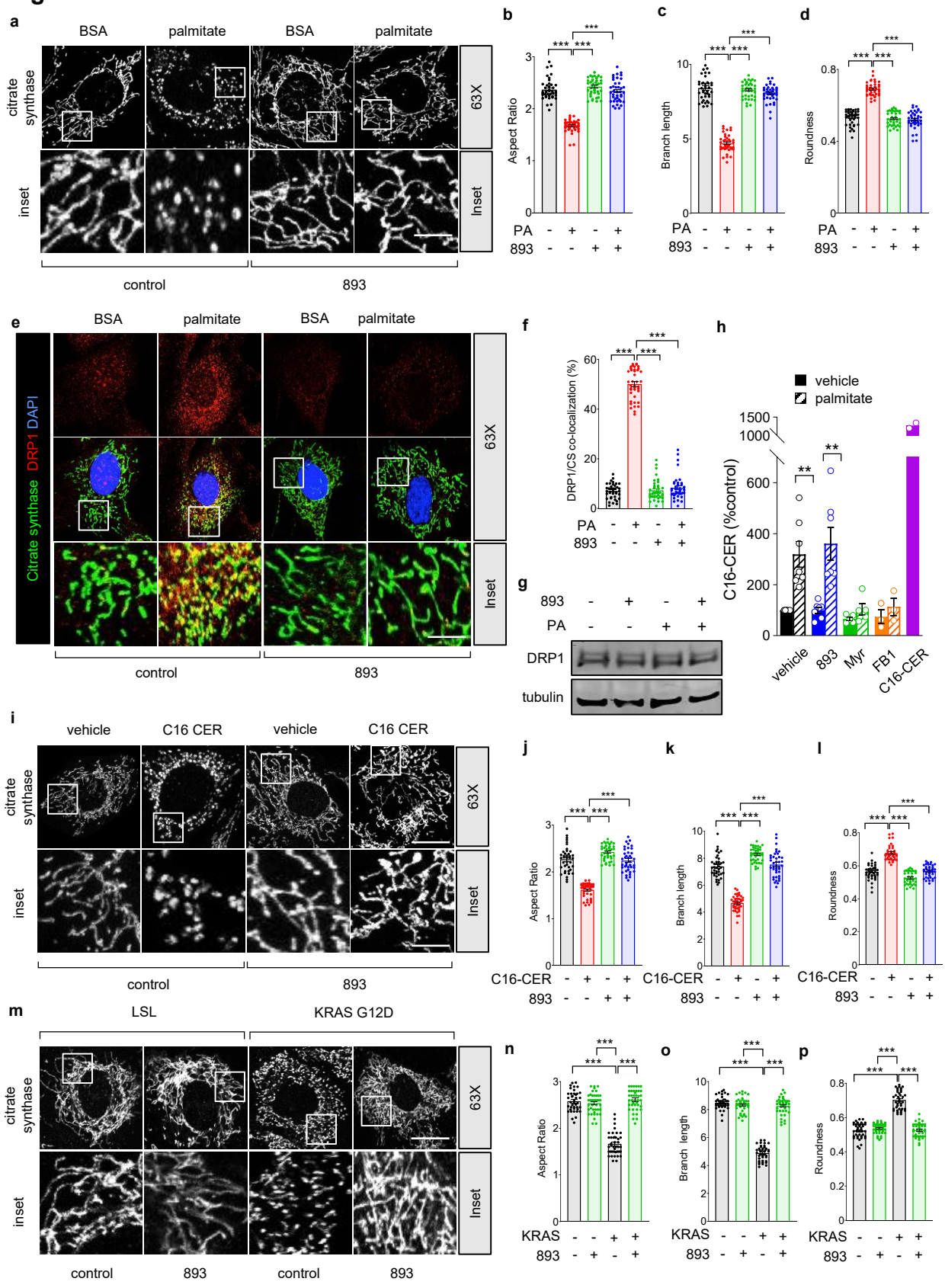
a
BSA
palmitate
BSA
palmitate
citrate synthase
inset
63X
Inset
control
893
b
Aspect Ratio
PA
893
c
Branch length
d
Roundness
e
Citrate synthase DRP1 DAPI
f
DRP1/CS co-localization (%)
g
DRP1
tubulin
h
vehicle
palmitate
C16-CER (%control)
vehicle
893
Myr
FB1
C16-CER
i
vehicle
C16 CER
j
k
l
C16-CER
m
LSL
KRAS G12D
n
o
p
KRAS

**Figure 2.6: 893 prevents ceramide-induced mitochondrial fission**
**a**, Citrate synthase staining in MEFs treated for 3 h with vehicle (BSA in ethanol) or BSA-conjugated palmitic acid (250 μM) after a 3 h pre-treatment with vehicle (water) or 893 (5 μM). **b-d,** ImageJ was used to calculate aspect ratio (**b**), branch length (**c**), and roundness (**d**) in the cells in (**a**). Forty cells from 2 biological replicates were examined. **e,** MEFs treated as in (**a**) but evaluated for Drp1 (red) and citrate synthase (green) co-localization (yellow) using confocal immunofluorescence microscopy. Nuclei are labeled with DAPI (blue). **f,** Mander's overlap coefficient (MOC) for Drp1 and citrate synthase for the cells in (**e**) calculated using ImageJ on a per cell basis from 40 cells from 2 biological replicates. **g**, Western blot for Drp1 on cells treated as in (**e**), n=1. **h**, C16:0 ceramide (C16-CER) levels in MEFs pre-treated for 3 h with vehicle (ethanol, n=7), 893 (5 μM, n=7), myriocin (Myr, 10 μM, n=5), or Fumonisin B1 (FB1, 20 μM, n=3) then treated with BSA in vehicle (ethanol) or BSA-conjugated palmitic acid (250 μM) for 3 h; n=3. MEFs were treated with C16-CER (100 μM, n=2) for 3 h as a positive control. **i,** MEFs were treated with vehicle (ethanol) or C16-CER (100 μM) for 3 h after a 3 h pre-treatment with vehicle (water) or 893 (5 μM) and mitochondria stained as in (**a**). **j-l,** aspect ratio (**j**), branch length (**k**), and roundness (**l**) in the cells in (**i**). Forty cells from 2 biological replicates were examined. **m-p,** Citrate synthase staining in control LSL or $KRAS^{G12D}$ MEFs after a 6 h treatment with vehicle or 893 (5 μM). Forty cells from 2 biological replicates were examined. Means ± SEM shown in **b-d**, **f, h**, **j-l**, and **n-p**. Using a one-way ANOVA and Tukey's correction (**b-d**, **f**, **j-l**, and **n-p**) or two sided, two-tailed t tests (**h**), **, $P \leq 0.01$; ***, $P \leq 0.001$; unmarked, not significant, $P > 0.05$. Scale bars, 20 μm.

## Figure 2.7

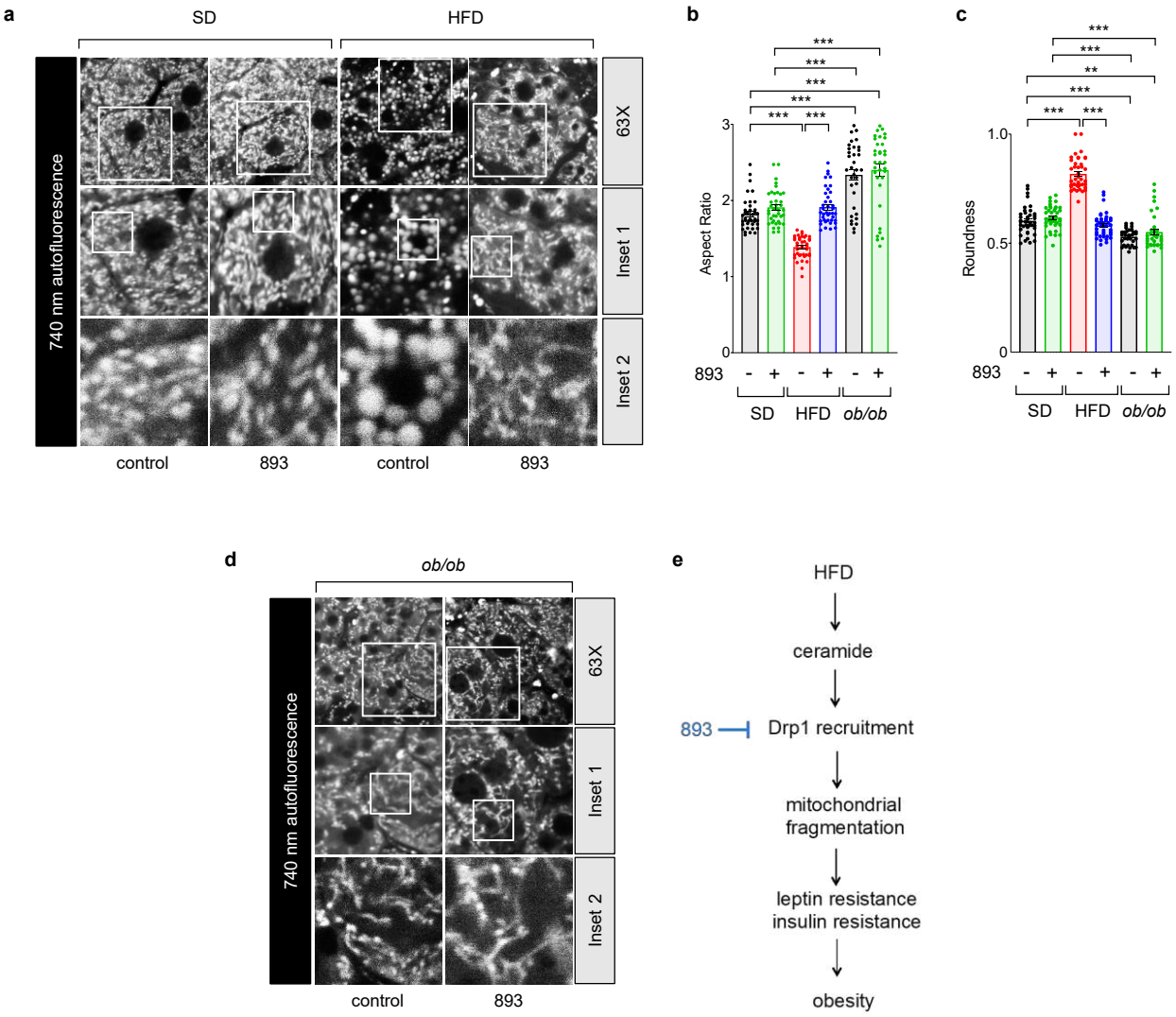


**Figure 2.7: 893 maintains normal mitochondrial morphology in HFD-fed mice**

**a**, NADH/NADPH autofluorescence evaluated by confocal microscopy in freshly resected livers from mice that had consumed a SD for 22 weeks or a HFD for 26 weeks after acute treatment with vehicle or 120 mg/kg 893 by gavage at ZT8.5. Mice were sacrificed in pairs between ZT12.5 and ZT18. **b,c**, Aspect ratio (**b**) and roundness (**c**) of mitochondrial in the livers shown in (**a** or **d**). Mean ± SEM shown; 6-8 fields were examined per mouse, n=4 in all groups. Using a one-way ANOVA and Tukey's correction, **, $P \leq 0.01$; ***, $P \leq 0.001$; unmarked, not significant, $P > 0.05$. For clarity, all *P*-values are provided in Extended Data Fig. 9. **d**, As in (**a**), but in livers from 12 week old *ob/ob* mice treated with vehicle or 893. **e,** Model for the metabolic actions of 893.

## 2.11 Supplemental figures

## Figure S2.1

**a**

| | Fig. 1b | | | | | | Fig. 1c | Fig. 1d | Fig. 1f | Fig. 1j | Fig. 1l | Fig. 1n |
|---|---|---|---|---|---|---|---|---|---|---|---|---|
| | Day 45 | Day 49 | Day 53 | Day 60 | Day 67 | Day 73 | Rx Day 25 | Rx Day 25 | Rx Day 25 | Rx Day 25 | Rx Day 25 | Rx Day 25 |
| SD vs HFD | 0.001 | <0.001 | <0.001 | <0.001 | <0.001 | <0.001 | 0.569 | 0.251 | 0.729 | 0.607 | 0.225 | 0.936 |
| SD vs HFD + 60 mpk 893 | 0.007 | 0.008 | 0.068 | 0.172 | 0.336 | 0.320 | <0.001 | 0.927 | <0.001 | | | |
| SD vs HFD + 120 mpk 893 | 0.008 | 0.008 | 0.108 | 0.906 | 0.999 | 1.000 | <0.001 | <0.001 | <0.001 | <0.001 | <0.001 | <0.001 |
| SD vs HFD + wheel | | | | | | | | | | <0.001 | 0.029 | 0.009 |
| SD vs HFD + 120 mpk 893 + wheel | | | | | | | | | | <0.001 | <0.001 | <0.001 |
| HFD vs HFD + 60 mpk 893 | 0.991 | 0.960 | 0.345 | 0.185 | 0.087 | 0.074 | <0.001 | 0.086 | 0.001 | | | |
| HFD vs HFD + 120 mpk 893 | 0.975 | 0.938 | 0.191 | 0.004 | 0.001 | <0.001 | <0.001 | <0.001 | <0.001 | <0.001 | <0.001 | 0.001 |
| HFD + 60 mpk 893 vs HFD + 120 mpk 893 | 1.000 | 1.000 | 1.000 | 0.719 | 0.572 | 0.375 | <0.001 | 0.001 | 0.967 | | | |
| HFD vs HFD + wheel | | | | | | | | | | <0.001 | <0.001 | 0.086 |
| HFD vs HFD + 120 mpk 893 + wheel | | | | | | | | | | <0.001 | <0.001 | <0.001 |
| HFD + wheel vs HFD + 120 mpk 893 + wheel | | | | | | | | | | <0.001 | <0.001 | 0.036 |
| HFD + wheel vs HFD + 120 mpk 893 | | | | | | | | | | 0.008 | 0.176 | 0.699 |
| HFD + 120 mpk 893 vs HFD + 120 mpk 893 + wheel | | | | | | | | | | 0.008 | 0.018 | 0.403 |

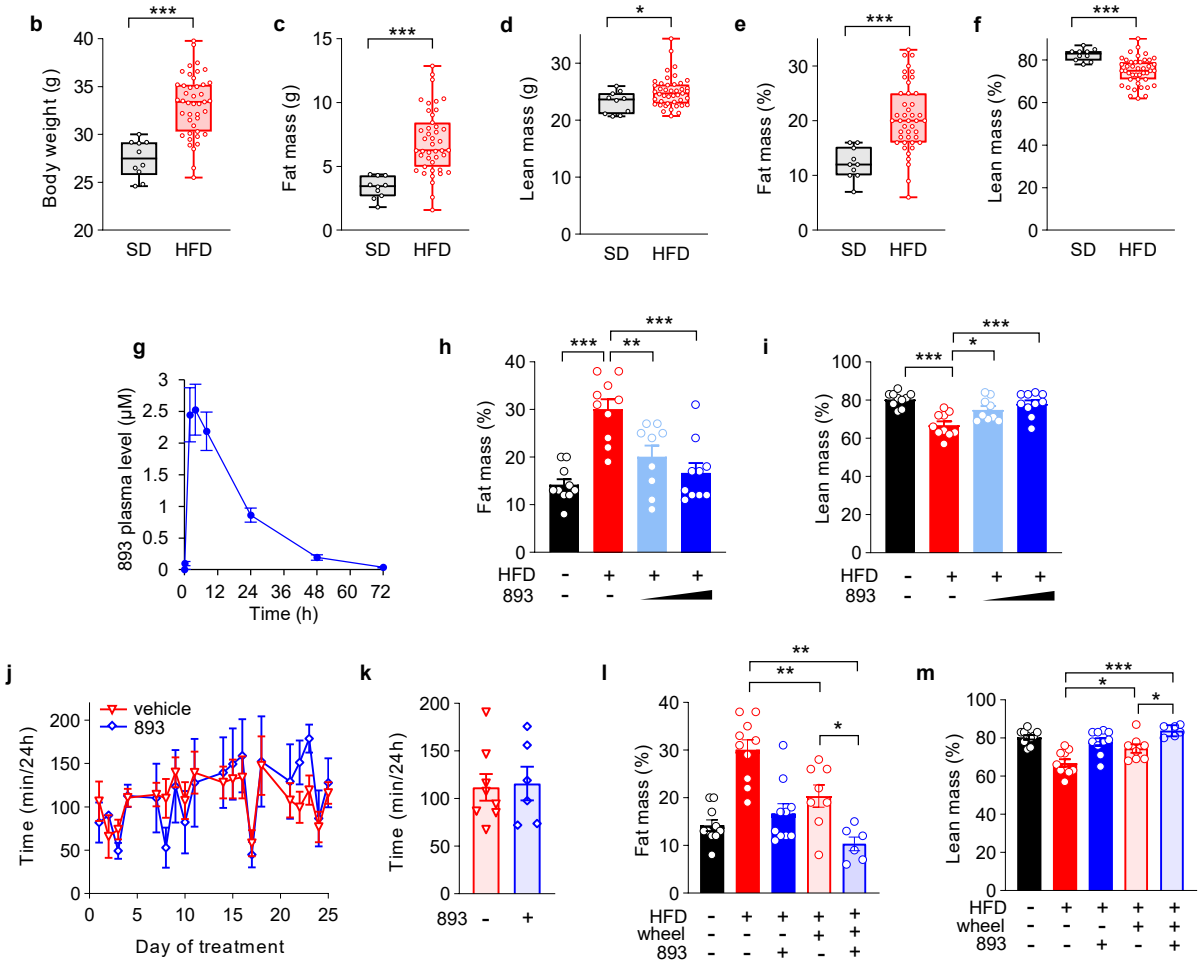

**Figure S2.1: 893 restores normal weight in mice maintained on a high fat diet**
**a,** *P*-values for **Figure 2.1b-d**, **f**, **j**, **l**, and **n** using a one-way ANOVA and Tukey's correction. **b-f,** Body weight (**b**), fat mass (**c**), lean mass (**d**)**,** body composition as % fat mass (**e**)**,** or % lean mass (**f**) for mice fed a SD (n=10) or HFD (n=40). In box plots, the center line is the median and the box is delimited by the 25$^{th}$ to 75$^{th}$ percentile, whiskers represent minimum and maximum values. **g,** Plasma pharmacokinetics in mice after a single dose of 120 mg/kg 893 given by gavage (n=3). **h,i,** Fat (**h**) or lean (**i**) mass as measured by EchoMRI after 25 days of treatment with vehicle (n=10), 60 (n=9), or 120 mg/kg 893 (n=10) p.o. Mon/Wed/Fri expressed as percent body weight. **j,k,** Average daily (**j**) or cumulative average per 24 h over the entire treatment period (**k**) time spent on running wheels by mice maintained on a HFD and treated with vehicle (n=8) or 120 mg/kg 893 (n=6) p.o. Mon/Wed/Fri. **l,m,** As in (**h,i**) but including mice housed with running wheels and treated with vehicle (n=8) or 120 mg/kg 893 (n=6). For (**g-m**), mean ± SEM shown. Using an unpaired, two-tailed t test (**b-f, j,** and **k**) or a one-way ANOVA and Tukey's correction (**h**, **i**, **l**, and **m**), *, $P < 0.05$; **, $P \leq 0.01$; ***, $P \leq 0.001$; unmarked, not significant, $P > 0.05$ except in (**l,m**) where comparisons shown in (**h,i**) are not repeated.

## Figure S2.2

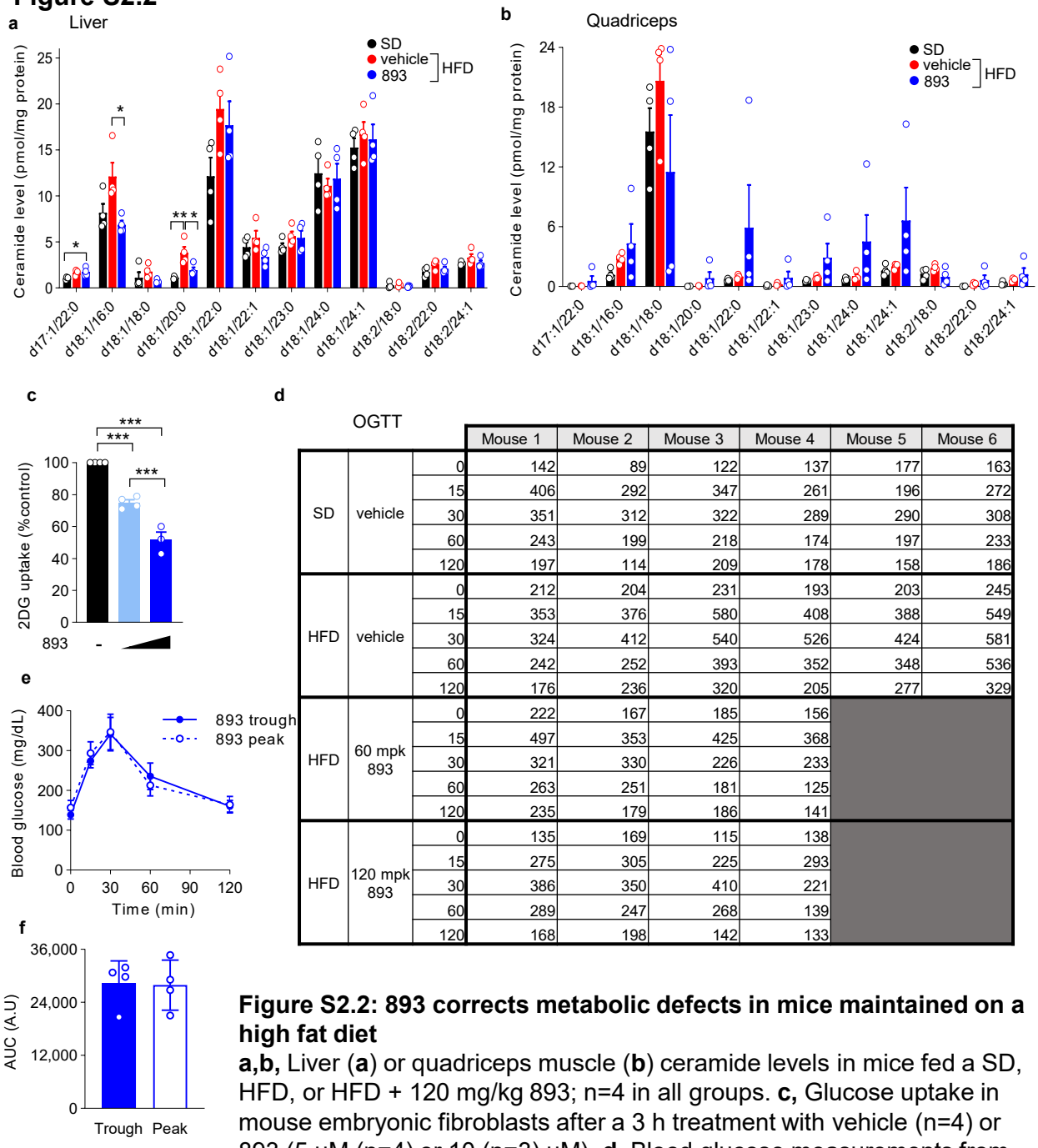


| | | | Mouse 1 | Mouse 2 | Mouse 3 | Mouse 4 | Mouse 5 | Mouse 6 |
|---|---|---|---|---|---|---|---|---|
| SD | vehicle | 0 | 142 | 89 | 122 | 137 | 177 | 163 |
| | | 15 | 406 | 292 | 347 | 261 | 196 | 272 |
| | | 30 | 351 | 312 | 322 | 289 | 290 | 308 |
| | | 60 | 243 | 199 | 218 | 174 | 197 | 233 |
| | | 120 | 197 | 114 | 209 | 178 | 158 | 186 |
| HFD | vehicle | 0 | 212 | 204 | 231 | 193 | 203 | 245 |
| | | 15 | 353 | 376 | 580 | 408 | 388 | 549 |
| | | 30 | 324 | 412 | 540 | 526 | 424 | 581 |
| | | 60 | 242 | 252 | 393 | 352 | 348 | 536 |
| | | 120 | 176 | 236 | 320 | 205 | 277 | 329 |
| HFD | 60 mpk 893 | 0 | 222 | 167 | 185 | 156 | | |
| | | 15 | 497 | 353 | 425 | 368 | | |
| | | 30 | 321 | 330 | 226 | 233 | | |
| | | 60 | 263 | 251 | 181 | 125 | | |
| | | 120 | 235 | 179 | 186 | 141 | | |
| HFD | 120 mpk 893 | 0 | 135 | 169 | 115 | 138 | | |
| | | 15 | 275 | 305 | 225 | 293 | | |
| | | 30 | 386 | 350 | 410 | 221 | | |
| | | 60 | 289 | 247 | 268 | 139 | | |
| | | 120 | 168 | 198 | 142 | 133 | | |

**Figure S2.2: 893 corrects metabolic defects in mice maintained on a high fat diet**

**a,b,** Liver (**a**) or quadriceps muscle (**b**) ceramide levels in mice fed a SD, HFD, or HFD + 120 mg/kg 893; n=4 in all groups. **c,** Glucose uptake in mouse embryonic fibroblasts after a 3 h treatment with vehicle (n=4) or 893 (5 μM (n=4) or 10 (n=3) μM). **d**, Blood glucose measurements from individual mice for the oral glucose tolerance test (OGTT) shown in main Fig. 2g. **e,f** Blood glucose levels (**e**) or area under the curve (AUC, **f**) during an OGTT performed when 893 levels were at their peak (4 h after dosing) or trough (24 h after dosing); n=4 for both groups. In **a-c**, **e**, and **f**, means ± SEM shown. Using a one-way ANOVA with Tukey's correction (**a-c**) or an unpaired, two-tailed t test (**e**,**f**),*, $P < 0.05$; **, $P < 0.01$; ***, $P < 0.001$; unmarked, not significant, $P > 0.05$.

## Figure S2.3

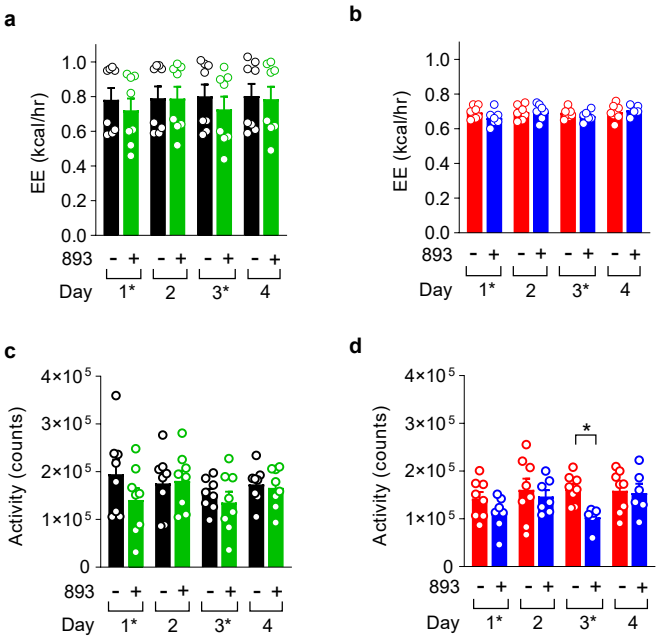


**Figure S2.3: 893 reduces the respiratory exchange ratio**
**a,b,** Average energy expenditure between ZT12 and ZT24 in mice fed a SD (**a**) or a HFD (**b**) for 10 weeks and then treated with either vehicle (n=8) or 120 mg/kg 893 (n=8) by gavage on days 1 and 3 (*). **c,d,** As in (**a,b**) but showing activity measured by XY beam breaks by mice fed a SD (**c**) or a HFD (**d**) and treated with either vehicle (n=8) or 120 mg/kg 893 (n=8). Means ± SEM shown. Using an unpaired, two-tailed t test to compare ± 893, *, $P \leq 0.05$; unmarked, not significant, $P > 0.05$.

## Figure S2.4

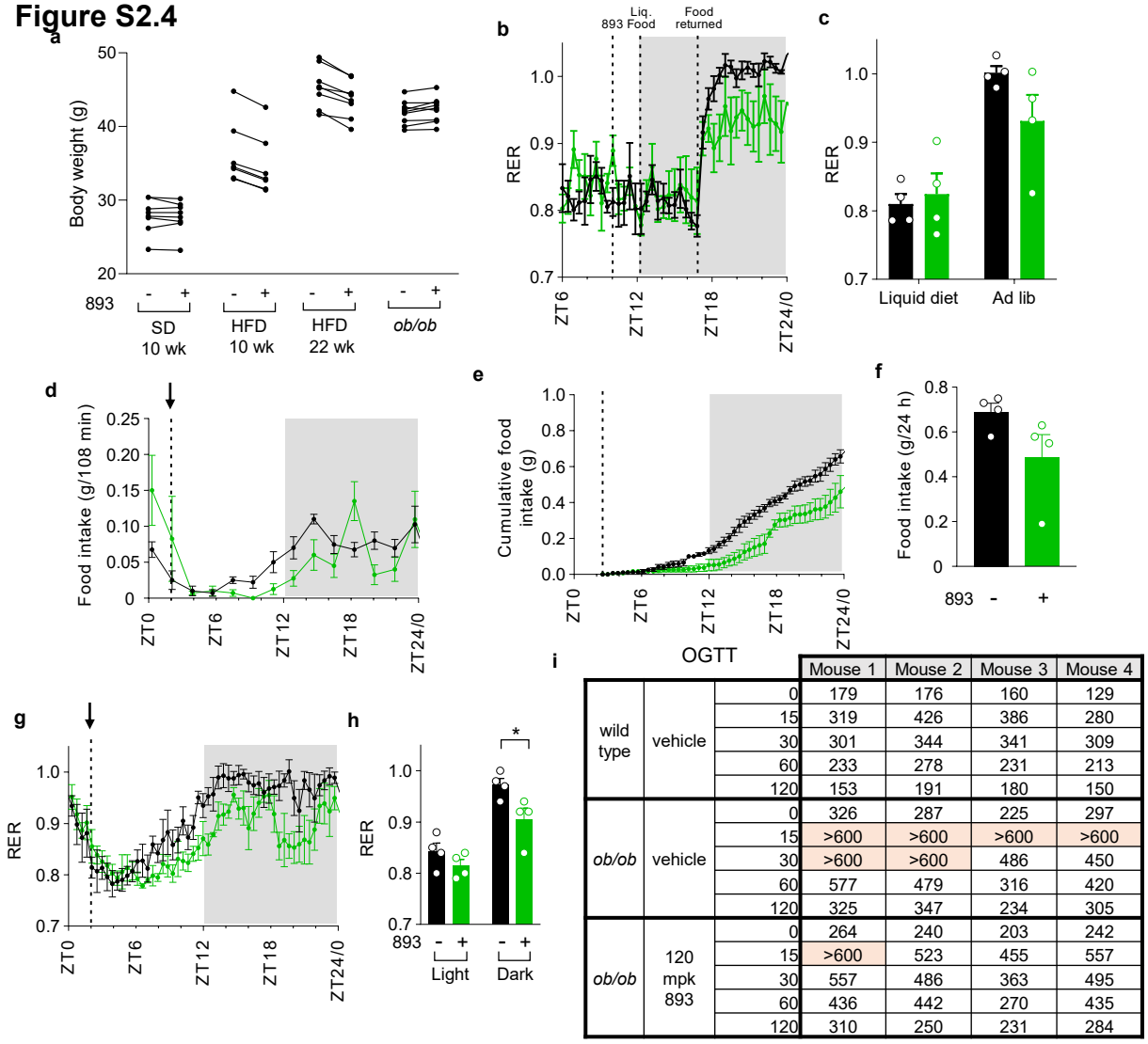


i

| | | | Mouse 1 | Mouse 2 | Mouse 3 | Mouse 4 |
|---|---|---|---|---|---|---|
| wild type | vehicle | 0 | 179 | 176 | 160 | 129 |
| | | 15 | 319 | 426 | 386 | 280 |
| | | 30 | 301 | 344 | 341 | 309 |
| | | 60 | 233 | 278 | 231 | 213 |
| | | 120 | 153 | 191 | 180 | 150 |
| *ob/ob* | vehicle | 0 | 326 | 287 | 225 | 297 |
| | | 15 | >600 | >600 | >600 | >600 |
| | | 30 | >600 | >600 | 486 | 450 |
| | | 60 | 577 | 479 | 316 | 420 |
| | | 120 | 325 | 347 | 234 | 305 |
| *ob/ob* | 120 mpk 893 | 0 | 264 | 240 | 203 | 242 |
| | | 15 | >600 | 523 | 455 | 557 |
| | | 30 | 557 | 486 | 363 | 495 |
| | | 60 | 436 | 442 | 270 | 435 |
| | | 120 | 310 | 250 | 231 | 284 |

**Figure S2.4: 893 reduces food intake**

**a,** Body weight before or 24 h after treatment with 120 mg/kg 893 p.o.; values from individual mice are connected by a line. Wild type mice were maintained on the SD or HFD for the indicated interval (n=8); *ob/ob* mice eating a 16% kcal from fat chow diet (n=9) were 9 weeks of age. **b,c**, RER of SD-fed mice where food pellets were removed at ZT9, mice were treated with vehicle (n=4) or 120 mg/kg 893 (n=4) by gavage at ZT8.5, and then gavaged with 0.4 kcal of liquid diet at ZT12. Access to food pellets was restored at ZT16. Continuous (every 27 min, **b**) or average (**c**) measurements shown for liquid diet (ZT12-ZT16) or ad libitum consumption of pellets (ZT16-ZT24). **d-f,** Food intake of mice eating the SD and treated with vehicle (n=4) or 120 mg/kg 893 (n=4) p.o. at ZT2 showing the averages of 4 measurements over 108 min (**d**), cumulative intake (**e**), or the total consumed between ZT2 and ZT24 (**f**). **g,h,** Average RER every 27 min (**g**) or averaged between ZT0 and ZT12 (light) or ZT12 and ZT24 (dark) (**h**) in the same mice as in (**d-f**). **i**, Blood glucose values for individual mice used in OGTT shown in main Fig. 5l. Mice were deprived of food at ZT4, treated with 120 mg/kg 893 p.o. at ZT6, and the OGTT performed 4 h later at ZT10. In **b-h**, means ± SEM shown. Using two-tailed, unpaired t test in (**c**, **f**, and **h**), *, $P \leq 0.05$; unmarked comparisons are not significant, $P > 0.05$.

**Figure S2.5**

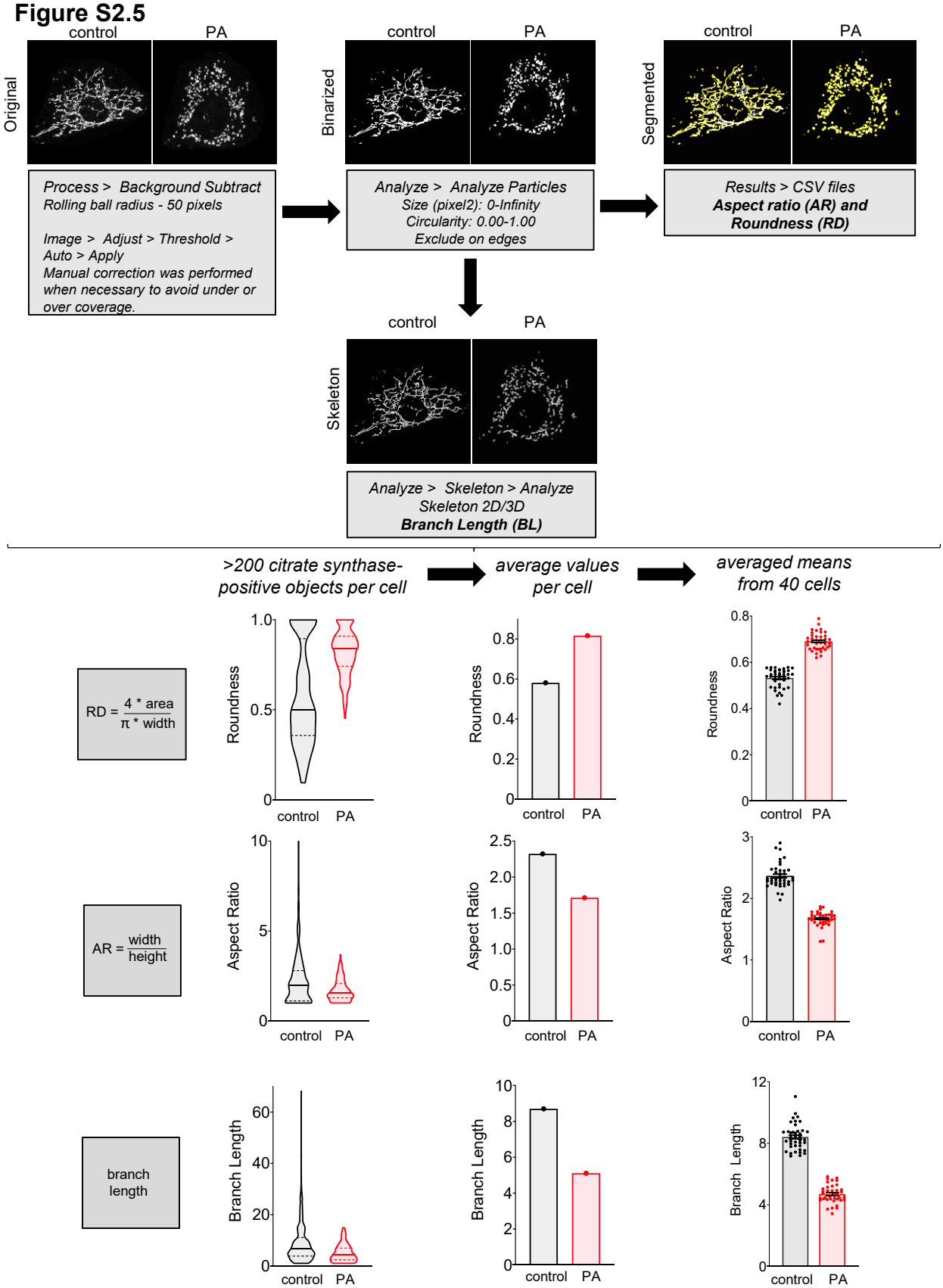
control
PA
Original
Binarized
Segmented
Process > Background Subtract
Rolling ball radius - 50 pixels
Image > Adjust > Threshold >
Auto > Apply
Manual correction was performed
when necessary to avoid under or
over coverage.
Analyze > Analyze Particles
Size (pixel2): 0-Infinity
Circularity: 0.00-1.00
Exclude on edges
Results > CSV files
Aspect ratio (AR) and
Roundness (RD)
Skeleton
Analyze > Skeleton > Analyze
Skeleton 2D/3D
Branch Length (BL)
>200 citrate synthase-positive objects per cell
average values per cell
averaged means from 40 cells
RD = 4 * area / π * width
AR = width / height
branch length
Roundness
Aspect Ratio
Branch Length

**Figure S2.5: Strategy for morphometric analysis of mitochondrial networks in vitro**
Representative images of citrate synthase staining in MEFs treated with vehicle (left panel) or palmitate (PA, right panel). Images are maximum intensity Z-projections derived from 8 Z-slices. Binarized mitochondrial networks were segmented to tag individual objects. Aspect ratio (tubule width/length) as well as roundness ((4 × area)/(π × width)) were measured from the all citrate synthase-positive objects on a per cell basis. Skeletonized networks were used to quantify branch length of the tubules.

## Figure S2.6

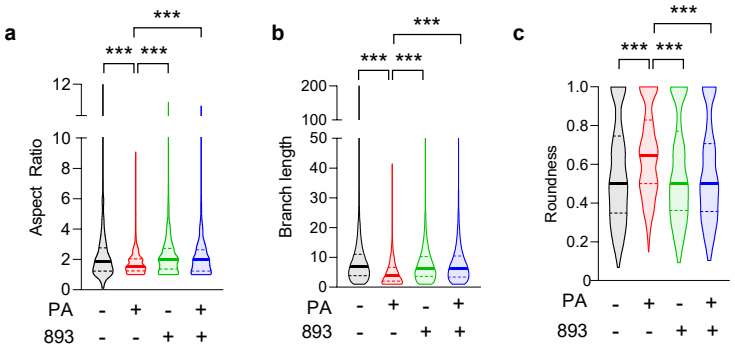


**Figure S2.6: 893 prevents palmitate-induced mitochondrial fission.**
**a-c**, MEFs were pre-treated with vehicle or pre-treatment with 5 μM 893for 3 h and then treated with BSA or 250 μM BSA-palmitate for an additional 3 h. Cells were then fixed, stained for citrate synthase, and analyzed as described in Extended Data Fig. 5. Data for individual citrate synthase-positive objects from 20 cells from 2 biological replicates (3,000-8,000 objects) shown. Complements main Fig. 6b-d where average values from 40 cells from 2 biological replicates are shown.

## Figure S2.7

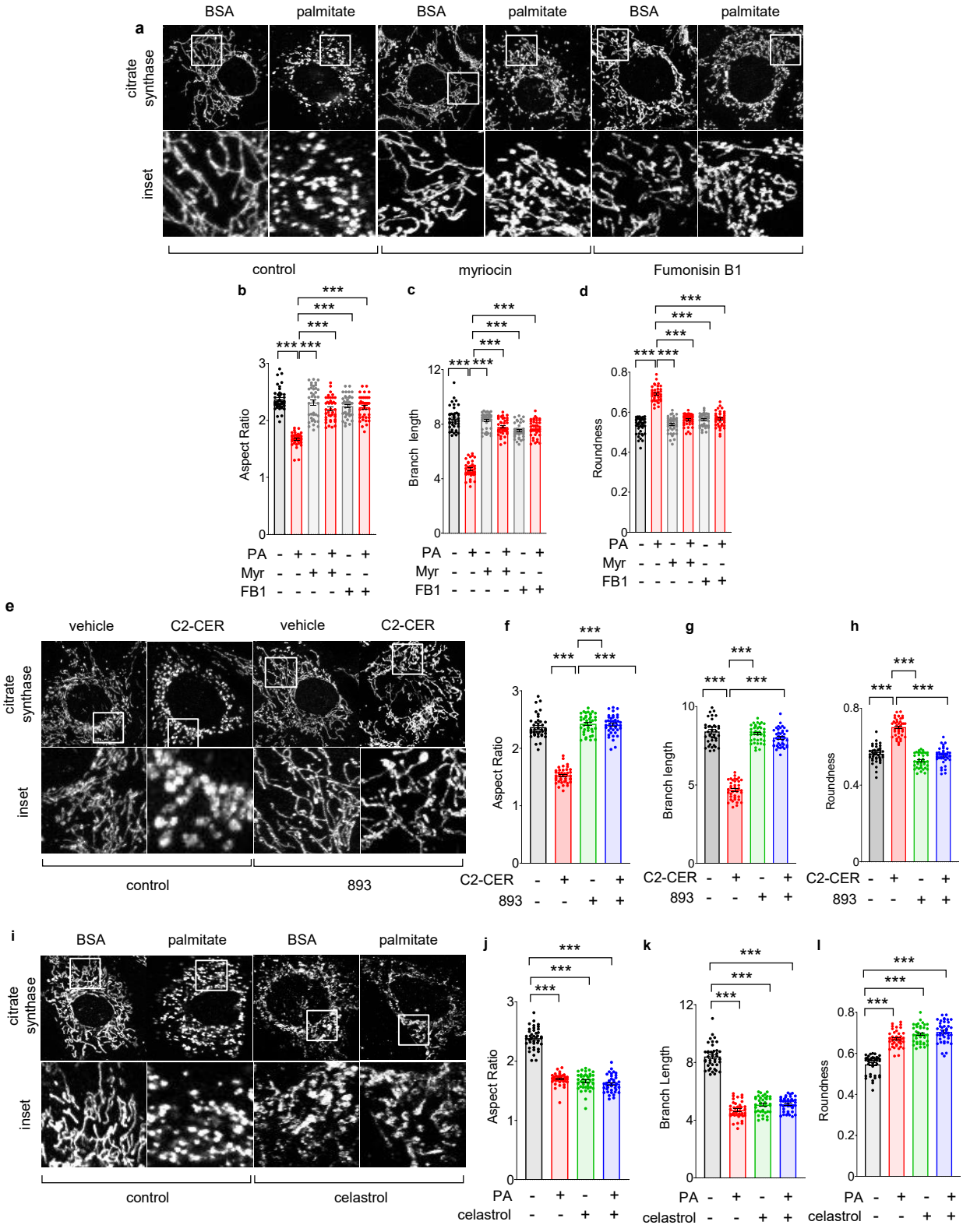
a
BSA
palmitate
BSA
palmitate
BSA
palmitate
citrate synthase
inset
control
myriocin
Fumonisin B1
b
Aspect Ratio
PA
Myr
FB1
c
Branch length
d
Roundness
e
vehicle
C2-CER
vehicle
C2-CER
citrate synthase
inset
control
893
f
Aspect Ratio
C2-CER
893
g
Branch length
h
Roundness
i
BSA
palmitate
BSA
palmitate
citrate synthase
inset
control
celastrol
j
Aspect Ratio
PA
celastrol
k
Branch Length
l
Roundness

**Figure S2.7: 893 reverses unbalanced mitochondrial fission.**
**a**, After a 3 h pre-treatment with Fumonisin-B1 (FB1, 30 μM) or myriocin (Myr, 10 μM), MEFs were treated for 3 h with BSA in vehicle (ethanol) or BSA-conjugated palmitate (250 μM) and stained for citrate synthase. **b-d,** Aspect ratio (**b**), branch length (**c**), and roundness (**d**) in the cells in (**a**); 40 cells were evaluated from 2 biological replicates. **e-h,** As in (**a-d**) but in MEFs pre-treated with vehicle or 893 (5 μM) for 3 h then treated with vehicle (DMSO) or C2-ceramide (50 μM) for an additional 3 h; 40 cells from 2 biological replicates examined. **i-l,** As in (**a-d**) but in MEFs pre-treated with vehicle or celastrol (500 nM); 40 cells from 2 biological replicates examined. Using a one-way ANOVA and Tukey's correction, ***, $P \leq 0.001$; unmarked, not significant, $P > 0.05$.

## Figure S2.8

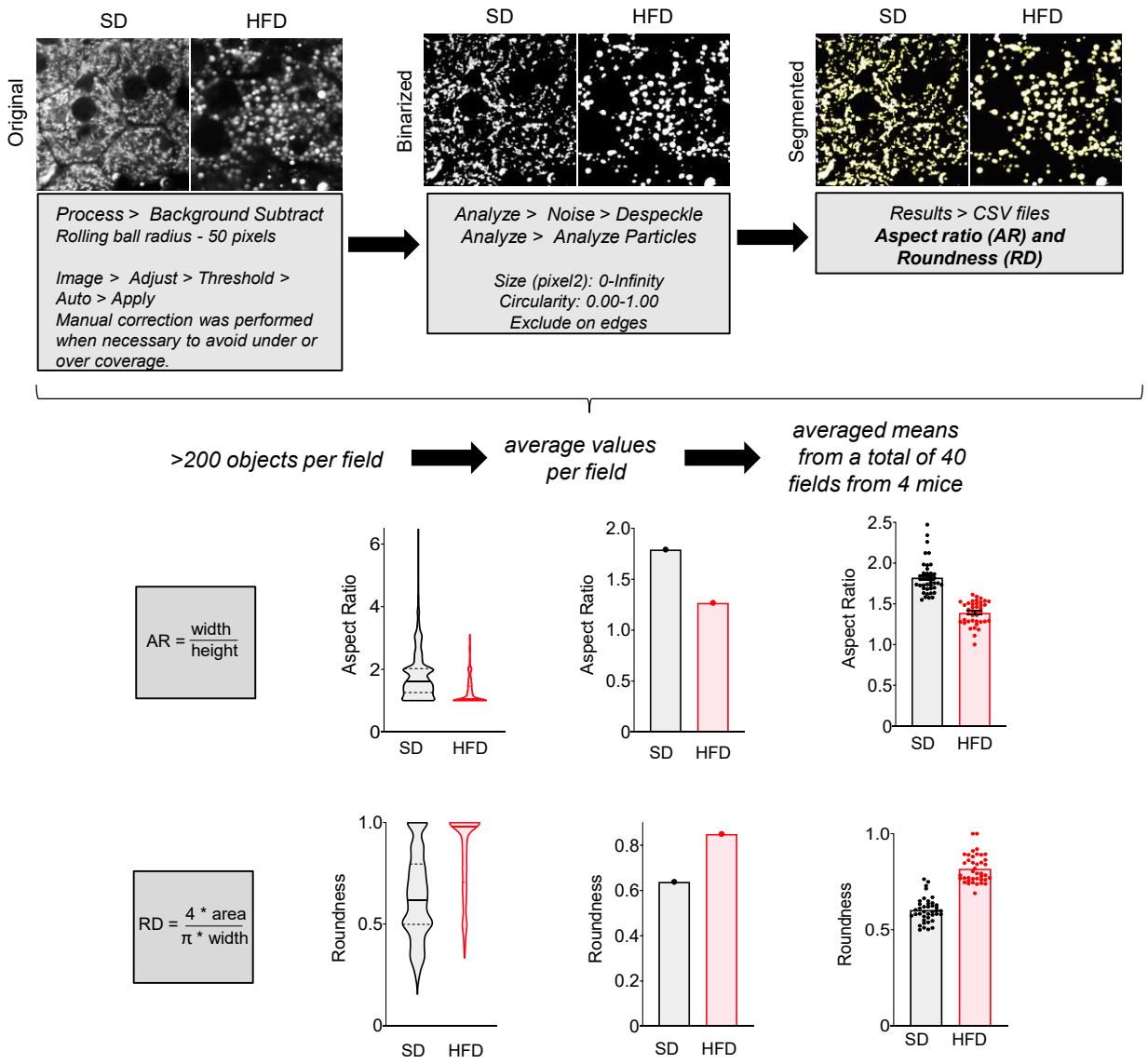


**Figure S2.8: Strategy for morphometric analysis of hepatic mitochondrial networks in vivo.**
Mitochondrial networks were visualized in freshly resected livers from mice fed a SD (left panel) or a HFD (right panel) using NADH/NADPH autofluorescence. Images are maximum intensity Z-projections derived from 6 Z-slices. Binarized mitochondrial networks were segmented to tag individual objects. Aspect ratio (tubule width/length) as well as roundness (4 × area/π × width) were measured on a per field basis. In main Fig. 7b,c, graphs represent 5,000-20,000 data points averaged from 6-8 fields of view taken from each of 4 mice per group.

## Figure S2.9

| | Fig 7b | Fig 7c |
|---|---|---|
| Vehicle:SD vs. 893:SD | 0.7738 | 0.9017 |
| Vehicle:SD vs. Vehicle:HFD | <0.0001 | <0.0001 |
| Vehicle:SD vs. 893:HFD | 0.7366 | 0.6457 |
| Vehicle:SD vs. Vehicle:OBOB | <0.0001 | <0.0001 |
| Vehicle:SD vs. 893:OBOB | <0.0001 | 0.0062 |
| 893:SD vs. Vehicle:HFD | <0.0001 | <0.0001 |
| 893:SD vs. 893:HFD | >0.9999 | 0.1077 |
| 893:SD vs. Vehicle:OBOB | <0.0001 | <0.0001 |
| 893:SD vs. 893:OBOB | <0.0001 | 0.0001 |
| Vehicle:HFD vs. 893:HFD | <0.0001 | <0.0001 |
| Vehicle:HFD vs. Vehicle:OBOB | <0.0001 | <0.0001 |
| Vehicle:HFD vs. 893:OBOB | <0.0001 | <0.0001 |
| 893:HFD vs. Vehicle:OBOB | <0.0001 | 0.0053 |
| 893:HFD vs. 893:OBOB | <0.0001 | 0.3009 |
| Vehicle:OBOB vs. 893:OBOB | 0.9507 | 0.6928 |

**Figure S2.9: Statistical analysis of mitochondrial networks in vivo**
*P*-values for Figure 2.7b and c using a one-way ANOVA and Tukey's correction.

# CHAPTER 3

## Summary and Conclusions

### 3.1 Summary of results

The aim of this work was to examine the utility of synthetic sphingolipid 893 in the treatment of diet-induced obesity. We demonstrated that, in a dose dependent manner, 893 was able to reverse excessive adiposity on a high fat diet, correlating to a resolution of hepatic steatosis and glucose intolerance. Importantly, mice treated with 893 showed no difference in their willingness to engage in voluntary exercise and providing a running wheel further enhanced the effects of 893 on body composition. Whole body metabolism in 893-treated mice was shifted towards a more oxidative state, in agreement with previous observations *in vitro* (S. M. Kim et al., 2016). The observed changes in metabolism were at least partially attributable to a reduction in food intake in a manner that correlated to adiposity in DIO mice, suggestive of re-sensitization to leptin and/or insulin. Chronic consumption of a HFD promotes excessive mitochondrial fission, which underlies both leptin and insulin resistance. 893 blocked saturated fatty acid-induced recruitment of Drp1 and mitochondrial fragmentation, and the ability for 893 to cause weight loss correlated with the ability to enhance mitochondrial fusion *in vivo.* In summary, the work here implies that 893 likely promotes weight-loss through its ability to oppose mitochondrial fusion, thereby promoting satiety and whole-body changes in metabolism.

In DIO mice, the reduction in food intake likely contributed to the changes observed in metabolism, given that pair-feeding mice to the amount consumed after 893 treatment recapitulated the shift to oxidative metabolism, and 893 failed to further decrease RER when caloric intake was normalized (Figure S2.4c). Paradoxically, although 893 still exerted strong anorectic effects in *ob/ob* mice they were resistant to weight loss (Figure 2.5i). A decrease in food consumption without a change in bodyweight implies that either the metabolizable energy of the diet decreased or, more likely, total energy output decreased. Indeed, pair feeding *ob/ob* mice to the level of those treated with recombinant leptin does not fully recapitulate the weight loss observed upon leptin repletion, likely because leptin also enhances energy expenditure (Levin, Nelson, Gurney, Vandlen, & de Sauvage, 1996). While we didn't detect an increase in overall energy expenditure in DIO mice, our experiment was not designed in such a way to resolve individual components of total daily energy expenditure (TDEE). Contributions to TDEE come from basal metabolic rate (BMR), thermoregulation, the energy expenditure associated with food intake (referred to as the thermic effect of food, or TEF), and physical activity. Thus to accurately measure BMR, an animal must therefore be euthermic, at rest, and in the post-absorptive state (Speakman, 2013). As we did not perform measurements under extended periods of fasting, 893-induced decreases in food intake would decrease the TEF, in which may mask any upregulation in other components of EE. That is, if 893 was altering BMR or thermogenic metabolism, it would appear as if there was no difference observed. This could be possible, as mitochondrial fusion is associated with an increased oxidative capacity, and mice with liver-specific Drp1 knockout, which would limit fission, have an increased rate

of EE (Wang et al., 2015). It follows that if 893-induced blockade in mitochondrial fission is contributing to weight loss, then 893 shouldn't provide benefit if mitochondria were already tubulated to begin with. The lack in weight loss in *ob/ob* mice, whose mitochondria were not fragmented like those of DIO mice at similar adiposity (Figure 2.7a,d), is consistent with the model that 893-induced decreases in mitochondrial fission are necessary to promote weight loss. In *ob/ob* mice, the complete lack of leptin creates an apparent "starvation" phenotype and considering starvation promotes hepatic mitochondrial fusion (Gomes, Di Benedetto, & Scorrano, 2011), this could conceivably explain why their liver mitochondria were not fragmented. Alternatively, the lack of fragmentation may be explained by the circadian regulation of mitochondrial morphology (Jacobi et al., 2015; Schmitt et al., 2018). Circadian clock genes and their downstream targets exhibit dampened rhythmicity in both DIO and *ob/ob* mouse livers (Ando et al., 2011; Jacobi et al., 2015). Leptin administration in *ob/ob* mice rescues the oscillations in core clock genes such as *Clock* and *Bmal1,* while calorie restriction alone has no effect. Liver-specific Bmal1 knockout hepatocyte mitochondria show no rhythmicity in mitochondrial dynamics and cannot adapt to nutritional challenges (Jacobi et al., 2015). Therefore, it is possible that the defect in clock gene regulation of the fusion and fission machinery in leptin-deficient animals is sufficient to explain the difference in mitochondrial morphology. In all, while the mechanism is not well defined, our data and that of others suggests that mitochondrial fragmentation may not be the primary driver of weight gain and metabolic dysfunction in *ob/ob* mice.

The molecular mechanism by which 893 lowers food intake remains unclear. Because the degree of suppression was greater in DIO mice, this suggested that 893 engaged signaling pathways that communicate energy stores and thus we turned our attention to leptin. Interestingly, after prolonged treatment the body weight of the 893 treated group plateaued at that of the standard chow group, corresponding to when fat mass was normalized. As leptinemia decreases as fat stores are depleted, and reduction of leptin can restore endogenous leptin sensitivity in DIO mice, this suggests that weight loss occurred in a leptin-dependent manner (Enriori et al., 2007; Zhao et al., 2019). In lean mice, exogenous leptin had no effect but in combination with 893 trended toward a larger reduction in food intake and bodyweight than just 893 alone (Figure 2.5). While suggestive of leptin sensitization, it is difficult to interpret the results without knowing the baseline circulating levels of leptin in these mice. The lack of response to leptin alone possibly was a result of intra-peritoneal administration, as leptin is maximally effective when delivered intracerebroventricularly (Halaas et al., 1997). It is not known why leptin fails to induce a response in leptin resistant animals, but has been hypothesized to be a result of either an inability for leptin to cross the blood brain barrier, or impaired signal transduction downstream of receptor engagement (Münzberg & Myers, 2005). However, 893's anorectic effects in *ob/ob* mice suggested that food intake suppression was at least partially independent of leptin or occurred downstream of leptin signaling. To more rigorously address this model, future experiments should address the effects that 893 has on circulating leptin levels and its downstream signaling cascade in both leptin-deficient and leptin-replete states. Although leptin is the prototypic adiposity signal, feeding behavior can also be controlled by insulin. Mice

lacking the insulin receptor in neurons become hyperphagic and obese (Brüning et al., 2000). As is the case for leptin, POMC and AgRP neurons express the insulin receptor (Varela & Horvath, 2012). In fact, many of the same perturbations to mitochondrial dynamics that affect leptin sensitivity also apply to insulin in various tissues (Nasrallah & Horvath, 2014). It is possible that these two signaling nodes exert coordinated actions to control feeding behavior and metabolic homeostasis, as both the leptin and insulin signaling pathways converge to promote POMC transcription and processing into a-MSH, which acts on downstream target neurons to reduce food intake (Benoit et al., 2002; Brown, Clegg, Benoit, & Woods, 2006). Re-sensitization to leptin and/or insulin could be directly tested by performing electrophysiological assays on populations of ARC neurons in response to hormones +/- 893. However, it has been suggested that receptors for leptin and insulin aren't necessarily co-expressed on the same POMC neuron, rather they exist in distinct anatomical regions of the ARC (Williams et al., 2010). Moreover, not all POMC cells are activated in response to hormonal stimulation; for example, insulin can have opposite effects on POMC neurons, either hyper-polarizing or de-polarizing them (Varela & Horvath, 2012; Williams et al., 2010). Thus, for further insight, single-cell transcriptomics could be used to define both the neuronal populations that 893 affects and what pathways are engaged. In summary, 893 suppresses appetite possibly through effects on neuronal control of feeding by blocking mitochondrial fission and further experiments will be aimed at defining the precise changes that 893 exerts on signaling in various populations of hypothalamic neurons.

### 3.2 Speculations into mechanism

Precisely how 893 is able to maintain a fused mitochondrial network under conditions of over nutrition remains to be determined; 893-induced mitochondrial elongation likely results from a decrease in mitochondrial fission. Although we do not directly rule out a concomitant increase in mitochondrial fusion, our data suggests that 893 blocks PA-induced Drp1 recruitment to the mitochondria (Figure 2.6e,f). Drp1 recruitment and activity at the mitochondria is highly dependent on a series of post translational modifications that occur in response to different stimuli. Drp1 is primarily diffuse in the cytosol but is recruited to fission sites by adaptor proteins such as Mff, allowing Drp1 to oligomerize into helical complexes to constrict mitochondria (Friedman et al., 2011; Otera et al., 2010). Our previous studies have demonstrated that 893 induces nutrient stress downstream activation of PP2A, and both nutrient stress and PP2A activity could plausibly affect mitochondrial dynamics. Under conditions of nutrient stress mitochondria elongate into tubular structures due to a reduction of Drp1 recruitment and unopposed fusion (Gomes et al., 2011), in support of the latter hypothesis. Alternatively, a PP2A-dependent mechanism may be involved either by directly de-phosphorylation of Drp1, of upstream regulators that would prevent Drp1 recruitment. We observed that other PP2A activators that phenocopy the effects of 893 on endosomal trafficking 893 do not protect from PA-induced mitochondrial fragmentation (data not shown). Ceramide also activates PP2A but enhances mitochondrial fission by binding to Mff and promoting Drp1 recruitment (Dobrowsky, Kamibayashi, Mumby, & Hannun, 1993; Hammerschmidt et al., 2019). A PP2A-

dependent mechanism may be valid if 893 were activating a distinct subset of PP2A heterotrimers, a plausible hypothesis considering both ceramide and 893 have differing effects on Akt (Kubiniok et al., 2019; S A Summers, Garza, Zhou, & Birnbaum, 1998). Interestingly, treatment of rat adrenal tumor cells with the small molecule PP2A inhibitors okadaic acid (OA) and calyculin A (CA) increase Drp1 phosphorylation at unknown sites (Cribbs & Strack, 2007). These molecules are selective for PP2A at low doses but are by no means specific as both molecules can inhibit PP1, PP2A, and other PPP family members at nanomolar concentrations (Swingle, Ni, & Honkanen, 2007). Moreover, they are extremely cytotoxic which precludes their use in many functional assays. In fact, manipulating PP2A activity in most cells is lethal further complicating the use of traditional genetic approaches to validate this mechanism of action. Our previous attempts to demonstrate necessity for PP2A have included the use of small molecules like OA and CA, as well as shRNAs against various different subunits of the PP2A holoenzyme, have not been successful largely due to either lethality or clonal adaptation to PP2A manipulation. New technologies are now available that facilitate temporal control of gene and protein expression, such as CRISPRi/a and auxin-inducible degron (AiD) systems. Current efforts in our lab are directed towards establishing stable cell lines using these technologies which would allow us to more readily tease apart the contributions of PP2A to the activity of 893. In all, results from the work shown here suggest a mechanism independent of PP2A and definitive experiments are in progress.

With the assumption that 893 has other molecular targets besides PP2A, our lab has performed rigorous unbiased chemoproteomics screens to identify direct protein targets of 893. The only PP2A component identified was Ppp2r1a, one of two isoforms of the scaffolding subunit. Even so, it was not the most highly enriched target, and multiple members of the importin-β family of nuclear import proteins were identified. 893 dramatically excludes a number of proteins from the nucleus, suggesting that 893 inhibits this subset of importins. FoxO1 is phosphorylated downstream of insulin signaling leading to its nuclear exclusion, and this is necessary for insulin and leptin to reduce food intake (M.-S. Kim et al., 2006). Conversely, silencing FoxO1 is sufficient to reduce food intake (Ropelle et al., 2009). FoxO1 is able to antagonize leptin signaling by binding to STAT3 and prevents it from activating *Pomc* transcription (Yang et al., 2009). Is possible that through binding importins 893 excludes FoxO1 from the nucleus, which in turn would relieve STAT3 inhibition and promote POMC expression. This proposed mechanism would possibly occur independent of changes in mitochondrial dynamics and offers an alternative explanation to the discordant results on food intake in *ob/ob* mice.

Aside from importins, an intriguing target identified in our chemoproteomic assays was voltage-dependent anion channel 2 (VDAC2), a voltage-gated channel that localizes to the outer mitochondrial membrane (OMM). In mice and humans there are 3 VDAC isoforms having about 75% sequence similarity (Naghdi & Hajnóczky, 2016). All VDACs have been isolated in mitochondrial associated membrane (MAM) fractions of

the ER, regions where the two organelles interact to coordinate $Ca^{2+}$ transfer from the ER to the mitochondria (Naghdi & Hajnóczky, 2016; Rowland & Voeltz, 2012). What effect would this have on mitochondrial dynamics? There is debate within the field regarding the relationship between MAMs and mitochondrial morphology. Both enhanced MAM formation and MAM disruption have been observed under conditions of metabolic dysfunction, implying that the role for these domains is much more nuanced and is likely to be context dependent. However, given that changes in MAMs underlies both insulin resistance and leptin resistance, and 893 may directly interact with a MAM associated protein like VDAC2, one hypothesis is that 893 may inhibit VDAC2 and decrease ER-mitochondrial contact sites. Probing whether 893 inhibits calcium uptake by the mitochondria would be informative in this sense. MAMs are not only important for $Ca^{2+}$ homeostasis but are also platforms necessary for phospholipid synthesis, and many lipid synthesizing enzymes are enriched in MAMs (Flis & Daum, 2013). Notably, in our unbiased hepatic lipidomics, the most significantly increased species in HFD + 893 treated livers were particular phosphatidylglycerol (PG) lipids. PG lipids are precursors for cardiolipin (CL) which compose a significant fraction of mitochondrial phospholipids, although PG lipids do not appear to accumulate under normal conditions (Osman, Voelker, & Langer, 2011). In yeast, CL is exclusively synthesized in the mitochondrial inner membrane (IMM) from PG by the enzyme Cls1 (Flis & Daum, 2013). Disruption of phosphatidylglycerophosphate synthase (PGS) causes PG and CL deficiency, and this mutant yeast strain shows impaired mitochondrial oxidative metabolism suggesting dysfunctional, fragmented mitochondria (Chang, Heacock, Clancey, & Dowhan, 1998). However not much is known about a direct role of PG in

mitochondrial dynamics in mammalian cells. One hypothesis is that 893-induced accumulation of PG could be a result of decreased MAMs, preventing PG from reaching the IMM where CL synthesis occurs. Notably, Drp1 interacts with CL and this may facilitate membrane constriction and fission (Dudek, 2017; Stepanyants et al., 2015). Thus, it is possible that 893 decreases Drp1 recruitment by limiting PG remodeling into CL. In all, the above data suggests that 893 may cause a decrease in ER-mitochondria contact sites, altering ion and/or lipid exchange, which could explain how 893 maintains mitochondria in a tubulated state.

### 3.3 Implications for the treatment of metabolic diseases

Past and current pharmacologic approaches that target satiety have had poor safety profiles resulting from targeting pleotropic neuronal pathways. Drugs that target the release of neurotransmitters such as serotonin (5-HT) have been pursued given that they can be potent appetite suppressors (Garfield & Heisler, 2009). However this approach has been met with high risk and little reward owing to toxicities associated to systemic accumulation of 5-HT (Fishman, 1999), exemplified by the rapid ban of the fen/phen combination due to high risk of pulmonary hypertension and valvular heart disease (Garfield & Heisler, 2009; Rodgers, Tschöp, & Wilding, 2012). These serotonergic agents elicit their appetite suppressive effects by inhibiting AgRP neurons and stimulating POMC neurons through specific 5-HT receptor family members (Heisler et al., 2002, 2006). Although engaging this pathway would enhance anorectic melanocortin signaling independent of leptin, the modest weight loss from the use of

more selective 5-HT receptor agonists like the recently approved Lorcaserin in the absence of long-term safety data poses more risk relative to benefit. Our data suggests that 893 engages satiety by enhancing leptin and/or insulin sensitivity by restoring mitochondrial fusion, but we have not ruled out any effects on 5-HT activity. We have shown that the acute administration of 893 does not affect heart-rate (Perryman et al., 2016), but further validation of cardiovascular safety is required before conclusions can be drawn. Centrally acting agents have also garnered concern due to increased risks of psychiatric adverse events such as anxiety and suicide (Sam, Salem, & Ghatei, 2011). 893 treated mice appear overtly normal to blinded individuals, although psychological distress is difficult to observe in animals without controlled behavioral assays. However, our data measuring voluntary wheel running activity does not suggest any adverse effects as anxiety can manifest in mice as changes in physical activity. Additionally, a comprehensive blood chemistry panel previously performed after 11 weeks of chronic treatment with 893 did not indicate systemic toxicity. As this was performed in a GEMM of aggressive prostate cancer, these results should be validated in both obese and healthy lean mice. Although the precise target is unknown, 893 appears to have a very good safety profile likely owing to the oscillating levels in the blood; constitutive mitochondrial fusion in excess of fission would surely have its ramifications. Most studies rely on stable knockout of the fusion/fission machinery making it difficult to evaluate the tolerability of preventing fission, although thus far the effects on metabolic health observed are largely beneficial (Wai & Langer, 2016). In summary, the excellent drug properties and potentially novel mechanism of action of 893 may be a safe and

effective approach to enhance satiety, warranting longer term studies to evaluate chronic safety.

It is well established that positive energy balance causes obesity, but it is largely disputed whether relative macronutrient content plays a considerable role. There is a correlation between the rise of obesity and an increase in sugar consumption, similar to that seen with fat (Softic, Cohen, & Kahn, 2016). Considering the ubiquity of heavily sweetened beverages and added sugars in most processed foods, intervention studies in both high fat and high sugar models would be informative (Softic et al., 2016). High intake of fructose in particular promotes non-alcoholic fatty liver disease (NAFLD), defined as excessive hepatic fat accumulation in the absence of prior liver disease in humans (Softic et al., 2016). NAFLD is part of the sequelae associated with HFD-induced obesity. However, at least in mice, high fructose diets alone do not cause obesity, although they do accelerate weight gain when combined with a HFD (Shapiro et al., 2008). Excess dietary fructose is shunted to the liver where it promotes de-novo lipogenesis, where if prolonged can cause progressive damage to mitochondria (Jegatheesan & De Bandt, 2017; Softic et al., 2019). By blocking mitochondrial fission, 893 may increase the metabolic flexibility of hepatic mitochondria by allowing them to oxidize excess lipids. It has been speculated that disruption of MAMs could promote the progression of NAFLD to more severe forms of hepatic disease such as non-alcoholic steatohepatitis (NASH), hepatocellular carcinoma and cirrhosis (Léveillé & Estall, 2019; Tubbs et al., 2014). Notably, a decrease in hepatic Mfn2 is associated with progression to NASH in human patients (Hernández-Alvarez et al., 2019) which

would represent an imbalance of fission in mitochondrial networks. By limiting Drp1 recruitment 893 may tip the balance back towards proper levels of fusion and thus 893 may have the potential to prevent the onset of severe liver disease. An additional caveat of the HFD model implemented here is that the diets are fixed in composition. A feeding model that allows animals to choose from high fat, high sugar, or standard food would allow us to assess whether 893 alters feeding preference, as one possibility for the more profound decrease in food intake could be that 893 interferes with the reward value of high fat foods that are proposed to promote hyperphagia (Barrett, Mercer, & Morgan, 2016; Hu et al., 2018). In summary, testing 893 in other models of DIO would provide a greater understanding of its mechanism of action and would potentially increase its therapeutic impact.

Cancer is another disease that has been proposed to be promoted by excessive mitochondrial fission (Senft & Ronai, 2016). Cancer is characterized by unrestrained growth, which requires a large influx of nutrients for continued anabolism and survival. Many oncogenic mutations enhance the acquisition of amino acids, lipids and sugars, and rewire metabolic pathways to support sustained growth (Pavlova & Thompson, 2016). Activating mutations in RAS are some of the most commonly occurring mutations in a number of tumors promoting anabolic metabolism and proliferation (Pylayeva-Gupta, Grabocka, & Bar-Sagi, 2011). Activation of RAS promotes Drp1 phosphorylation and mitochondrial fission, and cells with oncogenic RAS mutations require Drp1 both for transformation and tumor growth (Kashatus et al., 2015; Serasinghe et al., 2015). A dependency on increased fission makes sense given the

role that mitochondrial dynamics plays in coordinating nutrient supply with metabolism, stress responses, and cell life/death (Liesa & Shirihai, 2013). Mitochondrial fission promotes a less “efficient” way of generating ATP but spares carbon from being fully oxidized, allowing it to instead be shunted into biosynthetic pathways. Thus, targeting mitochondrial dynamics may be a novel strategy to treat cancer. However, targeting a single pathway rarely leads to tumor eradication as most tumors acquire compensatory mutations and emerge as refractory disease. In the case of RAS tumors in which Drp1 activity is reduced, surviving tumor cells adapt by restoring glucose flux (Nagdas et al., 2019), suggesting that combining Drp1 inhibition with inhibitors of glucose uptake would be a strategy to avoid the inevitable drug resistance that comes from targeted monotherapies. Because 893 blocks mitochondrial fission in KRAS MEFs (Figure 2.6m) and also reduces glucose uptake (Figure S2.2c), 893 could act as a poly-pharmacological approach to treating RAS-driven tumors. Additionally, obesity is a risk factor for a number of different cancers on its own. Hyperlipidemia in DIO would provide readily available lipids to support tumor growth. For example, particularly aggressive prostate cancers require exogenous lipid uptake for their migration and survival and fulfil this need by upregulating fatty acid uptake (Watt et al., 2019; Yue et al., 2014). 893 downregulates LDL uptake and the LDLr in vitro, and in our prostate cancer GEMM 893 reduced total circulating cholesterol even in the absence of DIO (S. M. Kim et al., 2016). Given what we now know about mitochondria, it is uncertain how much of 893’s activity can be attributed to substrate limitation and/or mitochondrial morphology. Collectively, 893’s effects on mitochondrial dynamics and the decrease in adiposity observed likely contribute to its anticancer effects.

## 3.4 Broader Perspectives

The finding that 893 is able to oppose mitochondrial fission opens the opportunity to identify unexpected roles for endogenous sphingolipids other than ceramide in the regulation of metabolic homeostasis in both health and disease. While ceramides have been vilified as metabolites that accumulate in pathological states, structurally 893 is more closely related to sphingosine and phytosphingosine, and these sphingolipids may have distinct roles. One proposed hypothesis is that ceramides are a primary messenger indicating nutrient overload and initially act to defend cells from fatty-acid overload (Scott A. Summers, Chaurasia, & Holland, 2019). Under conditions of hyperlipidemia, exposing cells to free fatty acids may interfere with membrane integrity due to detergent like properties. Under these conditions, ceramide levels would increase and induce downregulation of nutrient transporters as a response to nutrient overload, possibly promoting the preferential use of fatty acids for ATP (Scott A. Summers et al., 2019). As ceramide also upregulates the fatty acid translocase CD36 (Xia et al., 2015), it may also increase fatty acid uptake and sequestration into TAGs. However, in the obese state where there is constitutive abundance of circulating nutrients, the capacity for adipocytes to store TAGs is exceeded and excess fatty acids spill over into sphingolipid synthesis pathways, further increasing ceramide generation to the point of excess (Chaurasia & Summers, 2015). Indeed, genetic and pharmacological interventions that limit ceramide generation and accumulation are almost unequivocally protective from obesity-associated comorbidities (Chaurasia & Summers, 2015). But what is less clear is the function of other sphingolipid metabolites

themselves. Surely, they are not just passive by-products of shifts in ceramide levels. This ceramide-centric view of SL metabolism is hard to dissociate for a number of reasons. Sphingolipids in general have greasy hydrophobic moieties, are rapidly metabolized and distributed among several different pathways with unique and sometimes opposing functions. Moreover, differential subcellular localization of metabolic enzymes and pools of distinct lipids complicate most biochemical analyses that use bulk cells. Because 893 is a structural analog, but isn't metabolized like endogenous sphingolipids, it may shed light onto the roles of these enigmatic signaling molecules. Although 893 and ceramide share PP2A as a target, the work here complements our previous observations highlighting that 893 is a distinct entity from ceramide. It may be that 893 may mimic one or more sphingolipid species; phytosphingosine and sphingosine which are intermediates in ceramide biosynthesis, also phenocopy the effects of 893 on endolysosomal trafficking (Perryman et al., 2016). Interestingly, supplementation of phytosphingosine in the diet can improve glucose homeostasis in mice and humans independent of changes in adiposity. One possibility is that the rheostat between ceramide and sphingosine (or some other sphingolipid) tunes the cellular response to energy status via its effects on the mitochondria, which is overridden by chronic nutrient excess. 893 may engage this signaling node and restore proper mitochondrial morphology. Collectively, sphingosine or phytosphingosine could also regulate mitochondrial dynamics and play a role in these diseases, and whether there are endogenous sphingolipids that share the effects of 893 is an intriguing possibility to be explored.

In conclusion, we identify a synthetic sphingolipid that is able to antagonize the detrimental effects of endogenous ceramide on mitochondrial dynamics. The findings here are of great interest considering the multitude of previous studies demonstrating the beneficial effects of reducing mitochondrial fission in metabolic disease. Given the high personal and economic burden from the growing obesity epidemic, characterizing the precise mechanism by which 893 ameliorates mitochondrial dysfunction could facilitate the development of safe and effective new anti-obesity agents. Moreover, because excessive mitochondrial fission can also drive neurodegenerative diseases, there may be value in exploring the utility of 893 for these debilitating conditions (Knott, Perkins, Schwarzenbacher, & Bossy-Wetzel, 2008).

## 3.5 References


Ando, H., Kumazaki, M., Motosugi, Y., Ushijima, K., Maekawa, T., Ishikawa, E., & Fujimura, A. (2011). Impairment of peripheral circadian clocks precedes metabolic abnormalities in ob/ob mice. *Endocrinology*, *152*(4), 1347–1354. doi:10.1210/en.2010-1068

Barrett, P., Mercer, J. G., & Morgan, P. J. (2016). Preclinical models for obesity research. *Disease Models & Mechanisms*, *9*(11), 1245–1255. doi:10.1242/dmm.026443

Benoit, S. C., Air, E. L., Coolen, L. M., Strauss, R., Jackman, A., Clegg, D. J., … Woods, S. C. (2002). The catabolic action of insulin in the brain is mediated by melanocortins. *The Journal of Neuroscience*, *22*(20), 9048–9052.

Brown, L. M., Clegg, D. J., Benoit, S. C., & Woods, S. C. (2006). Intraventricular insulin and leptin reduce food intake and body weight in C57BL/6J mice. *Physiology & Behavior*, *89*(5), 687–691. doi:10.1016/j.physbeh.2006.08.008

Brüning, J. C., Gautam, D., Burks, D. J., Gillette, J., Schubert, M., Orban, P. C., … Kahn, C. R. (2000). Role of brain insulin receptor in control of body weight and reproduction. *Science*, *289*(5487), 2122–2125. doi:10.1126/science.289.5487.2122

Chang, S. C., Heacock, P. N., Clancey, C. J., & Dowhan, W. (1998). The PEL1 gene (renamed PGS1) encodes the phosphatidylglycero-phosphate synthase of Saccharomyces cerevisiae. *The Journal of Biological Chemistry*, *273*(16), 9829–9836. doi:10.1074/jbc.273.16.9829

Chaurasia, B., & Summers, S. A. (2015). Ceramides - Lipotoxic Inducers of Metabolic Disorders. *Trends in Endocrinology and Metabolism*, *26*(10), 538–550. doi:10.1016/j.tem.2015.07.006

Cribbs, J. T., & Strack, S. (2007). Reversible phosphorylation of Drp1 by cyclic AMP-dependent protein kinase and calcineurin regulates mitochondrial fission and cell death. *EMBO Reports*, *8*(10), 939–944. doi:10.1038/sj.embor.7401062

Dobrowsky, R. T., Kamibayashi, C., Mumby, M. C., & Hannun, Y. A. (1993). Ceramide activates heterotrimeric protein phosphatase 2A. *The Journal of Biological Chemistry*, *268*(21), 15523–15530.

Dudek, J. (2017). Role of cardiolipin in mitochondrial signaling pathways. *Frontiers in cell and developmental biology*, *5*, 90. doi:10.3389/fcell.2017.00090

Enriori, P. J., Evans, A. E., Sinnayah, P., Jobst, E. E., Tonelli-Lemos, L., Billes, S. K., … Cowley, M. A. (2007). Diet-induced obesity causes severe but reversible leptin resistance in arcuate melanocortin neurons. *Cell Metabolism*, *5*(3), 181–194. doi:10.1016/j.cmet.2007.02.004

Fishman, A. P. (1999). Aminorex to fen/phen: an epidemic foretold. *Circulation*, *99*(1), 156–161. doi:10.1161/01.cir.99.1.156

Flis, V. V., & Daum, G. (2013). Lipid transport between the endoplasmic reticulum and mitochondria. *Cold Spring Harbor Perspectives in Biology*, *5*(6). doi:10.1101/cshperspect.a013235

Friedman, J. R., Lackner, L. L., West, M., DiBenedetto, J. R., Nunnari, J., & Voeltz, G. K. (2011). ER tubules mark sites of mitochondrial division. *Science*, *334*(6054), 358–362. doi:10.1126/science.1207385

Garfield, A. S., & Heisler, L. K. (2009). Pharmacological targeting of the serotonergic system for the treatment of obesity. *The Journal of Physiology*, *587*(1), 49–60. doi:10.1113/jphysiol.2008.164152

Gomes, L. C., Di Benedetto, G., & Scorrano, L. (2011). During autophagy mitochondria elongate, are spared from degradation and sustain cell viability. *Nature Cell Biology*, *13*(5), 589–598. doi:10.1038/ncb2220

Halaas, J. L., Boozer, C., Blair-West, J., Fidahusein, N., Denton, D. A., & Friedman, J. M. (1997). Physiological response to long-term peripheral and central leptin infusion in lean and obese mice. *Proceedings of the National Academy of Sciences of the United States of America*, *94*(16), 8878–8883. doi:10.1073/pnas.94.16.8878

Hammerschmidt, P., Ostkotte, D., Nolte, H., Gerl, M. J., Jais, A., Brunner, H. L., … Brüning, J. C. (2019). CerS6-Derived Sphingolipids Interact with Mff and Promote Mitochondrial Fragmentation in Obesity. *Cell*, *177*(6), 1536–1552.e23. doi:10.1016/j.cell.2019.05.008

Heisler, L. K., Cowley, M. A., Tecott, L. H., Fan, W., Low, M. J., Smart, J. L., … Elmquist, J. K. (2002). Activation of central melanocortin pathways by fenfluramine. *Science*, *297*(5581), 609–611. doi:10.1126/science.1072327

Heisler, L. K., Jobst, E. E., Sutton, G. M., Zhou, L., Borok, E., Thornton-Jones, Z., … Cowley, M. A. (2006). Serotonin reciprocally regulates melanocortin neurons to modulate food intake. *Neuron*, *51*(2), 239–249. doi:10.1016/j.neuron.2006.06.004

Hernández-Alvarez, M. I., Sebastián, D., Vives, S., Ivanova, S., Bartoccioni, P., Kakimoto, P., … Zorzano, A. (2019). Deficient Endoplasmic Reticulum-Mitochondrial Phosphatidylserine Transfer Causes Liver Disease. *Cell*, *177*(4), 881–895.e17. doi:10.1016/j.cell.2019.04.010

Hu, S., Wang, L., Yang, D., Li, L., Togo, J., Wu, Y., … Speakman, J. R. (2018). Dietary fat, but not protein or carbohydrate, regulates energy intake and causes adiposity in mice. *Cell Metabolism*, *28*(3), 415–431.e4. doi:10.1016/j.cmet.2018.06.010

Jacobi, D., Liu, S., Burkewitz, K., Kory, N., Knudsen, N. H., Alexander, R. K., … Lee, C.-H. (2015). Hepatic bmal1 regulates rhythmic mitochondrial dynamics and promotes metabolic fitness. *Cell Metabolism*, *22*(4), 709–720. doi:10.1016/j.cmet.2015.08.006

Jegatheesan, P., & De Bandt, J.-P. (2017). Fructose and NAFLD: The Multifaceted Aspects of Fructose Metabolism. *Nutrients*, *9*(3). doi:10.3390/nu9030230

Kashatus, J. A., Nascimento, A., Myers, L. J., Sher, A., Byrne, F. L., Hoehn, K. L., … Kashatus, D. F. (2015). Erk2 phosphorylation of Drp1 promotes mitochondrial fission and MAPK-driven tumor growth. *Molecular Cell*, *57*(3), 537–551. doi:10.1016/j.molcel.2015.01.002

Kim, M.-S., Pak, Y. K., Jang, P.-G., Namkoong, C., Choi, Y.-S., Won, J.-C., … Lee, K.-U. (2006). Role of hypothalamic Foxo1 in the regulation of food intake and energy homeostasis. *Nature Neuroscience*, *9*(7), 901–906. doi:10.1038/nn1731

Kim, S. M., Roy, S. G., Chen, B., Nguyen, T. M., McMonigle, R. J., McCracken, A. N., … Edinger, A. L. (2016). Targeting cancer metabolism by simultaneously disrupting parallel nutrient access pathways. *The Journal of Clinical Investigation*, *126*(11), 4088–4102. doi:10.1172/JCI87148

Knott, A. B., Perkins, G., Schwarzenbacher, R., & Bossy-Wetzel, E. (2008). Mitochondrial fragmentation in neurodegeneration. *Nature Reviews. Neuroscience*, *9*(7), 505–518. doi:10.1038/nrn2417

Kubiniok, P., Finicle, B. T., Piffaretti, F., McCracken, A. N., Perryman, M., Hanessian, S., … Thibault, P. (2019). Dynamic Phosphoproteomics Uncovers Signaling Pathways Modulated by Anti-oncogenic Sphingolipid Analogs. *Molecular & Cellular Proteomics*, *18*(3), 408–422. doi:10.1074/mcp.RA118.001053

Léveillé, M., & Estall, J. L. (2019). Mitochondrial Dysfunction in the Transition from NASH to HCC. *Metabolites*, *9*(10). doi:10.3390/metabo9100233

Levin, N., Nelson, C., Gurney, A., Vandlen, R., & de Sauvage, F. (1996). Decreased food intake does not completely account for adiposity reduction after ob protein infusion. *Proceedings of the National Academy of Sciences of the United States of America*, *93*(4), 1726–1730. doi:10.1073/pnas.93.4.1726

Liesa, M., & Shirihai, O. S. (2013). Mitochondrial dynamics in the regulation of nutrient utilization and energy expenditure. *Cell Metabolism*, *17*(4), 491–506. doi:10.1016/j.cmet.2013.03.002

Münzberg, H., & Myers, M. G. (2005). Molecular and anatomical determinants of central leptin resistance. *Nature Neuroscience*, *8*(5), 566–570. doi:10.1038/nn1454

Nagdas, S., Kashatus, J. A., Nascimento, A., Hussain, S. S., Trainor, R. E., Pollock, S. R., … Kashatus, D. F. (2019). Drp1 Promotes KRas-Driven Metabolic Changes to Drive Pancreatic Tumor Growth. *Cell reports*, *28*(7), 1845–1859.e5. doi:10.1016/j.celrep.2019.07.031

Naghdi, S., & Hajnóczky, G. (2016). VDAC2-specific cellular functions and the underlying structure. *Biochimica et Biophysica Acta*, *1863*(10), 2503–2514. doi:10.1016/j.bbamcr.2016.04.020

Osman, C., Voelker, D. R., & Langer, T. (2011). Making heads or tails of phospholipids in mitochondria. *The Journal of Cell Biology*, *192*(1), 7–16. doi:10.1083/jcb.201006159

Otera, H., Wang, C., Cleland, M. M., Setoguchi, K., Yokota, S., Youle, R. J., & Mihara, K. (2010). Mff is an essential factor for mitochondrial recruitment of Drp1 during

mitochondrial fission in mammalian cells. *The Journal of Cell Biology*, *191*(6), 1141–1158. doi:10.1083/jcb.201007152

Pavlova, N. N., & Thompson, C. B. (2016). The emerging hallmarks of cancer metabolism. *Cell Metabolism*, *23*(1), 27–47. doi:10.1016/j.cmet.2015.12.006

Perryman, M. S., Tessier, J., Wiher, T., O'Donoghue, H., McCracken, A. N., Kim, S. M., … Hanessian, S. (2016). Effects of stereochemistry, saturation, and hydrocarbon chain length on the ability of synthetic constrained azacyclic sphingolipids to trigger nutrient transporter down-regulation, vacuolation, and cell death. *Bioorganic & Medicinal Chemistry*, *24*(18), 4390–4397. doi:10.1016/j.bmc.2016.07.038

Pylayeva-Gupta, Y., Grabocka, E., & Bar-Sagi, D. (2011). RAS oncogenes: weaving a tumorigenic web. *Nature Reviews. Cancer*, *11*(11), 761–774. doi:10.1038/nrc3106

Rodgers, R. J., Tschöp, M. H., & Wilding, J. P. H. (2012). Anti-obesity drugs: past, present and future. *Disease Models & Mechanisms*, *5*(5), 621–626. doi:10.1242/dmm.009621

Ropelle, E. R., Pauli, J. R., Prada, P., Cintra, D. E., Rocha, G. Z., Moraes, J. C., … De Souza, C. T. (2009). Inhibition of hypothalamic Foxo1 expression reduced food intake in diet-induced obesity rats. *The Journal of Physiology*, *587*(Pt 10), 2341–2351. doi:10.1113/jphysiol.2009.170050

Rowland, A. A., & Voeltz, G. K. (2012). Endoplasmic reticulum-mitochondria contacts: function of the junction. *Nature Reviews. Molecular Cell Biology*, *13*(10), 607–625. doi:10.1038/nrm3440

Sam, A. H., Salem, V., & Ghatei, M. A. (2011). Rimonabant: from RIO to ban. *Journal of obesity*, *2011*, 432607. doi:10.1155/2011/432607

Schmitt, K., Grimm, A., Dallmann, R., Oettinghaus, B., Restelli, L. M., Witzig, M., … Eckert, A. (2018). Circadian control of DRP1 activity regulates mitochondrial dynamics and bioenergetics. *Cell Metabolism*, *27*(3), 657–666.e5. doi:10.1016/j.cmet.2018.01.011

Schneeberger, M., Dietrich, M. O., Sebastián, D., Imbernón, M., Castaño, C., Garcia, A., … Claret, M. (2013). Mitofusin 2 in POMC neurons connects ER stress with leptin resistance and energy imbalance. *Cell*, *155*(1), 172–187. doi:10.1016/j.cell.2013.09.003

Sebastián, D., Hernández-Alvarez, M. I., Segalés, J., Sorianello, E., Muñoz, J. P., Sala, D., … Zorzano, A. (2012). Mitofusin 2 (Mfn2) links mitochondrial and endoplasmic reticulum function with insulin signaling and is essential for normal glucose homeostasis. *Proceedings of the National Academy of Sciences of the United States of America*, *109*(14), 5523–5528. doi:10.1073/pnas.1108220109

Senft, D., & Ronai, Z. A. (2016). Regulators of mitochondrial dynamics in cancer. *Current Opinion in Cell Biology*, *39*, 43–52. doi:10.1016/j.ceb.2016.02.001

Serasinghe, M. N., Wieder, S. Y., Renault, T. T., Elkholi, R., Asciolla, J. J., Yao, J. L., … Chipuk, J. E. (2015). Mitochondrial division is requisite to RAS-induced transformation and targeted by oncogenic MAPK pathway inhibitors. *Molecular Cell*, *57*(3), 521–536. doi:10.1016/j.molcel.2015.01.003

Shapiro, A., Mu, W., Roncal, C., Cheng, K.-Y., Johnson, R. J., & Scarpace, P. J. (2008). Fructose-induced leptin resistance exacerbates weight gain in response to subsequent high-fat feeding. *American Journal of Physiology. Regulatory, Integrative and Comparative Physiology*, *295*(5), R1370–5. doi:10.1152/ajpregu.00195.2008

Softic, S., Cohen, D. E., & Kahn, C. R. (2016). Role of dietary fructose and hepatic de novo lipogenesis in fatty liver disease. *Digestive Diseases and Sciences*, *61*(5), 1282–1293. doi:10.1007/s10620-016-4054-0

Softic, S., Meyer, J. G., Wang, G.-X., Gupta, M. K., Batista, T. M., Lauritzen, H. P. M. M., … Kahn, C. R. (2019). Dietary Sugars Alter Hepatic Fatty Acid Oxidation via Transcriptional and Post-translational Modifications of Mitochondrial Proteins. *Cell Metabolism*, *30*(4), 735–753.e4. doi:10.1016/j.cmet.2019.09.003

Speakman, J. R. (2013). Measuring energy metabolism in the mouse - theoretical, practical, and analytical considerations. *Frontiers in physiology*, *4*, 34. doi:10.3389/fphys.2013.00034

Stepanyants, N., Macdonald, P. J., Francy, C. A., Mears, J. A., Qi, X., & Ramachandran, R. (2015). Cardiolipin's propensity for phase transition and its reorganization by dynamin-related protein 1 form a basis for mitochondrial membrane fission. *Molecular Biology of the Cell*, *26*(17), 3104–3116. doi:10.1091/mbc.E15-06-0330

Summers, S A, Garza, L. A., Zhou, H., & Birnbaum, M. J. (1998). Regulation of insulin-stimulated glucose transporter GLUT4 translocation and Akt kinase activity by ceramide. *Molecular and Cellular Biology*, *18*(9), 5457–5464. doi:10.1128/mcb.18.9.5457

Summers, Scott A., Chaurasia, B., & Holland, W. L. (2019). Metabolic Messengers: ceramides. *Nature Metabolism*, *1*(11), 1051–1058. doi:10.1038/s42255-019-0134-8

Swingle, M., Ni, L., & Honkanen, R. E. (2007). Small-molecule inhibitors of ser/thr protein phosphatases: specificity, use and common forms of abuse. *Methods in Molecular Biology*, *365*, 23–38. doi:10.1385/1-59745-267-X:23

Tubbs, E., Theurey, P., Vial, G., Bendridi, N., Bravard, A., Chauvin, M.-A., … Rieusset, J. (2014). Mitochondria-associated endoplasmic reticulum membrane (MAM) integrity is required for insulin signaling and is implicated in hepatic insulin resistance. *Diabetes*, *63*(10), 3279–3294. doi:10.2337/db13-1751

Varela, L., & Horvath, T. L. (2012). Leptin and insulin pathways in POMC and AgRP neurons that modulate energy balance and glucose homeostasis. *EMBO Reports*, *13*(12), 1079–1086. doi:10.1038/embor.2012.174

Wang, L., Ishihara, T., Ibayashi, Y., Tatsushima, K., Setoyama, D., Hanada, Y., … Nomura, M. (2015). Disruption of mitochondrial fission in the liver protects mice from diet-induced obesity and metabolic deterioration. *Diabetologia*, *58*(10), 2371–2380. doi:10.1007/s00125-015-3704-7

Watt, M. J., Clark, A. K., Selth, L. A., Haynes, V. R., Lister, N., Rebello, R., … Taylor, R. A. (2019). Suppressing fatty acid uptake has therapeutic effects in preclinical models of prostate cancer. *Science Translational Medicine*, *11*(478). doi:10.1126/scitranslmed.aau5758

Williams, K. W., Margatho, L. O., Lee, C. E., Choi, M., Lee, S., Scott, M. M., … Elmquist, J. K. (2010). Segregation of acute leptin and insulin effects in distinct populations of arcuate proopiomelanocortin neurons. *The Journal of Neuroscience*, *30*(7), 2472–2479. doi:10.1523/JNEUROSCI.3118-09.2010

Xia, J. Y., Holland, W. L., Kusminski, C. M., Sun, K., Sharma, A. X., Pearson, M. J., … Scherer, P. E. (2015). Targeted induction of ceramide degradation leads to improved systemic metabolism and reduced hepatic steatosis. *Cell Metabolism*, *22*(2), 266–278. doi:10.1016/j.cmet.2015.06.007

Yang, G., Lim, C.-Y., Li, C., Xiao, X., Radda, G. K., Li, C., … Han, W. (2009). FoxO1 inhibits leptin regulation of pro-opiomelanocortin promoter activity by blocking STAT3 interaction with specificity protein 1. *The Journal of Biological Chemistry*, *284*(6), 3719–3727. doi:10.1074/jbc.M804965200

Yue, S., Li, J., Lee, S.-Y., Lee, H. J., Shao, T., Song, B., … Cheng, J.-X. (2014). Cholesteryl ester accumulation induced by PTEN loss and PI3K/AKT activation underlies human prostate cancer aggressiveness. *Cell Metabolism*, *19*(3), 393–406. doi:10.1016/j.cmet.2014.01.019

Zhao, S., Zhu, Y., Schultz, R. D., Li, N., He, Z., Zhang, Z., … Scherer, P. E. (2019). Partial leptin reduction as an insulin sensitization and weight loss strategy. *Cell Metabolism*, *30*(4), 706–719.e6. doi:10.1016/j.cmet.2019.08.005